UNIVERSIDADE DE SÃO PAULO
INSTITUTO DE GEOCIÊNCIAS

Multi-technical approach to evaluate the impacts caused by the Vazante Mine (MG) on the Santa Catarina River flow loss through the overexploitation of a fissure-karst aquifer and simulation of mitigating solutions by numerical modeling

OTÁVIO BARBOSA FERREIRA

Dissertação apresentada ao Programa Recursos Minerais e Hidrogeologia para obtenção do título de Mestre em Ciências

Área de concentração: Hidrogeologia

Orientadora: Profª. Drª. Alexandra Suhogusoff

Coorientadora: Profª. Drª. Tatiana Tavares

SÃO PAULO
2023

Serviço de Biblioteca e Documentação do IGc/USP
Ficha catalográfica gerada automaticamente com dados fornecidos pelo(a) autor(a)
via programa desenvolvido pela Seção Técnica de Informática do ICMC/USP

Bibliotecários responsáveis pela estrutura de catalogação da publicação:
Sonia Regina Yole Guerra - CRB-8/4208 | Anderson de Santana - CRB-8/6658

Barbosa Ferreira, Otávio
Multi-technical approach to evaluate the impacts caused by the Vazante Mine (MG) on the Santa Catarina River flow loss through the overexploitation of a fissure-karst aquifer and simulation of mitigating solutions by numerical modeling / Otávio Barbosa Ferreira; orientadora Alexandra Vieira Suhogusoff; coorientadora Tatiana Tavares. -- São Paulo, 2023.
87 p.

Dissertação (Mestrado - Programa de Pós-Graduação em Recursos Minerais e Hidrogeologia) -- Instituto de Geociências, Universidade de São Paulo, 2023.

1. Rio em secamento. 2. Terreno cárstico. 3. Modelagem de fluxo de águas subterrâneas. 4. Traçadores fluorescentes. 5. Mina subterrânea. I. Vieira Suhogusoff, Alexandra, orient. II. Tavares, Tatiana, coorient. III. Título.

UNIVERSIDADE DE SÃO PAULO
INSTITUTO DE GEOCIÊNCIAS

Multi-technical approach to evaluate the impacts caused by the Vazante Mine (MG) on the Santa Catarina River flow loss through the overexploitation of a fissure-karst aquifer and simulation of mitigating solutions by numerical modeling

OTÁVIO BARBOSA FERREIRA

Orientadora: Profª. Drª Alexandra Vieira Suhogusoff

Dissertação de Mestrado

Nº 920

COMISSÃO JULGADORA

Dra. Alexandra Vieira Suhogusoff

Dr. Paulo Henrique Ferreira Galvão

Dr. Lucas Padoan de Sá Godinho

SÃO PAULO

2023

Aos meus pais,

Armando e Vania

ao meu irmão,

Mario

aos companheiros,

Lourenço, Luiz, Melissa,

Renato e Ricardo

AGRADECIMENTOS

Gostaria de estender a minha gratidão às pessoas que contribuíram para a conclusão desta dissertação de mestrado:

Em primeiro lugar, quero expressar o meu mais profundo agradecimento à minha mãe Vania, ao meu pai Armando e ao meu irmão Mario. Seus incentivos inabaláveis têm sido a base das minhas realizações.

Às minhas orientadoras, Dra. Alexandra Suhogusoff e Dra. Tatiana Tavares, sou verdadeiramente grato pela sabedoria, orientação e companheirismo compartilhados ao longo desta pesquisa.

Ao hidrogeólogo Edmar Araújo, concedo um agradecimento especial pela sua disposição e paciência em me ensinar a operar um *software* que eu, até então, desconhecia.

Gostaria de agradecer o geólogo Vitor Losada pela sua participação ativa no trabalho de campo e análise de dados.

Ao Dr. Todd Kincaid, expresso minha gratidão pela irreverência, agilidade e conhecimento técnico demonstrados durante as atividades de campo.

Estendo meus sinceros agradecimentos aos Drs. Carlos Gamba e Otávio Gandolfo por fornecerem generosamente dados geofísicos essenciais para a conclusão desta dissertação.

Gostaria também de agradecer à equipe da Water Services and Technologies, liderada pelo Dr. Nilson Guiguer, pela sua cooperação durante os testes com traçadores fluorescentes.

Ao Dr. Luiz Ferrari, sou grato pelo compartilhamento da sua perspectiva acerca da modelagem numérica. Seus lampejos ampliaram minha compreensão sobre esse tema.

Gostaria também de parabenizar todos os colaboradores do Instituto de Pesquisas Tecnológicas do Estado de São Paulo (IPT) pela dedicação à excelência técnica e contribuição à comunidade científica.

Agradeço a bolsa de estudos concedida pela CAPES (Coordenação de Aperfeiçoamento de Pessoal de Nível Superior).

Por fim, gostaria de expressar a minha mais genuína gratidão ao Guga, ao Lourenço, à Melissa, ao Renato e ao Ricardo pelos preciosos momentos de relaxamento e diversão que partilhamos juntos.

Se podes olhar, vê. Se podes ver, repara.

José Saramago

SUMÁRIO

LISTA DE FIGURAS

LISTA DE TABELAS

APÊNDICES

RESUMO

A perda de água em rios e córregos é um dos efeitos imediatos da superexploração dos aquíferos. Particularmente no contexto da mineração subterrânea, mudanças notáveis no regime natural de fluxo dos aquíferos ocorrem devido à necessidade de manter as galerias subterrâneas drenadas por meio de bombeamento. Na região noroeste do estado de Minas Gerais, no município de Vazante, o Rio Santa Catarina (RSC) passa por um processo de secamento associado à operação da mina subterrânea de Vazante. Para compreender adequadamente este fenômeno, é necessário um amplo conhecimento sobre a dinâmica hidrogeológica da região, principalmente por se tratar de uma área de geologia complexa, com feições cársticas e sistemas de falhas e fraturas. Este estudo realizou uma abordagem multitécnica para espacializar e caracterizar as estruturas rúpteis hidraulicamente condutivas, bem como os condutos cársticos responsáveis pelas conexões hidráulicas entre o RSC e a mina subterrânea. A metodologia foi baseada em investigações de campo, avaliação estrutural, sensoriamento remoto (Interferometria Diferencial – DinSAR), geofísica (resistividade elétrica) e testes com traçadores fluorescentes. Uma modelagem numérica de fluxo de água subterrânea em regime transiente foi realizada para avaliar soluções de mitigação para o problema de secamento do RSC, bem como para prever os impactos que um possível evento de seca extrema na região poderia causar sobre a perda de fluxo do rio. A avaliação das descontinuidades mapeadas no interior da mina identificou que as falhas e fraturas hidraulicamente mais produtivas apresentam uma tendência estrutural subvertical com orientação NW/SE. Os ensaios com traçadores fluorescentes indicaram a existência de conexões hidráulicas entre o RSC e a mina subterrânea de Vazante. Os imageamentos por DinSAR sugeriram que os deslocamentos superficiais do terreno estão sendo controlados por estruturas hidrogeologicamente condutoras localizadas na porção rasa do aquífero. O levantamento de resistividade elétrica revelou zonas de baixa resistividade entre o RSC e a mina de Vazante, indicando a presença de caminhos preferenciais de fluxo. A abordagem multitécnica integrada permitiu classificar as estruturas rúpteis de acordo com seu potencial (alto ou médio) para controlar o fluxo das águas subterrâneas. Os condutos cársticos que ligam o rio à mina subterrânea também foram espacializados. Todas as simulações (adução de água a montante, impermeabilização do leito do rio, tamponamentos dos condutos cársticos e evento de seca extrema) mostraram uma tendência de aumento da perda de vazão do RSC relacionada ao avanço das galerias subterrâneas da mina, seguida de estabilização ao longo do período simulado (2022-2030). Os cenários de adução de água a montante e tamponamento dos condutos cársticos apresentaram, respectivamente, a maior e menor perda de vazão do rio (aumento de 35,1% e redução de 47,7%, respectivamente) e taxa de bombeamento da mina (aumento de 7,0% e redução de 37,9%, respectivamente). O cenário de impermeabilização do leito do rio provocou a maior expansão no cone de rebaixamento (513 m) em direção ao município de Vazante até 2030.

Palavras-chave: interação água subterrânea/água superficial, secamento de rio, terreno cárstico, mina subterrânea, geofísica, traçadores fluorescentes, sensoriamento remoto, modelagem de fluxo de águas subterrâneas, soluções de mitigação.

ABSTRACT

The water loss in rivers and streams is one of the immediate effects of aquifer overexploitation. Particularly in the context of underground mining, notable changes in the natural groundwater flow regime are observed due to the pumping required to keep underground galleries drained. In the northwest region of the Brazilian state of Minas Gerais, in Vazante municipality, the Santa Catarina River (SCR) undergoes a drying up processes related to the Vazante underground mine dewatering. To properly understand this phenomenon, it is necessary to have a broad knowledge about the hydrogeological dynamics of the region, mainly in areas of complex geology with karst features and systems of faults and fractures. This study performed a multi-technical approach to spatialize and characterize the most hydraulically conductive brittle structures and karst conduits responsible for the hydraulic connections between the drying river and the underground mine. The methodology was based on field investigation, structural framework, remote sensing (Differential Interferometry – DinSAR), geophysics (electrical resistivity), and fluorescent tracer tests. A transient numerical groundwater flow modeling was carried out to evaluate mitigation solutions for the SCR drying-up problem and predict the impacts that a possible extreme drought event in the region could cause on the river flow loss. The assessment of discontinuities mapped inside the mine identified that the most productive water-bearing brittle structures show a subvertical NW/SE structural trend. Fluorescent dye tracers indicated the existence of hydraulic connections between the SCR and the Vazante underground mine. The DinSAR imagery suggested that the terrain surface movements are being controlled by hydrogeologically conductive structures located in the shallow portion of the aquifer. The electrical resistivity survey revealed low resistivity zones between the SCR to the Vazante mine, indicating the presence of preferential flow-paths. The integrated multi-technical approach allowed classifying the brittle structures according to their potential (high or medium) to control the groundwater flow. The karst conduits that connect the drying river to the underground mine were also spatialized. All simulations (upstream water supply, riverbed-waterproofing, obstruction of sinkholes and extreme drought) showed a trend of increase in the SCR flow loss related to the advance of the underground mine galleries, followed by stabilization over the simulated period (2022-2030). The upstream water supply and sinkholes obstruction scenarios showed the highest and lowest river flow loss (35.1% increase and 47.7% decrease, respectively) and mine pumping rates (7.0% increase and 37,9% decrease, respectively). The riverbed-waterproofing scenario caused the largest expansion in the depression cone (513 m) towards the municipality of Vazante until 2030.

Keywords: groundwater/surface water interaction, drying river, karst terrain, underground mine, geophysics, dye tracer test, remote sensing, groundwater flow modeling, mitigating solutions.

1. INTRODUCTION AND OBJECTIVES

Developing reliable hydrogeological conceptual models is essential for characterizing groundwater flow behavior. They can address environmental questions related to the dynamics of aquifers and their interactions with surface water bodies such as rivers, lakes, and reservoirs (Bonsor et al., 2017; Karlovic et al., 2021; Kresic & Mikszewski, 2012; Mukherjee et al., 2018). A hydrogeological conceptual model is a synthesis of geological, hydrogeological, hydrological, and climate information about a particular area capable of describing the groundwater system based on physical and chemical principles (Cook, 2003; Enemark et al., 2019; Singhal & Gupta, 2010; White, 1999; White, 2012; Zheng & Bennett, 2002).

In general, hydrogeological conceptual models are elaborated through observations of water level fluctuation, borehole description, tracer test, sinkhole discretization, geophysical survey (e.g., gravimetry, electrical resistivity, and self-potential), hydrogeochemical data, and other auxiliary information like pluviometric and fluviometric data (Anderson et al., 2015; Lekula et al., 2018). However, the approach through conventional methods may not be enough for karst aquifers. The availability of subsurface data, such as the discretization of well-developed karst zones and location and structural trends of faults and fractures may not be satisfactory for the accomplishment of a reliable hydrogeological framework (Banks et al., 2009; Trabelsi et al., 2011).

Fractured rocks characterize systems with a subordinate or even non-existent primary porosity cut by cracks, joints, fractures, and shear zones that characterize the secondary porosity (Anderson et al., 2015). This scenario can be even more complex when soluble rocks like dolomite and limestone develop fractured aquifer systems in which groundwater flows through horizontal and vertical connections (Hamad et al., 2018; Masciopinto & Palmiotta, 2012; NASEM, 2020; Petitta et al., 2018). The hydraulic conductivity in fractured carbonate aquifers varies over a wide range due to the advance of karstification processes (conduit development and fracture aperture enlargement by dissolution) and the heterogeneity of the medium. As a result, karst aquifers develop a highly efficient connection with surface water bodies through sinkholes and springs (White et al., 2012).

Properly comprehending the hydraulic potential and location of karst features and brittle structures plays a crucial role in understanding the groundwater and surface water interactions in such a complex hydrogeological environment. These interactions incorporate the terrain's physiography (topography, geology, and geomorphology) to its hydraulic characteristics and is

associated with the regional water balance estimate (Fleckenstein et al., 2006; Kalhor et al., 2019). Bonacci (2015) describes groundwater and surface water in karst terrains as “a single dynamic system (…) hydraulically connected through numerous karst forms which facilitate and govern the exchange of water between the surface and subsurface”. Therefore, any intervention in the fragile hydraulic dynamics of fractured carbonate aquifers should consider solutions to avoid adverse impacts, such as developing sinkholes, land subsidence, and flow loss in rivers and streams (Taheri et al., 2016).

The negative effect of aquifer systems overexploitation is a very current topic and has been discussed by many authors around the world (Changming et al., 2001; Custodio, 2002; Esteller & Diaz-Delgado, 2002; Jamali et al., 2020; Molina et al., 2009; Rupérez-Moreno et al., 2017; Saadé-Sbeih et al., 2018). For example, Custodio (2002) describes the water loss in rivers and streams through infiltration into the ground as one of the immediate main effects of aquifer overexploitation. This infiltration may result in land subsidence and sudden collapse by water-table lowering and hydrostatic pressure decrease, mainly on soluble rocks. In addition, particularly in the context of underground mining, notable changes in the natural groundwater flow regime are observed due to the pumping rate to keep underground galleries drained (Custodio et al., 2016; Mengistu et al., 2014; Mengistu et al., 2019; Rapantova et al., 2007; Stavric, 2004).

The Vazante underground mine is an example of groundwater management complexity. It is Brazil's largest zinc ore deposit and remains among the ten largest zinc producers worldwide. Vazante's galleries are developed in karstified, folded, and fractured dolomitic rocks, which create a highly complex hydrogeological framework (Bittencourt & Reis Neto, 2012). The most critical springs inside the mine occur in conduits and fractures with a certain degree of dissolution. Therefore, for the mining operation, it is necessary to lower the water level of the aquifer system through pumping stations.

Bittencourt et al. (2008) report a gradual regional lowering of the aquifer system over the last decades due to the increasing water pumping in the Vazante mine. The water inflows to the mine through karstified and fractured zones during the advance of the mine galleries. The dewatering potentiated the appearance of many sinkholes around the mine, mainly into the river floodplain. In addition to the regional impacts on geomorphology, the Santa Catarina River (SCR), the main river of the dolomitic watershed in which the mine is located, has been gradually losing flow rate over the last few years, representing a social issue for the local

community. High hydraulic gradients induced by the mine water capture zone caused an inversion in the hydraulic gradient between the river and the aquifer (Bittencourt et al., 2008). Closer to the mining area, the river becomes influent, representing an important source of recharge for the dolomitic aquifer system, with a direct hydraulic connection with the mine through fractures and conduits (Ninanya et al., 2018).

Due to low precipitation rates and base flow contribution during the dry season, the river losing stretch dries up downstream. Extreme drought events in the SCR drainage basin, as observed between 2016 and 2017, can severely impact the decrease in river flow, reaching up to 8 km of a dry riverbed in October 2017. Combined with the impacts of mine dewatering, deficient precipitation can result in an upstream advance of the river drying front.

This study aimed to identify and classify brittle structures and karst conduits that can generate hydraulic connections between a drying river and an underground mine. Furthermore, the study presents how a multi-technical approach based on: (1) field investigation; (2) structural framework analysis; (3) remote sensing; (4) geophysics; and (5) dye tracer tests can supply detailed information on groundwater flow in a highly complex geological setting. The results contribute to developing refined conceptual models that can lead to more robust investigations for drying river problems related to underground mine dewatering.

In addition, simulations were performed based on a mathematical groundwater flow model in a transient regime using the computational algorithm FEFLOW – Finite Element Subsurface Flow and Transport Simulation System (Diersch 2014) to evaluate some mitigation solutions for the river drying-up phenomenon. It was also estimated the possible impacts that extreme climate events of drought combined with mining activity might generate in the Santa Catarina River flow.

The present master's research is part of the project "*Análise de causas associadas ao processo de secamento em trecho do rio Santa Catarina, município de Vazante/MG - Etapa 2*" (Analysis of causes associated with the drying process in a Santa Catarina River's stretch, municipality of Vazante/MG - Stage 2), carried out by the *Cidades, Infraestrutura e Meio Ambiente* (Cities, Infrastructure, and Environment) unit of the *Instituto de Pesquisas Tecnológicas do Estado de São Paulo – IPT* (Institute for Technological Research of the State of São Paulo).

1.1. Dissertation Structure

This master's dissertation is organized into five chapters with a logical relationship in the context of the objectives proposed in the dissertation. Therefore, some overlap between them was inevitable. They are described below:

Chapter 1 describes the relevance of the studied subject, its state of the art and the objectives to be achieved.

Chapter 2 is presented as a scientific manuscript submitted to the Hydrological Processes Journal in January 2023. This chapter introduces all the research developed for the hydrogeological characterization of the brittle structures in the study area, including the study area description, methods, results and discussions, conclusions, and references.

Chapter 3 describes the conceptual hydrogeological model based on the results obtained in the Chapter 2. It also includes the numerical modelling objectives, description, results, and discussions.

Chapter 4 presents the general conclusions and recommendations of the dissertation.

Chapter 5 lists all references cited throughout the dissertation.

The Appendix 1 brings the abstract of the work presented at 47th International Association of Hydrogeologists (IAH) Congress (Brazil, August 2021) regarding to the results described in the Chapter 2.

2. HYDROGEOLOGICAL CHARACTERIZATION OF BRITTLE STRUCTURES AND KARST CONDUITS CONNECTING A DRYING RIVER AND AN UNDERGROUND MINE USING A MULTI-TECHNICAL APPROACH (VAZANTE, BRAZIL)

Otávio B. Ferreira [1,2], Alexandra Suhogusoff [2], Tatiana Tavares [1], Edimar E. Araújo [3], Todd Kincaid [4], Vitor L. Díaz [1], Nilson Guiguer [5], Carlos C. Gamba [1], and Otavio Gandolfo [1]

[1] Institute of Technological Research, São Paulo, Brazil

[2] Geoscience Institute, University of São Paulo, São Paulo, Brazil

[3] Nexa Resources, Vazante, Brazil

[4] GeoHydros, Reno, USA

[5] Water Services and Technologies, Florianópolis, Brazil

Corresponding Author: Otávio B. Ferreira, Institute of Technological Research, 532 Professor Almeida Prado Ave, Butantã, São Paulo, Brazil; Geoscience Institute, University of São Paulo (USP), 562 do Lago St, Butantã, São Paulo, Brazil.

Email: otavio.barbosa.ferreira@usp.br

ABSTRACT

The water loss in rivers and streams is one of the immediate effects of aquifer overexploitation. Particularly in the context of underground mining, notable changes in the natural groundwater flow regime are observed due to the pumping required to keep underground galleries drained. In the northwest region of the Brazilian state of Minas Gerais, the Santa Catarina River undergoes a drying up processes related to the Vazante underground mine dewatering. To properly understand this phenomenon, it is necessary to have a broad knowledge about the hydrogeological dynamics of the region, mainly in areas of complex geology with karst features and systems of faults and fractures. This study performed a multi-technical approach to spatialize and characterize the most hydraulically conductive brittle structures and karst conduits responsible for the hydraulic connections between the drying river and the underground mine. The methodology was based on field investigation, structural framework analysis, remote sensing (Differential Interferometry – DinSAR), geophysics (electrical resistivity), and fluorescent tracer tests. The assessment of discontinuities mapped inside the mine identified the structural trend of the most productive water-bearing brittle structures inside the mine. Fluorescent dye tracers uranine and rhodamine-b indicated the existence of hydraulic connections between the SCR and the Vazante underground mine, being detected in eight different springs within mine. The DinSAR imagery suggested that the terrain surface movements, which are associated with the emergence of dolines and sinkholes in the riverbed, are being controlled by hydrogeologically conductive structures located in the shallow portion of the aquifer. The electrical resistivity survey revealed low resistivity zones between the SCR to the Vazante mine, indicating the presence of preferential flow-paths at depths greater than 90 m. The integrated multi-technical approach allowed classifying the brittle structures according to their potential (high or medium) to control the groundwater flow. The karst conduits that connect the drying river to the underground mine were also spatialized.

Keywords: groundwater/surface water interaction, drying river, karst terrain, underground mine, geophysics, dye tracer test, remote sensing, brittle structures

2.1. Introduction

Developing reliable hydrogeological conceptual models is essential for characterizing groundwater flow behavior. They can address environmental questions related to the dynamics of aquifers and their interactions with surface water bodies such as rivers, lakes, and reservoirs (Bonsor et al., 2017; Karlovic et al., 2021; Kresic & Mikszewski, 2012; Mukherjee et al., 2018). A hydrogeological conceptual model is a synthesis of geological, hydrogeological, hydrological, and climate information about a particular area capable of describing the groundwater system based on physical and chemical principles (Cook, 2003; Enemark et al., 2019; Singhal & Gupta, 2010; White, 1999; White, 2012; Zheng & Bennett, 2002).

In general, hydrogeological conceptual models are elaborated through observations of water level fluctuation, borehole description, dye tracer test, sinkhole discretization, geophysical survey (e.g., gravimetry, electrical resistivity, and self-potential), hydrogeochemical data, and other auxiliary information like pluviometric and fluviometric data (Anderson et al., 2015; Lekula et al., 2018). However, the approach through conventional methods may not be enough for karst aquifers. The availability of subsurface data, such as the discretization of well-developed karst zones and location and structural trends of faults and fractures may not be satisfactory for the accomplishment of a reliable hydrogeological framework (Banks et al., 2009; Trabelsi et al., 2011).

Fractured rocks characterize systems with a subordinate or even non-existent primary porosity cut by cracks, joints, fractures, and shear zones responsible for the formation of secondary porosity (Anderson et al., 2015). This scenario can be even more complex when soluble rocks like dolomite and limestone develop fractured aquifer systems in which groundwater flows through horizontal and vertical connections (Hamad et al., 2018; Masciopinto & Palmiotta, 2012; NASEM, 2020; Petitta et al., 2018). The hydraulic conductivity in fractured carbonate aquifers varies over a wide range due to the advance of karstification processes (conduits development and fracture aperture enlargement by dissolution) and the heterogeneity of the medium. As a result, karst aquifers develop a highly efficient connection with surface water bodies through sinkholes and springs (White et al., 2012).

Properly comprehending the hydraulic potential and location of karst features and brittle structures plays a crucial role in understanding the groundwater and surface water interactions in such a complex hydrogeological environment. These interactions incorporate the terrain's

physiography (topography, geology, and geomorphology) to its hydraulic characteristics and is associated with the regional water balance estimate (Fleckenstein et al., 2006; Kalhor et al., 2019). Bonacci (2015) describes groundwater and surface water in karst terrains as "a single dynamic system (…) hydraulically connected through numerous karst forms which facilitate and govern the exchange of water between the surface and subsurface". Therefore, any intervention in the fragile hydraulic dynamics of fractured carbonate aquifers should consider solutions to avoid adverse impacts, such as developing sinkholes, land subsidence, and flow loss in rivers and streams (Taheri et al., 2016).

The negative effect of aquifer systems overexploitation is a very current topic and has been discussed by many authors around the world (Changming et al., 2001; Custodio, 2002; Esteller & Diaz-Delgado, 2002; Jamali et al., 2020; Molina et al., 2009; Rupérez-Moreno et al., 2017; Saadé-Sbeih et al., 2018). For example, Custodio (2002) describes the water loss in rivers and streams through infiltration into the ground as one of the immediate main effects of aquifer overexploitation. This infiltration may result in land subsidence and sudden collapse by water-table lowering and hydrostatic pressure decrease, mainly on soluble rocks. In addition, particularly in the context of underground mining, notable changes in the natural groundwater flow regime are observed due to the pumping rate to keep underground galleries drained (Custodio et al., 2016; Mengistu et al., 2014; Mengistu et al., 2019; Rapantova et al., 2007; Stavric, 2004).

The Vazante underground mine is an example of groundwater management complexity. It is Brazil's largest zinc ore deposit and remains among the ten largest zinc producers worldwide. Vazante's galleries are developed in karstified, folded, and fractured dolomitic rocks, which create a highly complex hydrogeological framework (Bittencourt & Reis Neto, 2012). The most critical springs inside the mine occur in conduits and fractures with a certain degree of dissolution. Therefore, for the mining operation, it is necessary to lower the water level of the aquifer system through pumping stations.

Bittencourt et al. (2008) report a gradual regional lowering of the aquifer system over the last decades due to the increasing water pumping in the Vazante mine. The water inflows to the mine through karstified and fractured zones during the advance of the mine galleries. The dewatering potentiated the appearance of many sinkholes around the mine, mainly into the river floodplain. In addition to the regional impacts on geomorphology, the Santa Catarina River (SCR), the main river of the dolomitic watershed in which the mine is located, has been

gradually losing flow rate over the last few years. High hydraulic gradients induced by the mine water capture zone caused an inversion in the hydraulic gradient between the river and the aquifer (Bittencourt et al., 2008). Closer to the mining area, the river becomes influent, representing an important source of recharge for the dolomitic aquifer system, with a direct hydraulic connection with the mine through fractures and conduits (Ninanya et al., 2018).

Due to low precipitation rates and base flow contribution during the dry season, the river losing stretch dries up downstream. Extreme drought events in the SCR drainage basin, as observed between 2016 and 2017, can severely impact the decrease in river flow, reaching up to 8 km of a dry riverbed in October 2017. Combined with the impacts of mine dewatering, deficient precipitation can result in an upstream advance of the river drying front.

This study aimed to identify and classify brittle structures and karst conduits that can generate hydraulic connections between a drying river and an underground mine. Furthermore, the study presents how a multi-technical approach based on: (1) field investigation; (2) structural framework; (3) remote sensing; (4) geophysics; and (5) dye tracer tests can supply detailed information on groundwater flow in a highly complex geological setting. The results contribute to developing refined conceptual models that can lead to more robust investigations for drying river problems related to underground mine dewatering.

2.2. Study Site Description

2.2.1. Location, population, local climate, and geomorphology

The study area is located in the Vazante municipality (Figure 1), in the northwest region of the Brazilian state of Minas Gerais. With approximately 20,000 inhabitants, the most important economic activity that stands out in generating income for the municipality is industrial (39%) due to the implementation, since the 1950s, of a zinc ore extraction and processing plant (IBGE, 2010).

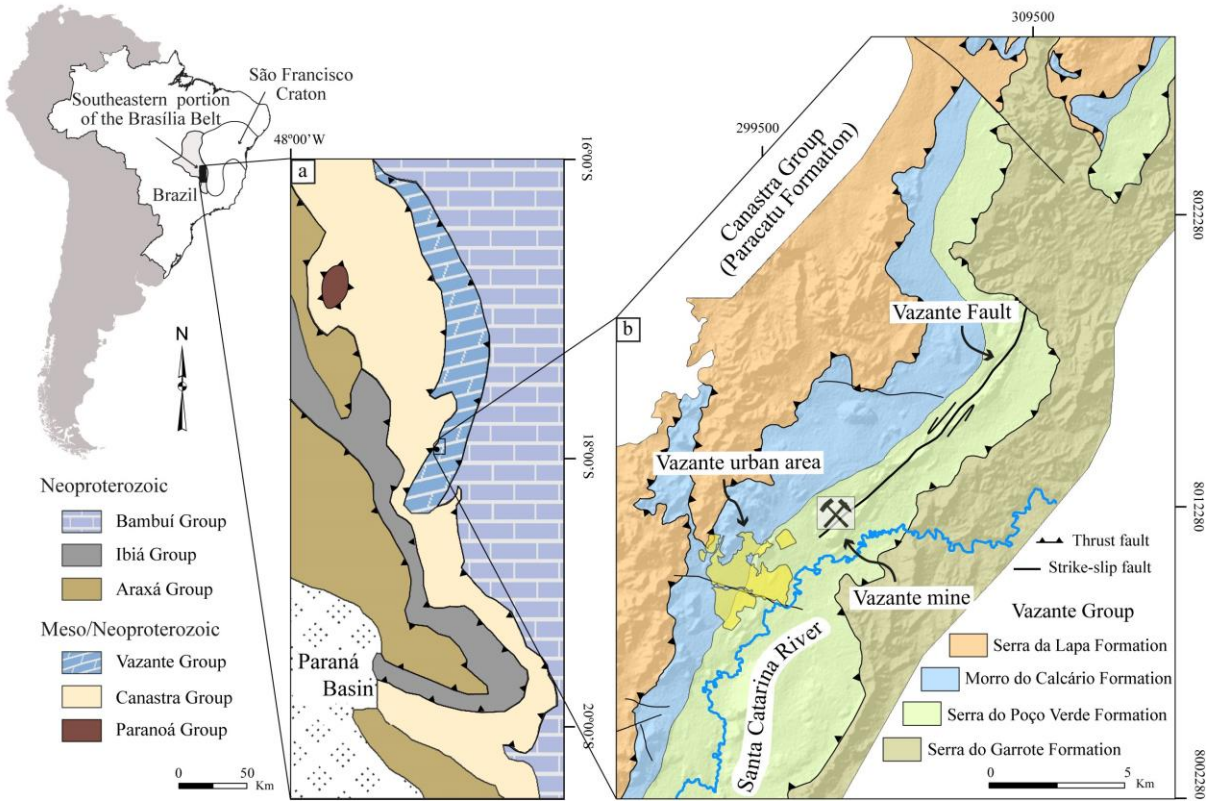

Figure 1 - Location map showing: a) Geological map of the Brazilia Fold Belt southeastern segment (after Dardenne, 2000); b) Geological map of the Vazante Group in the study area and locations of the Vazante urban area, Vazante mine, Santa Catarina River, and Vazante Fault.

The area is in the Cerrado biome (Brazilian Savanna) at approximately 650 m altitude. It has a continental tropical climate marked by dry winters (April to September) and rainy summers (October to March) with an average annual temperature of 21.6 ºC and 1,470 mm of mean annual precipitation (Rodrigues Filho & Viana 2011; Vasconcelos et al., 2012).

Geomorphologically, the Vazante region presents a relief with broad hills, low mountains, and tabular plateaus characterized as slightly elevated surfaces in relation to the adjacent lands (Machado & Silva, 2010). The local geomorphology corresponds to an area of approximately 60 km of flat relief, associated with the SCR floodplain and its tributaries, bordered by hilly terrain. Well-developed karst surfaces are described in the region, with the development of pinnacles and ruiniform relief (Bittencourt et al., 2008; Bittencourt et al., 2009).

2.2.2. Geology settings

The geological arrangement of the study area is associated with the southwestern portion of the Brasília Fold Belt (Figure 1a). It represents an orogen situated in the western margin of the São Francisco Craton (Almeida, 1977). The Brasilia Fold Belt extends more than 1,000 km in an overall N-S direction, comprehending sequences of rock thrust to the east, indicating tectonic transport towards the São Francisco Craton (Dardenne, 2000). This regional structure displays Meso-Neoproterozoic sedimentary and metasedimentary sequences; Paleo-Meso-Neoproterozoic igneous intrusions and volcano-sedimentary units; and Archean exotic granite-greenstone terranes (Dardenne, 2000; Fuck et al., 1994; Valeriano et al., 2004).

Located in the southeastern segment of the Brasília Fold Belt, the metasedimentary Meso-Neoproterozoic groups of Araxá, Ibiá, Canastra, and Vazante characterize a system of thrusts and nappes submitted by increasing deformation and metamorphism compared with the belt's northern segment (Pimentel et al., 2001). The geological deformation complexity makes recognizing the stratigraphic arrangement between these metasedimentary units difficult.

The Vazante Group extends up to 300 km in a N-S direction in the external zone of the Brasilia Fold Belt (Dardenne, 2000; Fuck et al., 1994), comprising mainly metasedimentary units (limestone, shale, and diamictite), into seven formations: Santo Antonio do Bonito, Rocinha, Lagamar, Serra do Garrote, Serra do Poço Verde, Morro do Calcário, and Serra da Lapa (Figure 2). Only the last four formations occur in the study area.

The Serra do Garrote Formation is composed of a sedimentary marine sequence with dark gray to black phyllites, sometimes containing zones of chlorite alteration, calcite veins, and pyrite-rich interbedded quartzite (Carvalho et al., 2016; Slezak et al., 2014). The overlying Serra do Poço Verde Formation has tectonic contact with the Serra do Garrote Formation (Slezak et al., 2014).

The Serra do Poço Verde Formation, which hosts the Vazante non-sulfide hypogenic zinc deposit (Monteiro et al., 2007), consists of metadolomitic and metapelitic sequences. According to Dardenne (2000), this formation is divided into four members, described below from base to

top. The Morro do Pinheiro Lower Member consists of light grey and pink laminated dolomite with cyanobacteria mats intercalated with oncolitic dolarenite, intraformational breccia and lens of dolomite with columnar stromatolites. The Morro do Pinheiro Upper Member is composed of dark grey laminated dolomite with cyanobacteria mats, birdseye features, dolarenite, breccia, and carbonaceous shale. The Pamplona Lower Member comprises grey to purple siltstone intercalated with micritic dolomite with cyanobacteria mats and grey to green slates. The Pamplona Middle Member is composed of dolomite with cyanobacteria mats intercalated with lamellar breccia, dolarenite, dolomite with columnar stromatolites, and shale lens.

The Morro do Calcário Formation comprises gray dolarenite with stromatolitic bioherms (Carvalho et al., 2019; Monteiro et al., 2006) and comprehends the Upper Pamplona Member described by Rigobello et al. (1988).

The Serra da Lapa Formation is the upper unit of the Vazante Group (Carvalho et al., 2019), consisting of black carbonaceous phyllite, carbonatic metasiltstone lenses, dolostone and quartzite lens (Monteiro et al., 2007; Pimentel et al., 2001).

The zinc silicate mineralization (willemite) of the Vazante deposit is hosted in a hydrothermal breccia composed of iron-rich dolomite, ankerite, and siderite (Hitzman et al., 2003; Monteiro et al., 2006; Monteiro et al., 2007). The Vazante Fault controlled the percolation of the mineralized hydrothermal fluids (Dias et al., 2015; Pinho et al., 1989; Slezak et al., 2014;). This important tectonic structure (Figure 1b) is 12 km long with strike N40º-50ºE and deep 50º-70NW, parallel to regional geologic contacts (Carvalho et al., 2016; Dardenne, 2000).

The Morro do Calcário and Serra do Poço Verde formations host a complex karst system with exokarst and endokarst features associated with important fracture and fault zones (Bittencourt & Reis Neto, 2012). Bittencourt et al. (2009) proposed epigenic and hypogenic processes influence on the karstification development over time. According to this model, the karst system has two primary altimetric levels. The first, located between 600 m and 450 m elevation, is controlled predominantly by epigenic processes and is associated with the main surface karst features in the region. The second one, located below the 450 m elevation, comprehends only relict features developed by hypogenic speleogenesis processes and is related to the formation of karst conduits that intercept the underground mine galleries in deeper portions of the aquifer system.

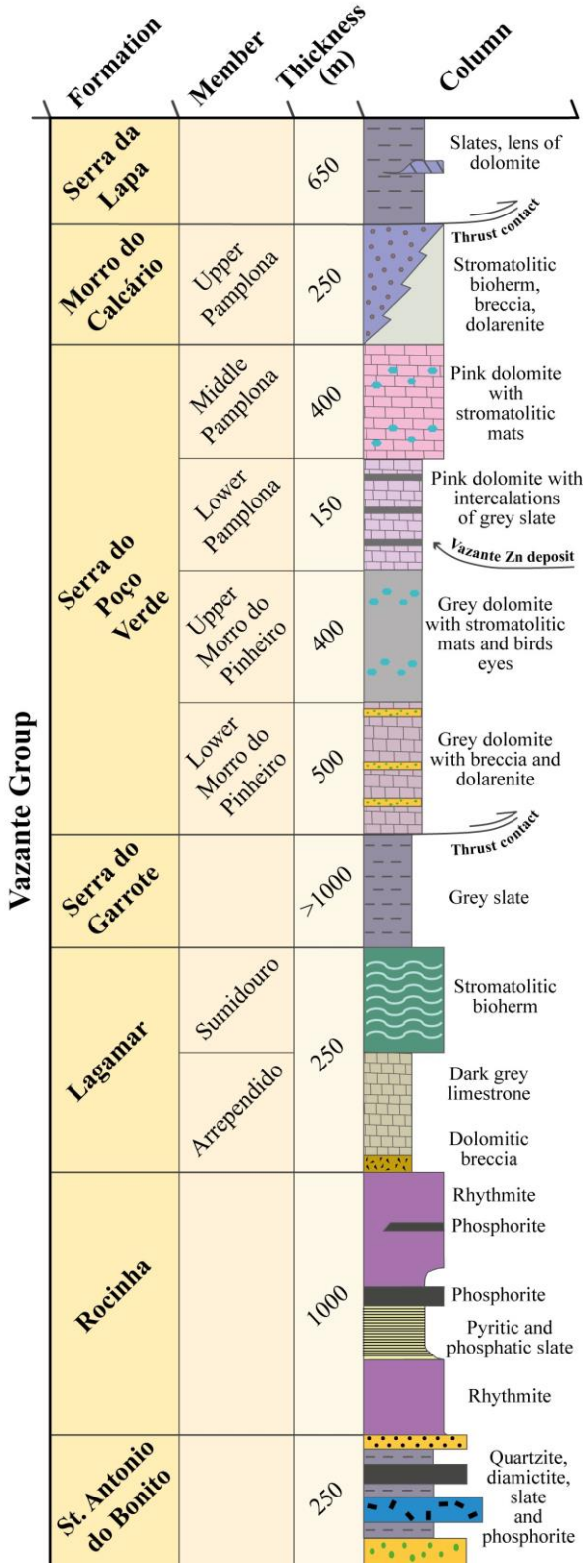

Figure 2 - Out-of-scale lithostratigraphic column of the Vazante Group with the Vazante zinc deposit location (after Azmy et al., 2006; Carvalho et al., 2016; Dardenne, 2000).

2.2.3. Hydrology and hydrogeology settings

The SCR is located in the Paracatu River drainage basin, representing one of its main left-side tributaries. With an average flow rate of approximately 13,000 m³/h near the mine region, SCR reaches peaks of more than 100,000 m³/h during the rainy season, according to the mining company data. Inside the dolomitic basin, formed by the Serra do Poço Verde and Morro do Calcário formations, the SCR flows from southwest to northeast and represents the local base level. Its main tributaries are the Carrapato, Carranca, and Guariroba streams, located upstream of the river watershed.

Ninanya et al. (2018) previously estimated the aquifer recharge from the river at 3,650 m³/h. Since then, the SCR water losses to the aquifer have been gradually increasing due to more severe dry seasons and internal erosion of flow-bearing structures that connect the river to the mine. Over time, hydraulic and geomorphological data of river flow rate variations, water levels, water quality, and changes in sinkhole formation patterns are closely monitored by the mining company through regular field inspections, automated river monitoring stations, and several monitoring wells installed in the study area.

The groundwater flow concentrates inside the dolomitic basin with a preferential direction towards the underground mine through the hydrogeological units Pink Dolomite, Black Philite, and Grey Dolomite (Figure 3). This units show the greatest groundwater drawdown in the region close to the mine. The groundwater flow occurs preferentially by secondary porosity formed by fracture systems and dissolution features developed and conditioned along the main fracture zones.

To the west of the dolomitic basin, the Serra da Lapa Formation acts as a drainage divide reaching altitudes between 832 m and 895 m. The eastern, northern and southern boundaries comprise the watershed divide formed by the Serra do Garrote Formation, which has elevations between 641m (NE portion) and 832m (SE portion). The surface runoff occurs mainly from these topographic highs towards the dolomitic basin with discharge into the SCR.

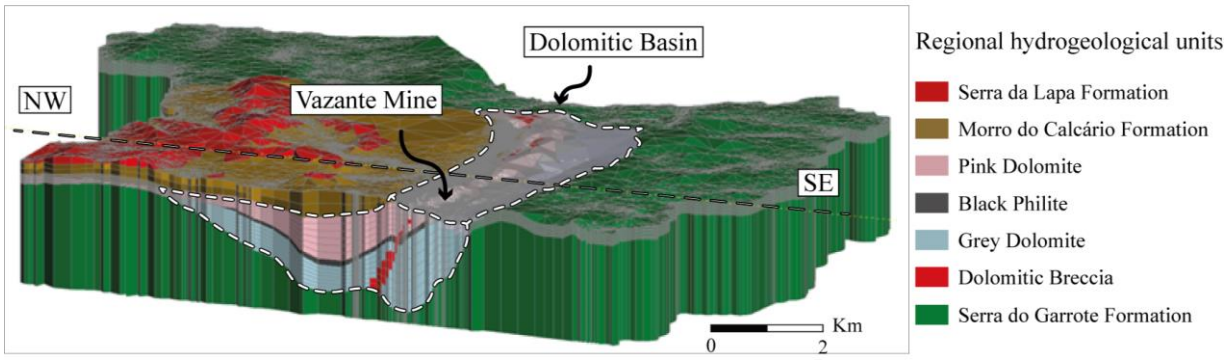

Figure 3 - Geological model of the study area in NW-SE section with the spatial distribution of regional hydrogeological units. Model generated in Leapfrog Geo.

The mining company defined the local hydrogeological units of the aquifer system based on the mineralized body and mine positions (Bittencourt et al., 2008). The groundwater level drawdown occurs heterogeneously depending on the mineralized body presence (Figure 4). The Upper and Lower Footwall aquifers consist of the grey dolomites of the Serra do Poço Verde Formation and show a high level of karstification and fracturing. Fractured black carbonaceous phyllite layers separates the Upper and Lower Footwal aquifers, behaving as inefficient local aquitards since the fractures allow hydraulic connections. The well-karstified pink dolomites of the Morro do Calcário Formation host the Hanging Wall aquifer, which has a less significant drawdown because of the smaller number of underground galleries in these rocks (Figure 4).

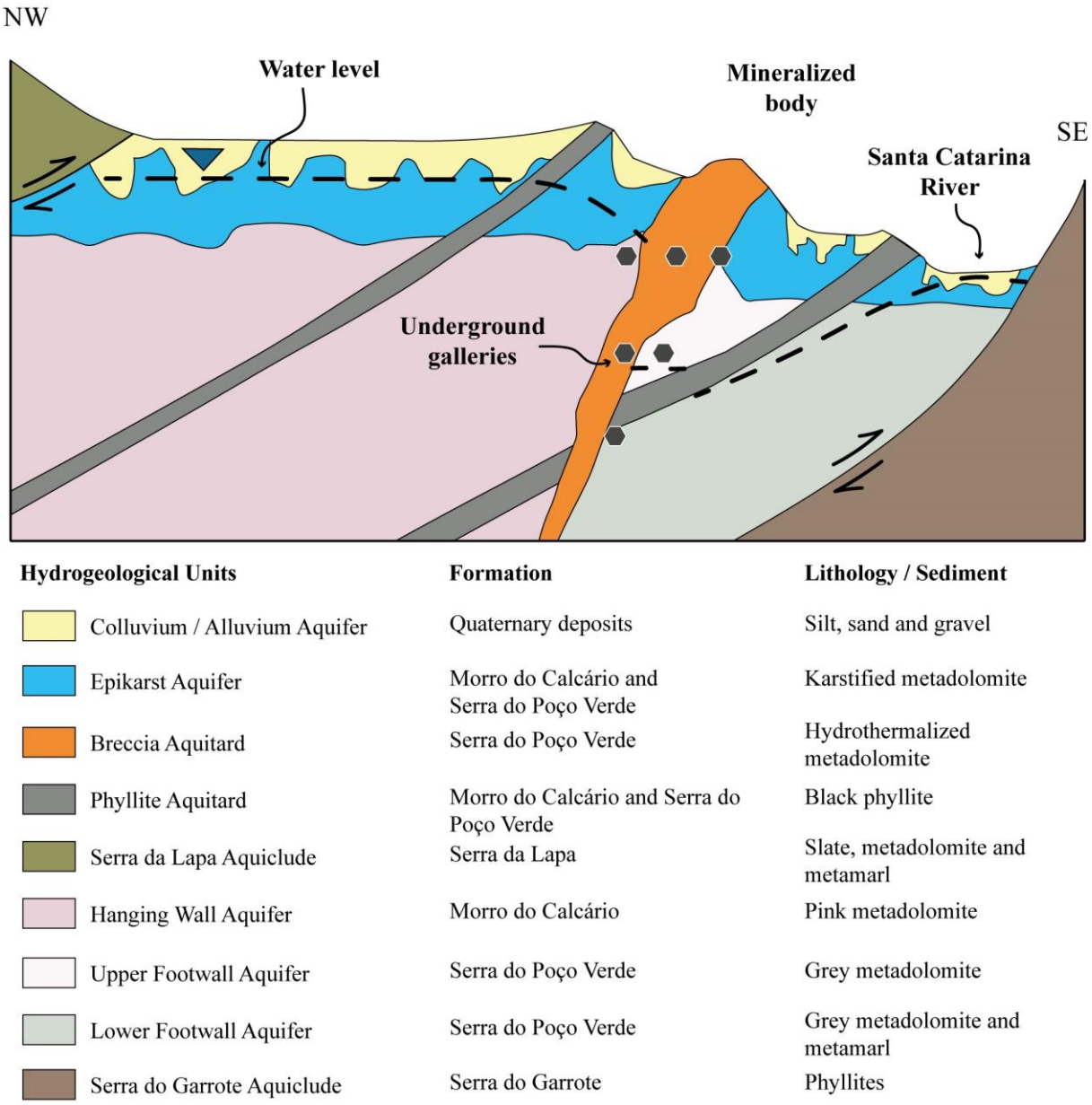

Figure 4 - Schematic hydrogeological section of the fractured aquifer system in the study area (modified from Bittencourt et al., 2008).

Although the mineralized body consists of dolomitic breccia, it represents an aquitard due to the low permeability caused by mineral precipitation from mineralized hydrothermal fluids. The set of epikarst and shallower conduit and cave systems extend to a depth of up to 100 m, promoting a highly effective hydraulic connectivity between the three aforementioned dolomitic aquifers (Bittencourt et al., 2008).

In the hydraulic interaction zone between the SCR and the aquifer, groundwater flows downward in the more superficial hydrogeological units (Colluvium-Alluvium Cover and Epikast) and between fractures and karst conduits developed in the carbonate rock massif

(Figure 5). The Colluvium-Alluvium Cover unit forms a shallow aquifer, of primary porosity, with a direct connection to the SCR. The Epikarst unit is located beneath the Colluvium-Alluvial unit, having a complex system of hydraulic connections through fractures and karst conduits that hydraulically connect the surface sediments to the carbonate massif.

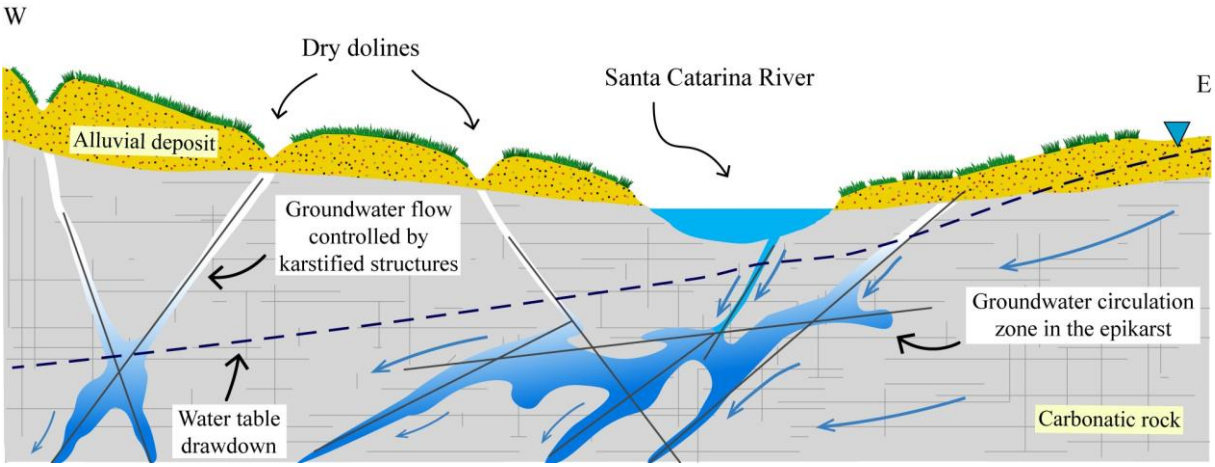

Figure 5 - Schematic diagram summarizing the conceptual groundwater circulation model of the Santa Catarina River losing stretch during the dry season.

2.3. Materials and Methods

The methodological approach was based on the integration and analysis of direct and indirect data from the geomorphological, hydrological, hydrogeological and structural framework of the region (Figure 6).

Direct data were obtained from: mapping dolines and sinkholes in the SCR drying stretches; classification of springs in hydraulically active faults and fractures inside the mine; and fluorescent dye tracer tests in the SCR. The recognition of surface sinkholes in the SCR and resurgences inside the mine guided the selection of injection and sampling points for the tracer tests.

The acquisition of indirect data was based on remote sensing (differential interferometry); and geophysics (electrical resistivity). These imageries contributed to the spatial discretization of the most relevant regional hydrogeological structures between the SCR and the underground mine. All data were crossed using a GIS platform to establish a logical association between the most significant potential zones for groundwater flow and the discontinuities located in the study area.

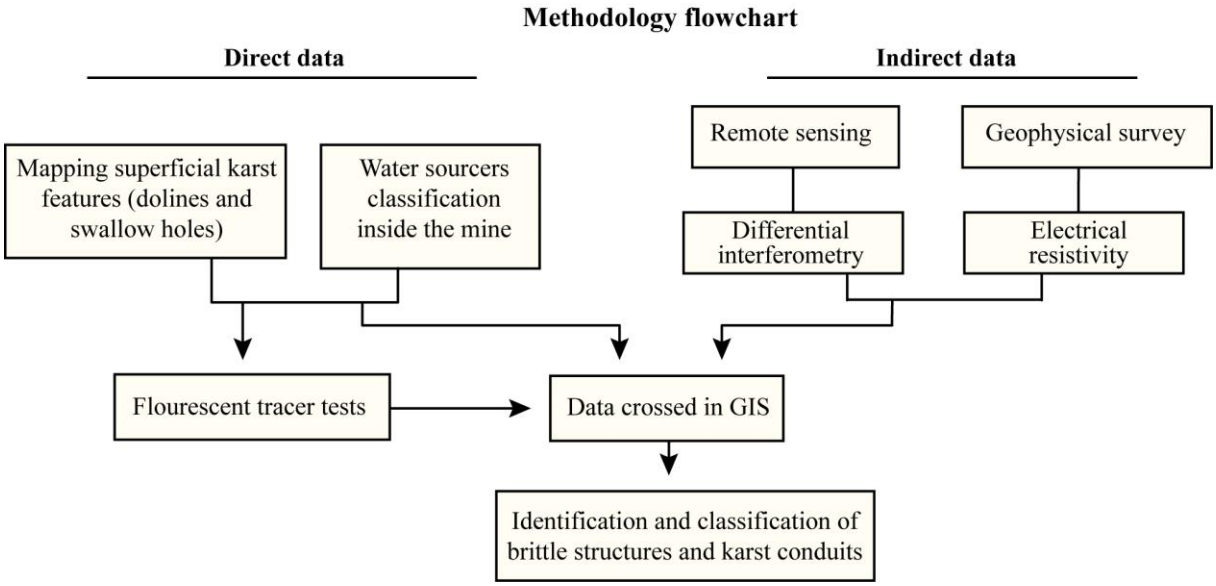

Figure 6 - Flowchart showing the data acquisition and interpretation sequence.

2.3.1. Minesprings typification

The hydrogeological assessment of discontinuities mapped inside the mine identified the faults and fractures (Figure 7a) that most influence groundwater leakage inside the mine. In

total, 283 brittle structures were evaluated based on their flow rates, enlargement by dissolution, and attitudes. The mining company provided all hydraulic and structural data.

Dry structures were discarded based on a preliminary evaluation of quantitative flow rate data. The water-bearing structures were classified into four types:

Type 1: poorly developed karstification, and flow rates under 0.1 m^3/h;
Type 2: varying levels of karstification, with flow rates between 0.1 m^3/h and 1 m^3/h;
Type 3: well-developed karstification, with flow rates between 1 m^3/h and 100 m^3/h;
Type 4: well-developed karstification, with flow rates over 100 m^3/h.

These water-bearing discontinuities have been correlated to regional fault zones and fracture systems, described in the region by several structural surveys carried out over the last few decades by the mining company.

2.3.2. Fluorescent dye tracer tests

The tests with fluorescent tracers aimed to recognize the possible groundwater flow-paths between the SCR losing stretch and the Vazante mine through discontinuities and karst conduits (Figure 7b,c). Tracers can improve conceptual models, especially in hydrogeologically complex aquifers (Cao et al., 2020; Divine & McDonnell, 2005; Silva et al., 2005). Through their concentration measurements, tracers can reveal hydraulic and geometric characteristics of the aquifer, such as preferential flow-paths and zones with disparate hydraulic conductivities (Leibundgut et al., 2009).

Fluorescein (uranine), rhodamine-B and PTSA (1,3,6,8-pyrenetetrasulfonic acid) were injected into the SCR in two distinct periods and river segments for better discretization. The first injection was made at the beginning of the losing stretch (Figure 7d) in January 2020, while the second was downstream, in February 2020. Among the fluorescent substances used as hydrogeological tracers, the three tracers used in this survey have high fluorescence intensity, favoring their detection even at concentrations of µg/l (ppb). The water background fluorescence from the SCR and the mine was measured before injecting the tracer. These measurements attest to whether the apparent fluorescence generated by colloidal particles of organic matter and clay minerals in the water will not overwhelm the fluorescence induced by the tracers (Ferreira et al., 2021; Suhogusoff et al., 2005).

The mass estimate of each injected dye tracer was based on a study carried out in the SCR in 2013 with the same fluorescent tracers (GeoHydros & DHI 2013). In this study, the amount

of tracer was calculated based on Equation (1), defined by Worthington & Smart (2003) for sink-to-spring tests in karst aquifers:

$$M = 19 \,.\, (L \cdot Q \cdot C)\ 0{,}95 \quad (1)$$

Where M = mass of the tracer in kg; L = 2000 m (approximate distance between injection and sampling points); Q = 11,678 m^3/h (discharge flow rate based on mine discharge channel); and C = 50 µg/l (peak concentration at sampling points).

Equations (2) and (3) takes into account the dilution and dispersion of dye tracers injected into the river channel, not directly into sinkholes. GeoHydros & DHI (2013) developed these equations to estimate the amount of tracer needed to be injected into the river to produce desired concentration peaks at mine sampling points.

$$MRiv = CRiv \,.\, QRiv \,.\, (tInj + (D / VRiv)) \quad (2)$$

$$C = CRiv / (Q / QLoss) \quad (3)$$

Where MRiv = mass of the tracer injected in the river in kg; CRiv = 250 µg/l (maximum dye tracer concentration in the river); QRiv = river flow rate during the injection in m^3/h; tInj = 60 s (injection time); D = longitudinal dispersivity (between 500 m and 1,500 m); VRiv = 0.89 m/s (river flow velocity); QLoss = 7,200 m^3/h (river flow loss to the aquifer).

During the first and second dye injections, the river flow rate was at 5,200 m^3/h and 20,000 m^3/h, respectively. Based on these values, the first injection required 10 kg of PTSA, 5 kg of fluorescein, and 10 kg of rhodamine-b. The second demanded 15 kg of fluorescein and 10 kg of rhodamine-b. The upstream automated flow rate monitoring stations provided the flow rate variations hourly during the injections.

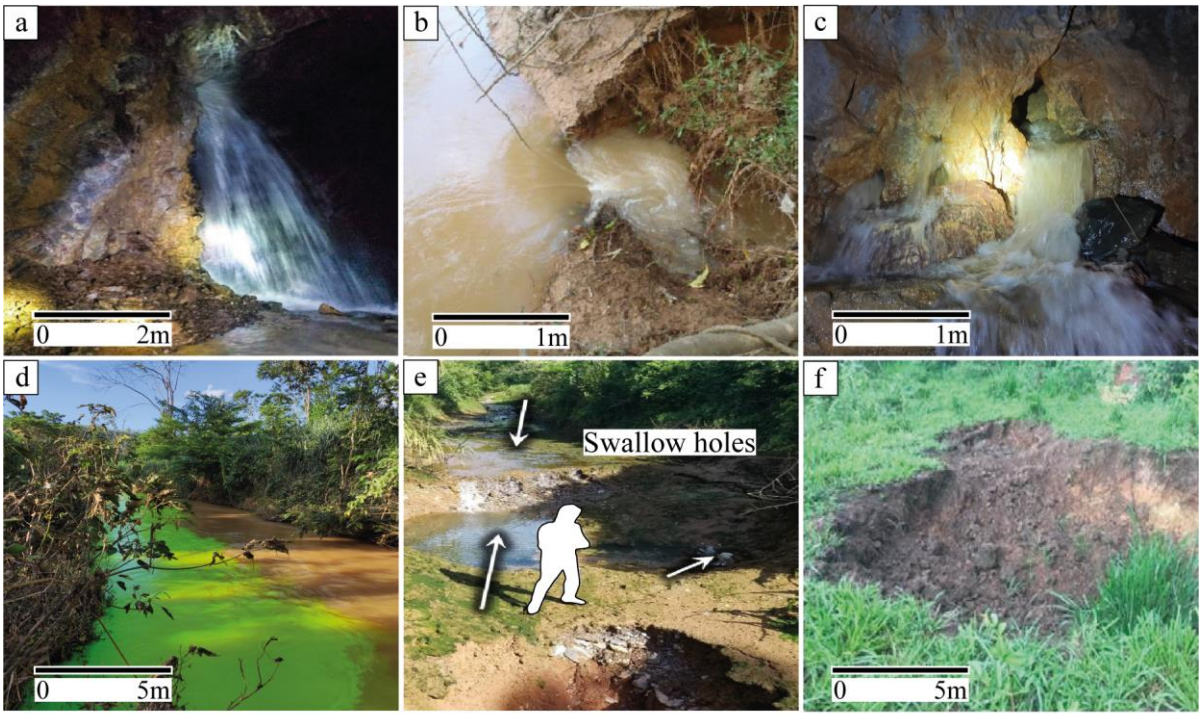

Figure 7 - Photographs of the study area showing: a) Water-bearing fracture inside the mine with an approximate flow rate of 500 m³/h; b) A sinkhole capturing a significant volume of water from the Santa Catarina River; c) Karst conduit developed in a fracture zone; d) Fluorescein (uranine) fluorescent tracer injected into the Santa Catarina River; e) Santa Catarina River drying stretch in a region with sinkholes; f) Recently formed decametric doline near the mine.

The interpretations were based on detection curves of tracer concentration versus time (Figure 8). Three components of each positive detection curve described the hydraulic system along the flow-paths between the SCR and the underground mine. These components are first detection interval; peak intensity; and response duration. Tracer arrival interval marks the travel time between the injection point and the sampling stations in the mine, indicating possible preferential flow-paths. The response magnitude and duration indicate how much the river water has been mixed with the aquifer water.

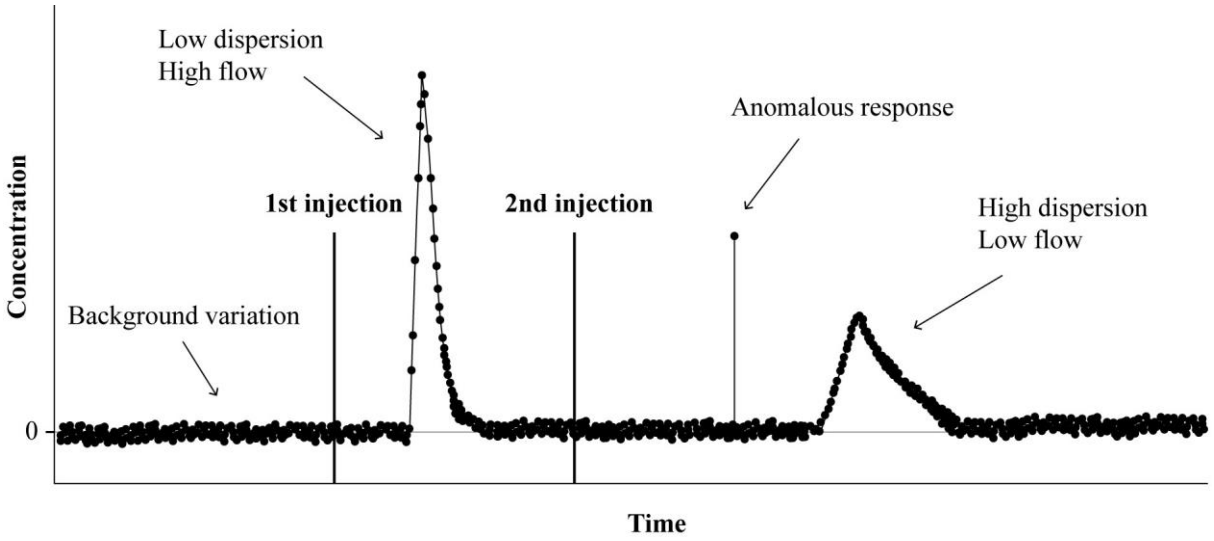

Figure 8 - Schematic fluorescence detection curve representing expected patterns for tracer transport in fast advective flow with low dispersion conditions; and slow advective flow with high dispersion conditions.

Field investigation guided the selections of the injection points. Dolines and sinkholes were mapped along the entire SCR losing stretch (Figure 7e,f), as well as their morphological dynamics (reactivation, recent collapse, and river capture points) at different precipitation rates over approximately one month of observations. Seventeen sampling points were selected in galleries between 50 m and 400 m depth (Figure 9), based on the most hydraulically relevant faults, fractures, karst conduits, and water convergence and storage sites (Table 1).

Table 1 - Description of tracer sampling points inside the mine.

Sampling point	**Mine gallery level (m)[1]**	**Description**
M1	455	Water surge in a mining shaft
M2	326	Artificial surge in shutters
M3	326 - 345	Karst conduit in the gallery wall
M4	345	Piped water from the gallery level 345
M5	370	Gallery ceiling karstified fracture
M6	345	Surge in a karstified contact zone between phyllite and dolomite
M7	345	Karst conduit in the gallery ceiling
M8	420	Surge in a borehole that intercepted a water-bearing karstified fracture
M9	370	Artificial emergence in shutter located in karst conduit
M10	345	Karst conduit in the gallery ceiling
M11	345 - 388	Water bearing fracture

M12	326	Water bearing fracture
M13	326	Surge in a borehole that intercepted a water-bearing fracture
M14	326	Water bearing fracture
M15	140	Surge in a borehole that intercepted a water-bearing fracture
M16	388	Water tank that stores water from the gallery level 484

[1]Above mean sea level.

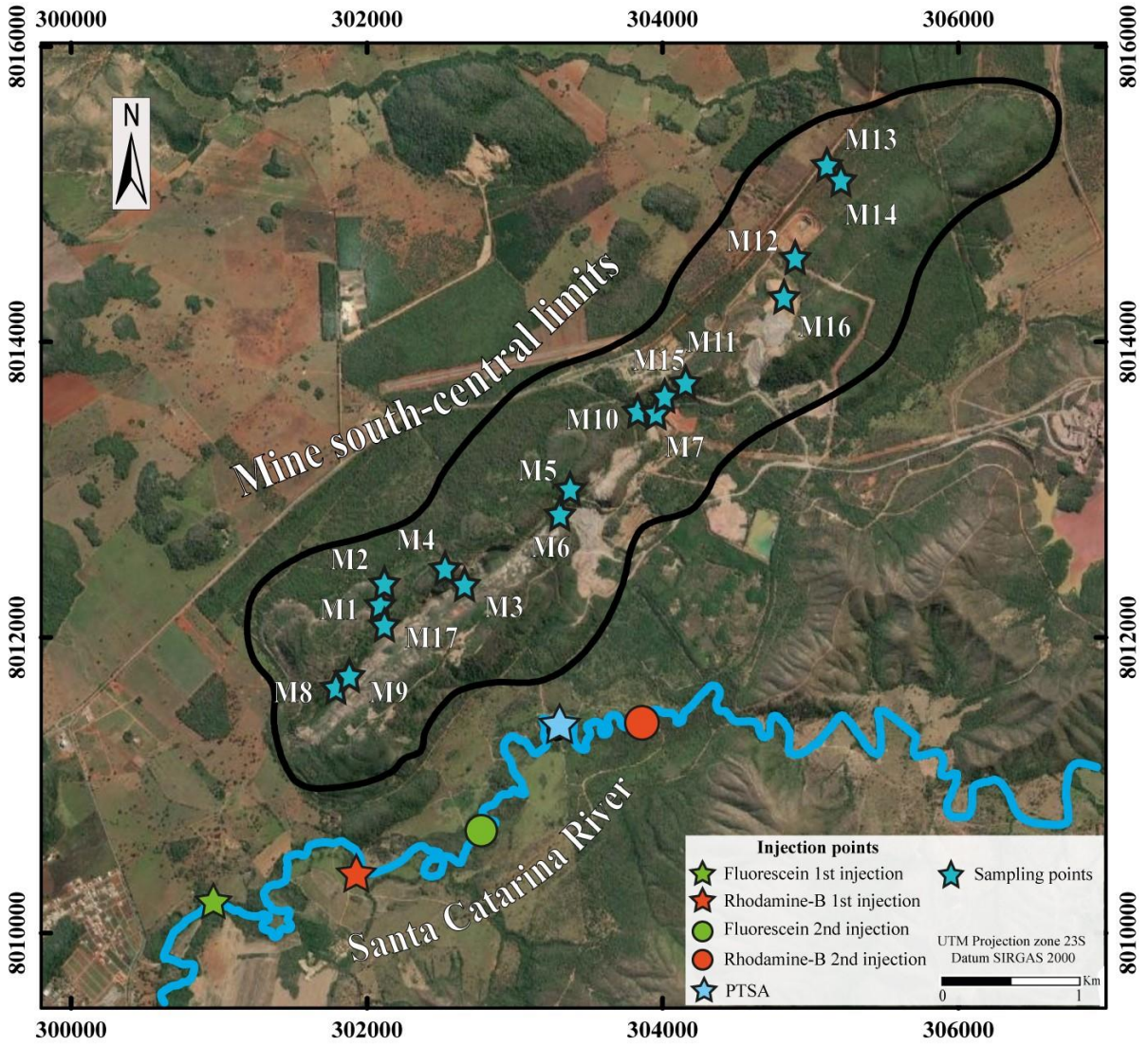

Figure 9 - Tracer injection points in the river and sampling points inside the mine. The river flows to the east.

Turner C3 submersible optical fluorometers, configured to take readings at 3-minute intervals, provided the fluorescence analyses within the optical spectra of each tracer. Fluorescein, rhodamine-B, and PTSA have distinct excitation/emission wavelength ranges, allowing each to be identified independently by the fluorometer without mutual interference.

At the tracer measurement sites, activated charcoal (fluorescein and rhodamine-B adsorbent) and white cotton (PTSA adsorbent) samplers provided a qualitative tracer detection backup in case of an eventual malfunction of any optical fluorometer.

2.3.3. Remote sensing and geophysical survey

Indirect data supported hydrogeological interpretations about the location and continuity of the brittle structures that exert control over the hydrogeological flow in the region between the SCR losing stretch and the underground mine. The analyses were based on differential interferometry (DInSAR) and electrical resistivity methods.

Differential interferometry obtained by Synthetic Aperture Radar (DInSAR) is a remote sensing technique that allows mapping small magnitude altimetric changes that occur slowly on the land surface, often imperceptible to the human eye (Gallowey & Hoffmann 2007). The application of this technique aimed to investigate morphological rearrangements in a highly dynamic karst environment that may be conditioning the SCR flow loss phenomena. The initial data acquisition was carried out in June 2019 to obtain the reference image (t0) to acquire surface information at an initial moment for later comparison on subsequent dates. Eight imaging were performed until September 2020, accounting for 16 months of observations. For data acquisition, a remotely piloted aircraft, also known as a drone, carried three radar antennas operating with C-, L- and P-band. This process essentially used data from the P- and L- bands as they provided information from below the treetops.

The electrical resistivity survey allowed the assessment of conductive zones in the carbonate rocks. They may be associated with groundwater circulation controlled and confined by discontinuities (faults and fractures) and areas with well-developed karstification. Sixteen lines for geoelectric acquisition data were performed (Figure 10), which recorded vertical values up to 140 meters depth from the ground surface. The surveys were acquired using a dipole-dipole array with an electrode spacing of 10 m. The equipment used was a Syscal Pro model that operates with a multi-electrode acquisition system in which 72 electrodes switch automatically allowing the spacing between them to be gradually increased in multiples of the initial spacing to reach depths with a reliable signal.

The lines have high sampling density, resulting in high-resolution geoelectric imaging (electrical resistivity tomography), with minimum length of 450 m (Line 11) and maximum of 2000 m (Line 4). The AGI EarthImager 2D software was used to model the resistivity pseudosections, in the process known as 2D inversion. It is an iterative process that, starting

from an initial model (measured resistivity mean value), searches for a 2D modeled resistivity section capable of reproducing an observed pseudosection within an acceptable error.

Based on these 16 2D modeled resistivity sections generated by EarthImager 2D, interpolations were performed on GIS platform by Ordinary Kriging to create laterally continuous resistivity data maps. The interpolations comprised 24 levels, between 5 m and 140 m depth.

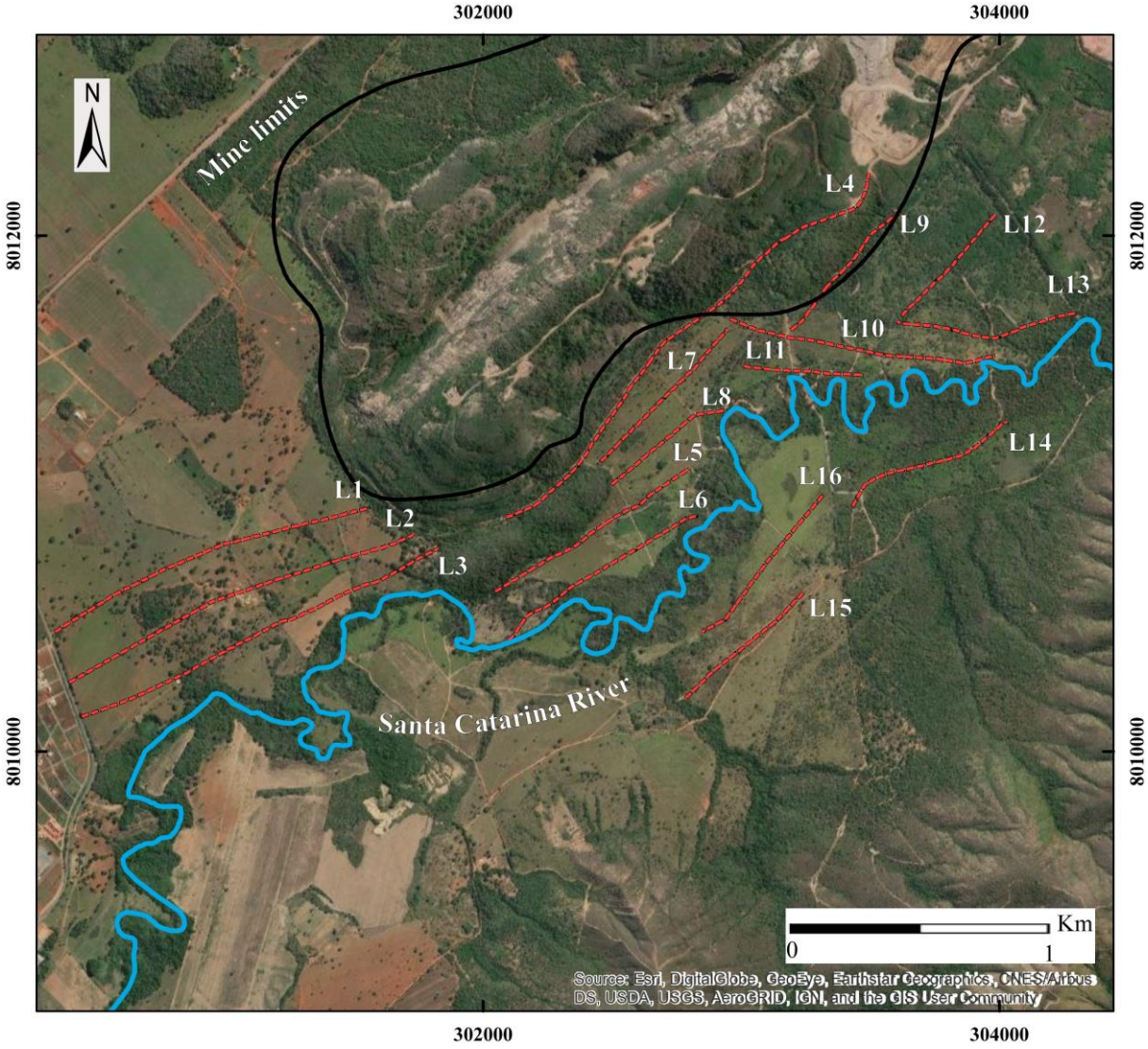

Figure 10 - Layout of the 16 electrical resistivity survey lines. The river flows to the east.

The differential interferometry outcomes deal with surface terrain displacement data, while the results obtained by electrical resistivity are related to underground geological features beyond the working interface of DInSAR. However, in most cases, soil movement phenomena in karstic terrains can be associated with subsurface geodynamics. The overlay of these two surveys allowed a three-dimensional visualization of relevant hydrogeological flow zones

related to structures capable of controlling the groundwater flow and karstification in the study area.

2.4. Results and Discussion

2.4.1. Spring types and structural trends

From 161 water-bearing structures mapped inside the mine, 85% were classified as Type 1 and Type 2, with low flow rates and karstification degrees. The most important hydrogeological structures, Type 3 and Type 4, represent 15% of the water-bearing structures and are responsible for more than 70% of the mine's total pumping rate.

Rose diagrams (Figure 11) give the preferred directions (strike and dip) of the most water-productive structures mapped inside the mine. Type 4 and Type 3 structures have, for the most part, sub-vertical dips, with an average of 84º and NW strike. Subordinately, some Type 4 structures have a NE strike with dips of smaller angles (57º on average) both for NW and SE. Approximately 70% of Type 1 and Type 2 structures are NW strikes oriented with high dip angles between 68° and 90°.

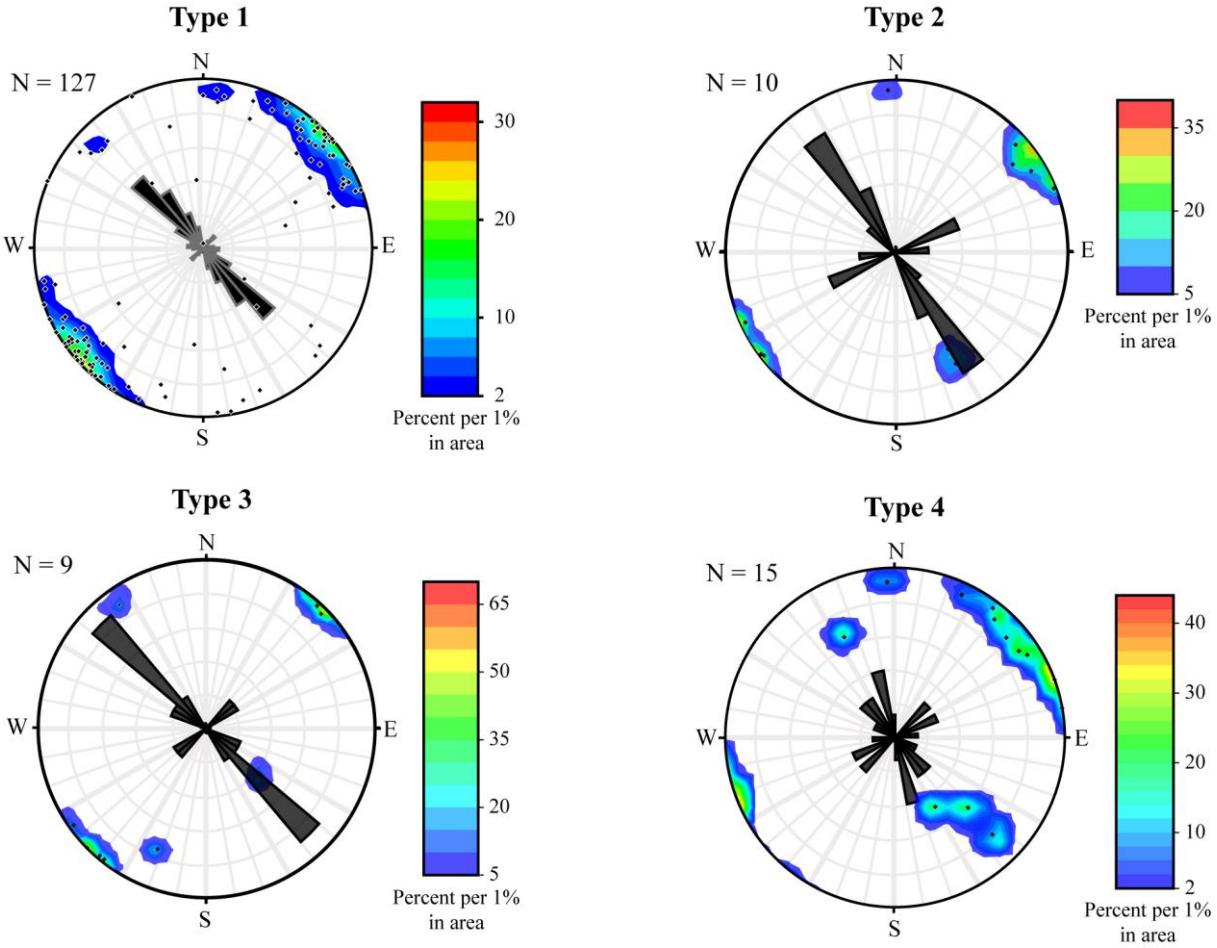

Figure 11 - Rose diagrams showing the water-bearing structures' attitude classified according to their flow rate range.

The structural trend found in hydraulically productive faults and fractures inside the mine corroborates the model proposed by Rostirolla et al. (2002). According to them, the aquifer system in the study region has undergone intense structural split up (Figure 12), essentially caused by brittle deformations. The last phase of regional tectonic deformation generated a grid of subvertical faults and exposed fracture systems with NW strike. They act as potential fluid percolation planes, controlled by the regional hydraulic gradient, and govern the hydrogeological flow and the advance of karstification in the aquifer system. The NW structural trend is more regional, controlling the epikarst groundwater circulation. It also promotes downward vertical water percolation, connecting the deep aquifer zone through dissolved fractures and faults.

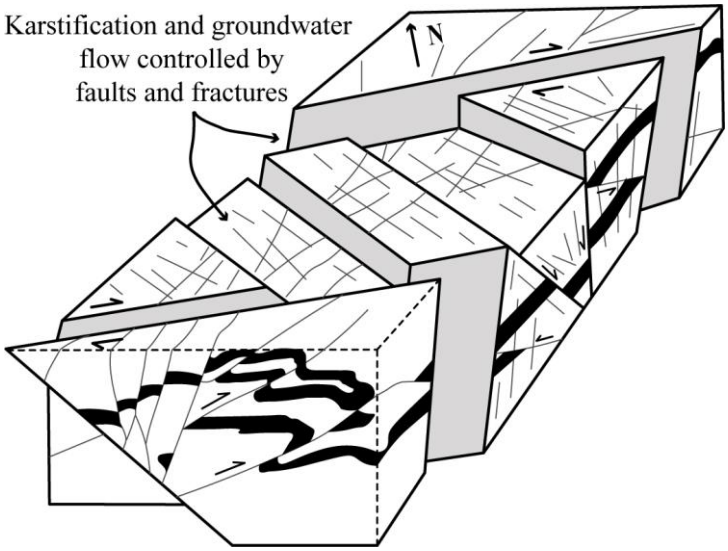

Figure 12 - Schematic block diagram showing the dolomitic aquifer tectonic compartmentation (modified from Rostirolla et al., 2002).

Although Type 4 structures are hydraulically important due to their groundwater transmission capacity, they did not show significant flow variations over 18 consecutive months of measurement (Figure 13), showing a tendency to equilibrium with a poorly responsive behavior to the rainy and dry seasons. On the other hand, structures that remain dry for most of the year begin to transmit water in the rainy season and Type 1 and Type 2 structures start to present a greater volume of water. This groundwater circulation dynamics may be associated with the saturation of Type 3 and 4 structures, forcing the excess volume of water to percolate through alternative paths.

The Type 4 structures located in the south portion of the mine were spatialized and projected onto the surface with their strike direction for correlations with the regional structures previously mapped by the mining company.

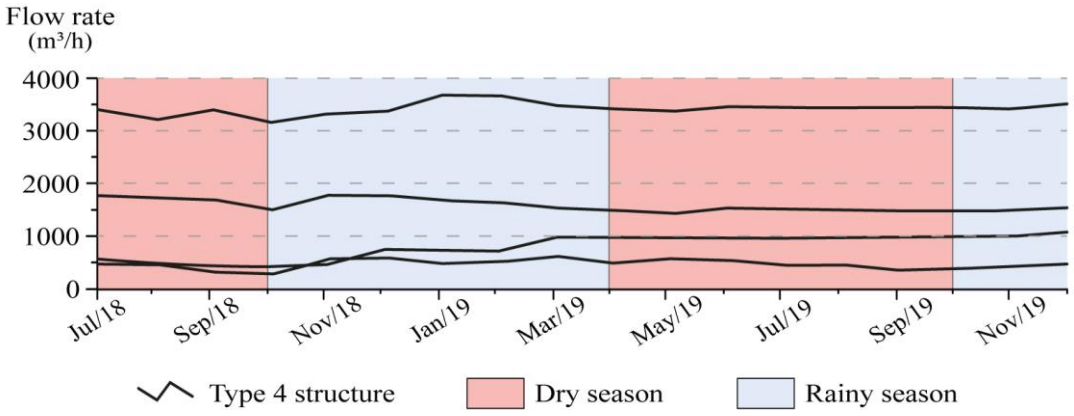

Figure 13 - Type 4 brittle structure located in the southern portion of the mine with flow rates measured between July 2018 and December 2019. The dry and rainy seasons are highlighted in red and blue, respectively.

2.4.2. Surface water-groundwater connections

Fluorescent dye tracers uranine and rhodamine-b revealed the existence of preferential flow-paths between the SCR and the Vazante underground mine. In the river stretch where the tracer injections occurred, the water infiltrated through the riverbed or sinkholes and flowed to eight different springs (M1, M3, M4, M5, M6, M8, M9, and M17) within the underground mine. No tracers were detected during the two injection stages at the measurement points located in the central part of the mine (northward to the positive detection points shown in Figure 14a). Only the water-bearing structures located in the southern portion of the mine received direct or indirect water from the SCR (Fig 14a). This may be associated with the geological contact between the dolomitic basin and the Serra do Garrote aquiclude, which prevents the groundwater flow towards the direct hydraulic gradient between the northeast river portion and the mine.

The PTSA tracers, whose injection was performed directly on a sinkhole in the SCR bed, were detected only at the sampling point M6. The hydraulic connection between these two points is possibly associated with continuous karst features capable of controlling the groundwater flow from the surface to depths greater than 300 m.

The first detection intervals varied between 2 h (point M6 after the first injection of rhodamine-b) and 16 h (point M3 after the first injection of fluorescein). Peak concentrations were reached between 11 h (point M5 after the first injection of fluorescein) and 50 h (point M7 after the first injection of rhodamine-b). Response durations ranged from 43 h (point M3) to 209 h (point M9) after the second fluorescein injection.

These results point to a system where the discrete river infiltration points are not necessarily directly connected to the flow-paths by fractures and conduits that transport water to the mine. Water infiltrated by sinkholes may percolate through the upper portion of the granular aquifer and/or through the epikarst before draining into the deeper fractured aquifer during a longer residence period compared to direct hydraulic connections through discontinuities. Another factor associated with the residence period is the dispersion phenomenon that tracers can undergo during transport through a network of fractures and conduits with varied openings.

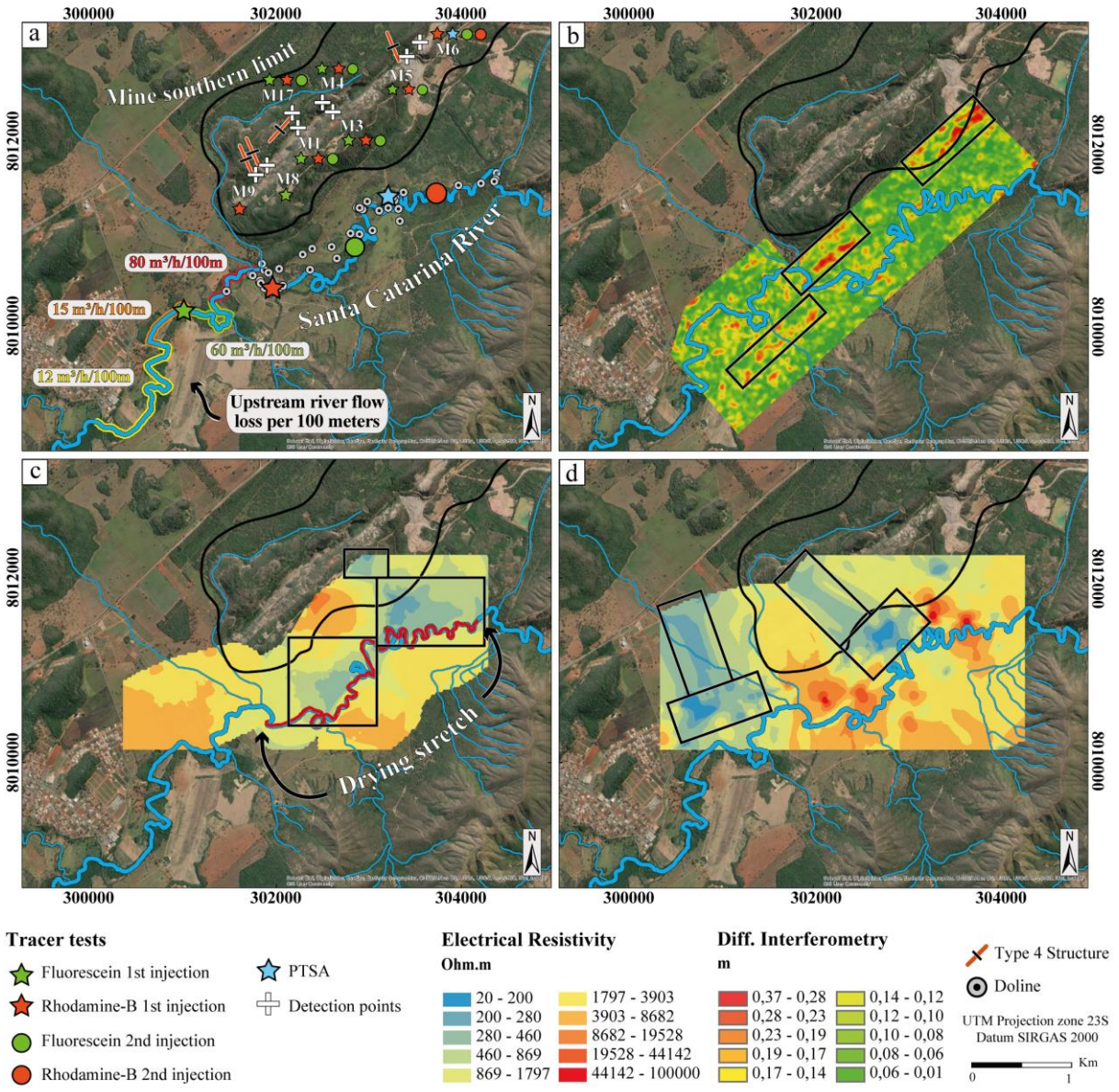

Figure 14 - Map of the region between the Santa Catarina River drying stretch and the southern portion of the Vazante underground mine showing: a) The Type 4 structures mapped within the mine represented with their respective strike directions; and the locations of the fluorescent tracers injection and detection points; b) Accumulated surface displacement obtained by DinSAR between June 2019 (t0) and September 2020 (t8) near the Santa Catarina River drying stretch. Rectangles outline the zones of greatest displacement. c) and d) Electrical resistivity maps for 10 m and 90 m depth, respectively. Rectangles outline the most electrically conductive regions.

2.4.3. Terrain displacements and preferential groundwater flow-paths

The differential interferometry and electrical resistivity data were interpreted together with structural and geomorphological mapping data based on the reactivation and emergence of new sinkholes in the SCR drying stretch. It is worth mentioning that the analyses of these

techniques integrated with field investigations create a more robust scenario for the definition of preferential groundwater flow-paths between the river and the underground mine through discontinuity zones and karst features.

The surface monitored by DinSAR has a very dynamic behavior (Figure 14b). Movements tend to occur throughout the monitored terrain, and it is impossible to identify specific areas where no displacement has occurred. This behavior was observed in all 16 months of imagery. Despite the intense surface dynamics observed in the entire monitored surface, it was possible to identify areas with persistent surface displacements that form continuous alignment patterns in time, which become more pronounced when observed in a long time series.

Based on the interpolation of the resistivity results obtained in the 2D pseudosections, as exemplified in Figure15, iso-depth electrical resistivity maps outlined the occurrence of low resistivity zones. The bluish tones in Figure 14c,d correspond to lower electrical resistivity values and are possibly related to regions with greater water saturation and percolation, which may be associated with fracture zones and hydraulically conductive structures.

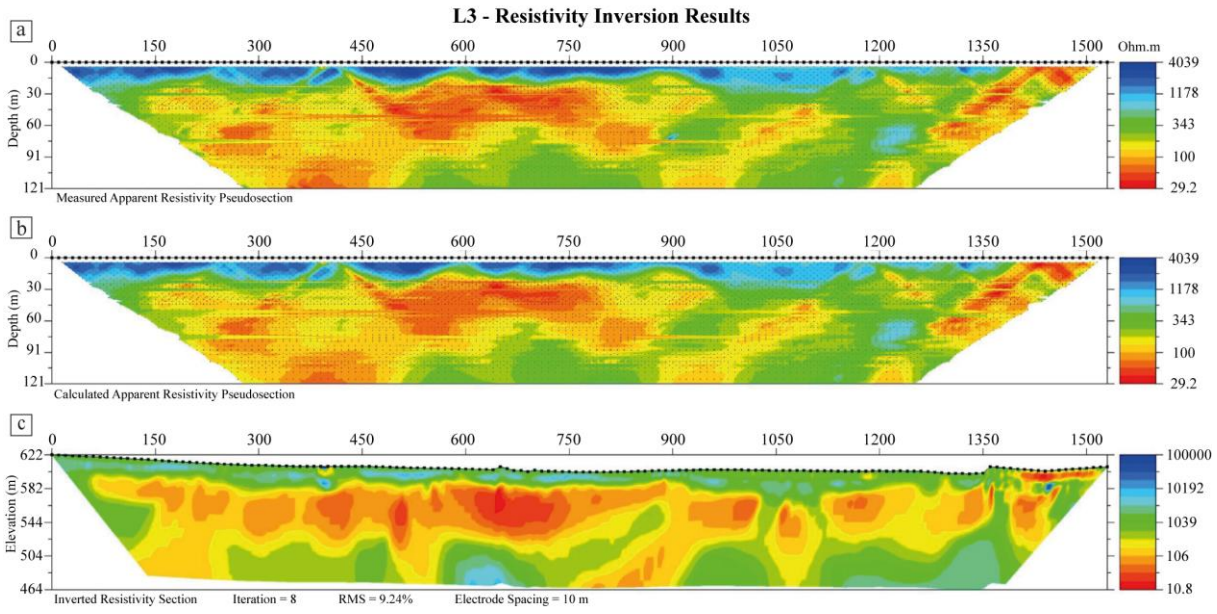

Figure 15 - Example of 2D resistivity inversion result for line L3 showing: a) Measured apparent pseudosection; b) Calculated apparent pseudosection; and c) 2D modeled resistivity section obtained by inversion. Note that the 2D modeled section (c) is extrapolated beyond the sampling limits. Therefore, the overestimation of features close to the section boundaries was avoided.

Electrical resistivity data corresponding to the aquifer upper portion (Colluvium/Alluvium Aquifer) correlates better with the differential interferometry imagery. The accumulated surface movement recorded by DInSAR highlights three zones of persistent displacements (Figure 14b) aligned with the NE-SW direction of higher electrical conductivity for shallow depths (10 m), shown in Figure 14c. The SCR bed and the sinkholes mapped close to the river also show the same alignment trend. These displacement zones parallel to the river are probably related to stress release fractures, as described by Sasowsky and White (1994), which may be controlling and guiding the emergence of new sinkholes.

The lower electrical resistivity zones at greater depths (90 m), corresponding to the Upper and Lower Footwall Aquifers, show two regions of water saturation following a pattern of NW-SE alignment different from that observed in the aquifer's upper portion (Figure 14d). These interpretations suggest that the terrain surface movements, which are associated with the emergence of dolines and sinkholes in the riverbed, are being controlled by hydrogeologically conductive structures located in the shallow portion of the aquifer. The low resistivity zones that connect the SCR to the underground mine indicate the presence of preferential flow-paths at depths greater than 90 m. They may be associated with developing of deep fracture zones capable of capturing the groundwater flow toward the underground mine.

2.4.4. Data crossing for brittle Structure classification and location of karst conduits

The results obtained in each direct and indirect survey were crossed with the mapping data of the main brittle structures in the region. These structures were classified into high or medium potential to control groundwater flow according to their location, attitude and correlation with karst features (Figure 16a).

Dolines and sinkholes alignment patterns mapped in the vicinity of the SCR indicated the location of possible regional structures that could lead to the emergence and development of geomorphological features characteristic of karst terrains. In addition, flow loss measurements upstream of the SCR drying stretch (Figure 14a) and the segments with remarkable structural control of the riverbed were also associated with regional brittle structures.

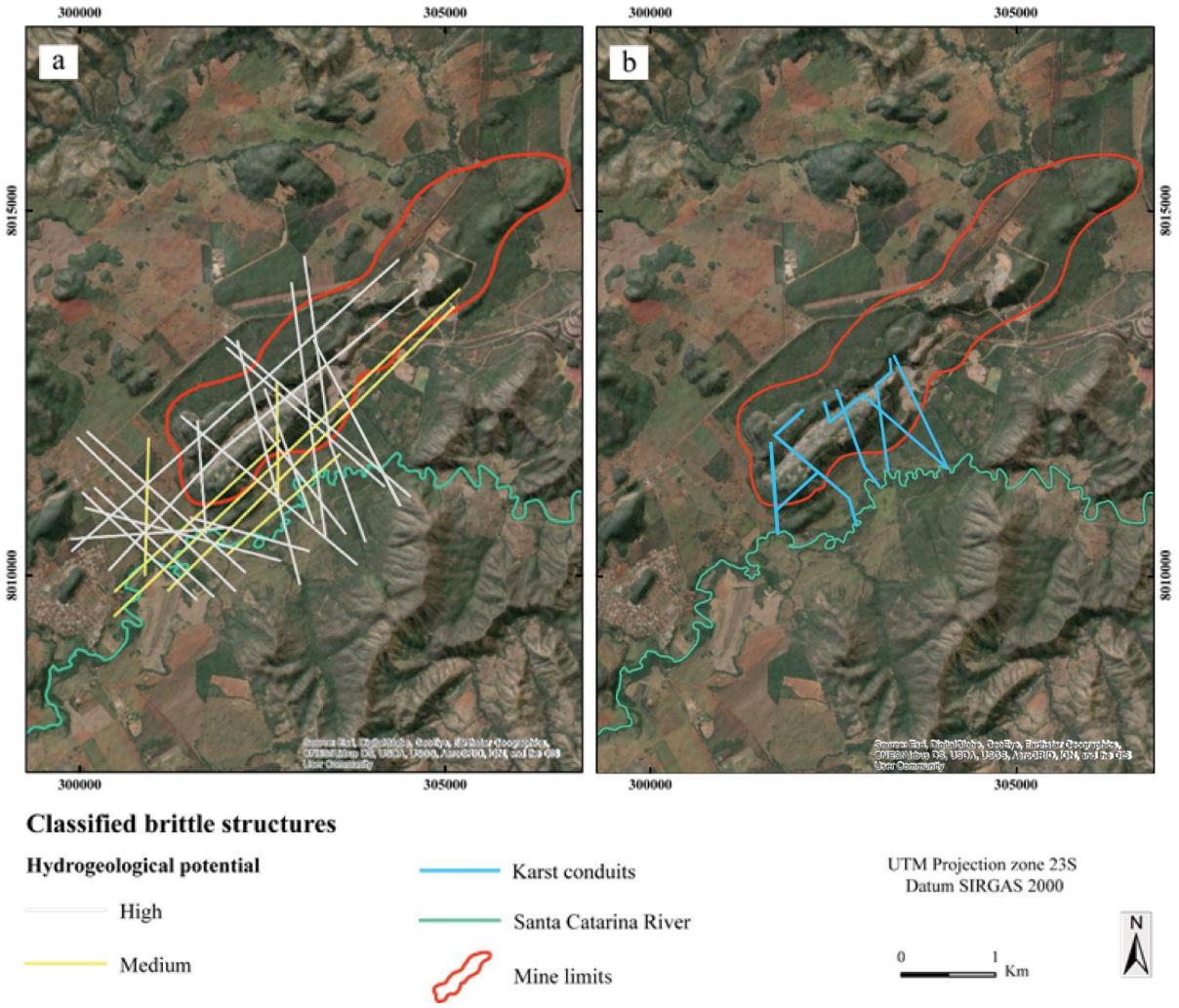

Figure 16 - Maps showing: a) The classified brittle structures of high and medium hydrogeological potential; and b) Possible direct flow-paths through karst conduits between the SCR and the Vazante underground mine.

The mapped sub-vertical fractures with NW-SE and E-W directions were classified as having high hydrogeological potential. Rostirolla et al. (2002) described these structures as open joints and fractures capable of exerting substantial control over the hydrogeological flow in the karst aquifer. On the other hand, the NE and NS sub-vertical structures, defined as having lower potential for fluid percolation, were classified either as high or as medium hydrogeological potential due to the integration of structural data with the other surveys. Differential interferometry (surface analysis) and electrical resistivity data up to 140 m depth defined the vertical continuity of the brittle structures. When these structures overlapped with the Type 3 or Type 4 fractures mapped inside the mine, the vertical continuity was then defined by the depth at which these fractures were located.

The proposed location of the karst conduits was inferred through the inflow features in the mine in which the tracer tests showed a connection with the SCR. The ends of the conduits

located in the SCR were based on observations of sinkholes along the riverbed and the tracer injection points. The subsurface continuities of the conduits, delimited between the sinks in the river and the resurgence in the mine, were inferred through the plans that define the brittle structures (Figure 16b) that hydraulically connect the region and exert control over the development of karst features.

The location and classification of these structures will serve as a basis for intervention work on the SCR drying up problem. Based on the local recognition of the sinkholes, it will be possible to waterproof specific stretches of the riverbed that were under the greatest influence of water capture by leakage through brittle structures and karst conduits. Local clogging of sinkholes in the riverbed could also be carried out, reducing the river flow loss and the underground mine dewatering. The spatialized structures could be also used in the elaboration of more detailed mathematical flow models that better represent the hydrogeological dynamics of the region.

2.5. Conclusions

The integration of a multi-technical approach based on field investigations, structural framework, remote sensing, geophysics and dye tracer tests allowed the following conclusions: (1) The NW structural trend hosts the most productive water-bearing brittle structures located between the SCR and the Vazante underground mine; (2) The surface displacements associated with the emergence of dolines and sinkholes in the riverbed are being controlled by hydrogeologically conductive structures located in the shallow portion of the aquifer; (3) The low resistivity zones that connect the SCR to the underground mine indicate the presence of preferential flow-paths at depths greater than 90 m. They may be associated with developing of deep fracture zones capable of capturing the groundwater flow toward the underground mine; (4) Fluorescent dye tracers indicated the existence of direct and indirect hydraulic connections between the SCR and the Vazante underground mine through fault and fracture networks.

Moreover, the hydrogeological classification of brittle structures and the proposed location of karst conduits will guide the work to mitigate the problem of drying up on the SCR. The results obtained in this study contributes to the development of hydrogeological conceptual models that can lead to more robust investigations for drying river problems related to underground mine dewatering in a complex geological framework.

2.6. References

Almeida F.F.M. (1977). O Cráton do São Francisco. Revista Brasileira de Geociências, 7:349-364.

Anderson, M. P., Woessner, W. W. & Hunt, R. J. (2015). Applied groundwater modeling: simulation of flow and advective transport. Academic press.

Azmy, K., Kaufman, A.J., Misi, A. & Oliveira, T.F. (2006). Isotope stratigraphy of the Lapa Formation, São Francisco Basin, Brazil: implications for Late Neoproterozoic glacial events in South America. Precam. Research, 149, 231–248.

Banks, E. W., Simmons, C. T., Love, A. J., Cranswick, R., Werner, A. D., Bestland, E. A. & Wilson, T. (2009). Fractured bedrock and saprolite hydrogeologic controls on groundwater/surface-water interaction: a conceptual model (Australia). Hydrogeology Journal, 17(8), 1969–1989. doi:10.1007/s10040-009-0490-7v.

Bittencourt, C., Auler, A. S., Reis Neto, J. M., Bessa, V. & Silva, M. V. A. (2009). The influence of hypogene and epigene speleogenesis in the evolution of the Vazante Karst, Minas Gerais state, Brazil. In Hypogene speleogenesis and karst hydrogeology of Artesian Basins, Simferopol. Conference, Chernivtsi, Ukraine.

Bittencourt, C., Bessa, V. & Araújo, E. E. (2008). The Vazante Underground Mine, Brazil — An Example of Controlled Water Table Drawdown in Karstic Areas. Sinkholes and the Engineering and Environmental Impacts of Karst. doi:10.1061/41003(327)71.

Bittencourt, C. & Reis Neto, J. (2012). O sistema cárstico de Vazante - carste em profundidade em metadolomitos do Grupo Vazante - MG. Revista Brasileira de Geociências, 42. 01-10. 10.25249/0375-7536.20124210110.

Bonacci, O. (2015). Surface Waters and Groundwater in Karst. In Karst Aquifers Characterization and Engineering. Professional Practice in Earth Sciences. doi:10.1007/978-3-319-12850-4.

Bonsor, H. C., MacDonald, A. M., Ahmed, K. M., Burgess, W. G., Basharat, M., Calow, R. C. & Zahid, A. (2017). Hydrogeological typologies of the Indo-Gangetic basin alluvial aquifer, South Asia. Hydrogeology Journal, 25(5), 1377–1406. doi:10.1007/s10040-017-1550-z.

Cao, V., Schaffer, M., Taherdangkoo, R. & Licha, T. (2020). Solute Reactive Tracers for Hydrogeological Applications: A Short Review and Future Prospects. Water, v.12, n. 3, p. 653.

Carvalho M.O., Valeriano C.M., Aparicio-González P.A., Oliveira G.D. & Impiccini A. (2016). The thrust contact between the Canastra and Vazante groups in the Southern Brasília Belt: structural evolution, white mica crystallinity and implications for the Brasiliano orogeny. Brazilian Journal of Geology, 46(4):567-583.

Carvalho, M.O., Valeriano, C.M., Aguiar Neto, C.C., Oliveira, G.D. & Heilbron, M. (2019). The Vazante and Canastra groups revisited: Sm-Nd and Sr isotopes - evidence for contribution from Tonian intraplate magmatism during passive margin development along the SW São Francisco margin, Brazil. Brazilian Journal of Geology, 49(1). doi:10.1590/2317-4889201920180081.

Changming, L., Jingjie, Y. & Kendy, E. (2001). Groundwater Exploitation and Its Impact on the Environment in the North China Plain. Water International, 26(2), 265–272. doi:10.1080/02508060108686913.

Cook, P. G. (2003). A guide to regional groundwater flow in fractured rock aquifers. Henley Beach, S. Aust: Seaview Press.

Custodio, E. (2002). Aquifer overexploitation: what does it mean? Hydrogeology Journal, 10, 254–277. doi:10.1007/s10040-002-0188-6.

Custodio, E., Andreu-Rodes, J. M., Aragón, R., Estrela, T., Ferrer, J., García-Aróstegui, J. L. & del Villar, A. (2016). Groundwater intensive use and mining in south-eastern peninsular Spain: Hydrogeological, economic and social aspects. Science of The Total Environment, 559, 302–316. doi:10.1016/j.scitotenv.2016.02.107.

Dardenne, M.A. (2000). The Brasília fold belt. In: Cordani, U.G., Milani, E.J., Thomaz-Filho, A., Campos, D.A. (Eds.), Tectonic Evolution of South America. 31st International Geological Congress, Rio de Janeiro, Brazil, pp. 231– 263.

Divine, C.E. & McDonnell, J.J. (2005). The future of applied tracers in hydrogeology. Hydrogeology Journal, 13, p. 255-258.

Dias, P., Marinho, M., Sotero, M., Vilela, F., Marques, E. & Matos, C. (2015). Metalogenia das Províncias Minerais do Brasil: distrito zincífero de vazante, MG. Belo Horizonte: Companhia de Pesquisa de Recursos Minerais - CPRM, 2015. 59p. v.5. (Série Províncias Minerais do Brasil).

Enemark, T., Peeters, L. J. M., Mallants, D. & Batelaan, O. (2019). Hydrogeological conceptual model building and testing: A review. Journal of Hydrology, 569, 310–329. doi:10.1016/j.jhydrol.2018.12.007.

Esteller, M. V. & Diaz-Delgado, C. (2002). Environmental Effects of Aquifer Overexploitation: A Case Study in the Highlands of Mexico. Environmental Management, 29(2), 266–278. doi:10.1007/s00267-001-0024-0.

Ferreira, O. B., Suhogusoff, A. V. & Tavares, T. S. (2021). Determinação do fator de retardamento da uranina em sedimentos quaternários do aquífero São Paulo. Águas Subterrâneas, 35(1), 65–77. https://doi.org/10.14295/ras.v35i1.29951.

Fleckenstein J. H., Niswonger R. G. & Fogg E. G. (2006). River-Aquifer Interactions, Geologic Heterogeneity, and Low-Flow Management. Groundwater, 44(6), 837–852. doi:10.1111/j.1745-6584.2006.00190.x.

Fuck R. A., Pimentel M. M. & Silva L. J. (1994). Compartimentação Tectônica na porção oriental da Província Tocantins In Congresso Brasileiro de Geologia, 38, Camboriú, Brazil, p.215-216.

Galloway, D.L. & Hoffmann, J. (2007). The application of satellite differential SAR interferometry-derived ground displacements in hydrogeology. Hydrogeology Journal, 15, 133–154. https://doi.org/10.1007/s10040-006-0121-5.

GeoHydros & DHI. (2013). Estudo da caracterização da dinâmica de fluxos subterrâneos a partir da injeção de técnicas baseadas na utilização de traçadores corantes. Technical Report. p.389.

Hamad, A., Hadji, R., Bâali, F., Houda, B., Redhaounia, B., Zighmi, K. & Hamed, Y. (2018). Conceptual model for karstic aquifers by combined analysis of GIS, chemical, thermal, and isotopic tools in Tuniso-Algerian transboundary basin. Arabian Journal of Geosciences, 11(15). doi:10.1007/s12517-018-3773-2.

Hitzman, M. W.; Reynolds, N. A.; Sangster, D. F.; Allen, C. R. & Carman, C. E. (2003). Classification, Genesis, and Exploration Guides for Nonsulfide Zinc Deposits. Economic Geology, 98(4), 685–714. doi:10.2113/gsecongeo.98.4.685.

IBGE - Instituto Brasileiro de Geografia e Estatística. (2010). Available in: <www.cidades.ibge.gov.br/brasil/mg/vazante/panorama>. Accessed in: March 7th, 2022.

Jamali, M. Y., Mustapha, N. & Amir, S. (2020). The Impact of Over-exploitation of Groundwater along the Irrigated Perimeter of Tadla, Oum Errabia Basin, Morocco. Desalination and water treatment, 195, 201-212. doi:10.5004/dwt.2020.25877.

Kalhor, K., Ghasemizadeh, R., Rajic, L. & Alshawabkeh, A. (2019). Assessment of groundwater quality and remediation in karst aquifers: A review. Groundwater for Sustainable Development, 8,104-121.https://doi.org/10.1016/j.gsd.2018.10.004.

Karlovic, I., Markovic, T., Vujnovic, T. & Larva, O. (2021). Development of a Hydrogeological Conceptual Model of the Varaždin Alluvial Aquifer. Hydrology, 8(1), 19. doi:10.3390/hydrology8010019.

Kresic, N. & Mikszewski, A. (2012). Hydrogeological conceptual site models: data analysis and visualization. CRC press.

Leibundgut, C., Maloszewski, P. & Kulls, C. (2009). Tracers in Hydrology. John Wiley e Sons, Ltda.

Lekula, M., Lubczynski, M. W. & Shemang, E. M. (2018). Hydrogeological conceptual model of large and complex sedimentary aquifer systems – Central Kalahari Basin (Botswana). Physics and Chemistry of the Earth, Parts A/B/C, 106, 47-62. doi:10.1016/j.pce.2018.05.006.

Machado, M. & Silva, S. (2010). Geodiversidade do estado de Minas Gerais. CPRM. 131 p.

Masciopinto, C. & Palmiotta, D. (2012). Flow and Transport in Fractured Aquifers: New Conceptual Models Based on Field Measurements. Transport in Porous Media, 96(1), 117–133. doi:10.1007/s11242-012-0077-y.

Mengistu, H., Demlie, M. B., Abiye, T. A., Xu, Y. & Kanyerere, T. (2019). Conceptual hydrogeological and numerical groundwater flow modeling around the moab khutsong deep gold mine, South Africa. Groundwater for Sustainable Development, 9, 100266. doi:10.1016/j.gsd.2019.100266.

Mengistu, H., Tessema, A., Abiye, T., Demlie, M. & Lin, H. (2014). Numerical modeling and environmental isotope methods in integrated mine-water management: a case study from the Witwatersrand basin, South Africa. Hydrogeology Journal, 23(3), 533–550. doi:10.1007/s10040-014-1216-z.

Molina, J. L., García Aróstegui, J. L., Benavente, J., Varela, C., de la Hera, A. & López Geta, J. A. (2009). Aquifers Overexploitation in SE Spain: A Proposal for the Integrated Analysis of Water Management. Water Resources Management, 23(13), 2737–2760. doi:10.1007/s11269-009-9406-5.

Monteiro, L.V., Bettencourt, J.S., Juliani, C. & Oliveira, T.F. (2006). Geology, petrography, and mineral chemistry of the Vazante non-sulfide and Ambrósia and Fagundes sulfide-rich carbonatehosted Zn-(Pb) deposits, Minas Gerais, Brazil. Ore Geology Reviews, 28, 201 – 234.

Monteiro, L.V., Bettencourt, J.S., Juliani, C. & Oliveira, T.F. (2007). Non-sulfide and sulfide-rich zinc mineralizations in the Vazante, Ambrosia and Fagundes deposits, Minas Gerais,

Brazil: mass balance and stable isotope characteristics of the hydro- thermal alterations. Gondwana Research, 11, 362–381.

Mukherjee, A., Bhanja, S. N., & Wada, Y. (2018). Groundwater depletion causing reduction of baseflow triggering Ganges River summer drying. Scientific Reports, 8(1). doi:10.1038/s41598-018-30246-7.

NASEM - National Academies of Sciences, Engineering, and Medicine. (2020). Characterization, Modeling, Monitoring, and Remediation of Fractured Rock. Washington, DC: The National Academies Press. https://doi.org/10.17226/21742.

Ninanya, H., Guiguer, N., Vargas, E. A., Nascimento, G., Araujo, E. & Cazarin, C. L. (2018). Analysis of water control in an underground mine under strong karst media influence (Vazante mine, Brazil). Hydrogeology Journal, 26, 2257–2282. doi:10.1007/s10040-018-1785-3.

Petitta, M., Mastrorillo, L., Preziosi, E., Banzato, F., Barberio, M. D., Billi, A. & Doglioni, C. (2018). Water-table and discharge changes associated with the 2016–2017 seismic sequence in central Italy: hydrogeological data and a conceptual model for fractured carbonate aquifers. Hydrogeology Journal, 26(4), 1009–1026. doi:10.1007/s10040-017-1717-7.

Pimentel, M.M., Dardenne, M.A., Fuck, R.A., Viana, M.G., Junges, S.L., Fischel, D.P., Seer, H.J. & Dantas, E.L. (2001). Nd isotopes and the provenance of detrital sediments of the Neoproterozoic Brasília Belt, central Brazil. Journal of South American Earth Sciences 14, 571– 585.

Pinho, J.M., Dardenne, M.A. & Rigobello, A.E. (1989). Evolução Tectônica da mineralização de zinco de Vazante. In: Simpósio de Geologia do Núcleo Minas Gerais, 110:275-276.

Rapantova, N., Grmela, A., Vojtek, D., Halir, J. & Michalek, B. (2007). Ground Water Flow Modeling Applications in Mining Hydrogeology. Mine Water and the Environment, 26(4), 264–270. doi:10.1007/s10230-007-0017-1.

Rigobello, A.E., Branquinho, J.A., Dantas, M.G.S., Oliveira, T.F. & Nieves Filho, W. (1988) Mina de zinco de Vazante, Minas Gerais. In: Principais depósitos minerais do Brasil, 1, 670.

Rodrigues Filho, S. & Viana, M. B. (2011). Gestão da água: o desafio do zinco em Vazante (MG). Recursos minerais & sustentabilidade territorial, Grandes minas, 1, 333-360.

Rostirolla, S. P., Mancini, F., Reis Neto, J. M., Figueira, E. G. & Araujo, E. C. (2002). Análise estrutural da mina de Vazante e adjacências: Geometria, cinemética, e implicacões para a hidrogeologia. Revista Brasileira de Geociências, 32, 59-68.

Rupérez-Moreno, C., Senent-Aparicio, J., Martinez-Vicente, D., García-Aróstegui, J. L., Calvo-Rubio, F. C. & Pérez-Sánchez, J. (2017). Sustainability of irrigated agriculture with overexploited aquifers: The case of Segura basin (SE, Spain). Agricultural Water Management, 182, 67–76. doi:10.1016/j.agwat.2016.12.008.

Saadé-Sbeih, M., Asaad, A. H., Shamali, O., Zwahlen, F. & Jaubert, R. (2018). Groundwater balance politics: Aquifer overexploitation in the Orontes River basin. Water Alternatives, 11(3), 663-683.

Sasowsky, D. & White, B. (1994). The role of stress release fracturing in the development of cavernous porosity in carbonate aquifers. Water Resources Research, 30(12), 3523–3530. doi:10.1029/94wr01727.

Silva, L.L., Donnici, C.L., Ayala, J.D., Freitas, C.H., Moreira, R.M. & Pinto, A.F. (2005). Traçadores: o uso de agentes químicos para estudos hidrológicos, ambientais, petroquímicos e biológicos. Química Nova, 32, 1576-1585.

Singhal, B. S. & Gupta, R. P. (2010). Applied hydrogeology of fractured rocks. Springer Science & Business Media.

Slezak, P., Olivo, G., Oliveira, G. & Dardenne, M. (2014). Geology, mineralogy, and geochemistry of the Vazante Northern Extension zinc silicate deposit, Minas Gerais, Brazil. Ore Geology Reviews, 56, 234-257.

Stavric, V. (2004). Aquifer overexploitation and groundwater mining. In Balwois Conference on Water Observation and Information System for Decision Support, Ohrid, Macedonia, 25-29.

Suhogusoff, A. V., Hirata, R. & Ferrari, L. M. (2005). Adsorção do traçador fluorescente uranina em sedimentos quaternários da Bacia de São Paulo. Revista Brasileira de Geociências, 35, 551-558. https://doi.org/10.25249/0375-536.200537551558.

Taheri, K., Taheri, M. & Parise, M. (2016). Impact of intensive groundwater exploitation on an unprotected covered karst aquifer: a case study in Kermanshah Province, western Iran. Environmental Earth Sciences, 75(17). doi:10.1007/s12665-016-5995-5.

Trabelsi, F., Tarhouni, J., Mammou, A. B. & Ranieri, G. (2011). GIS-based subsurface databases and 3-D geological modeling as a tool for the setup of hydrogeological framework: Nabeul–Hammamet coastal aquifer case study (Northeast Tunisia). Environmental Earth Sciences, 70(5), 2087–2105. doi:10.1007/s12665-011-1416-y.

Valeriano C.M., Dardenne M.A., Fonseca M.A., Simões L.S.A. & Seer H.J. (2004). A evolução tectônica da Faixa Brasília. In: Mantesso-Neto V. e Bartoreli A. (eds.). Geologia do

continente sul-americano: evolução da obra de Fernando Flávio Marques de Almeida. São Paulo, Beca, 575-593.

Vasconcelos, V. V., Martins Junior, P. P. & Hadad, R. M. (2012). Caracterização ambiental da bacia do Rio Paracatu. In Martins, P. P. Projeto SACD. Belo Horizonte Cetec.

White, W. B. (1999). Conceptual models for karstic aquifers. Karst modeling, 5, 11-16.

White, W.B. (2012). Conceptual Models for Carbonate Aquifers. Groundwater, 50: 180-186. doi: 10.1111/j.1745-6584.2012.00923.x.

Worthington, S. R. & Smart, C. C. (2003). Empirical Determination of Tracer Mass for Sink to Spring Tests in Karst. Sinkholes and the Engineering and Environmental Impacts of Karst, 287-298. doi:10.1061/40698(2003)26.

Zheng, C. & Bennett, G. D. (2002). Applied contaminant transport modeling, 2, 353. NewYork: Wiley-Interscience.

ACKNOWLEDGEMENTS

Otávio Barbosa Ferreira was financed through a postgraduate scholarship granted by the CAPES foundation. The authors would like to thank the Institute for Technological Research of the State of São Paulo, where the project was developed. We also acknowledge the support of the Nexa Resources and the Water Services and Technologies for providing essential data to complete the research.

DATA AVAILABILITY

The data that support the findings of this research are available on request from the corresponding author. The data are not publicly available due to privacy restrictions.

3. NUMERICAL MODELING OF MITIGATION SCENARIOS FOR THE SANTA CATARINA RIVER DRYING-UP PROBLEM

The initial methodological approach of this work was based on direct and indirect data surveys about the region's morphological, hydrological, hydrogeological, and structural dynamics. The first step was mapping and characterizing superficial karst features in the Santa Catarina River (SCR) drying stretch, such as dolines and sinkholes (Figure 17). Then underground resurgences inside the mine, such as hydraulically active dissolved faults and fractures, were mapped and classified. The location of these karst features provided a first approach to interconnected recharge and discharge points. It guided the selection of the injection points for the fluorescent tracers in the river, and the detection points associated with water sources inside the mine.

After that, indirect data acquisitions were made through remote sensing and geophysical methods of differential interferometry and electrical resistivity, respectively. These imageries contributed to the spatial discretization of the most hydrogeologically relevant regional structures between the SCR and the underground mine. All data were crossed using a GIS platform to establish a logical association between the greatest potential zones for groundwater flow and the discontinuities located in the study area.

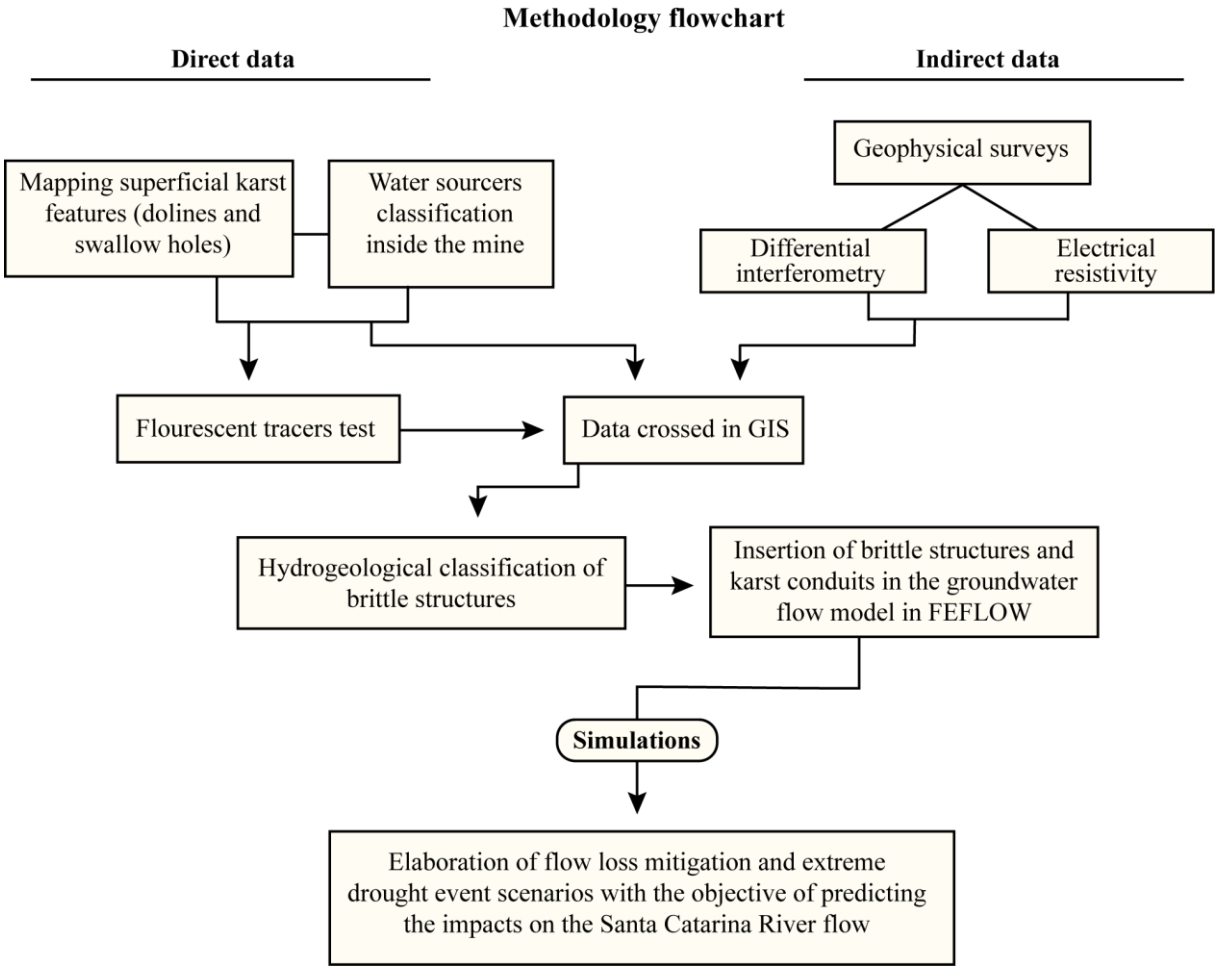

Figure 17 - Flowchart showing the data acquisition and work sequence.

A transient numerical groundwater flow modeling was carried out to evaluate mitigation solutions for the SCR drying-up problem, and predict the impacts that a possible extreme drought event in the region could cause on the river flow loss. The estimates for the SCR flow loss provided for each simulated scenario served as a basis for future planning of the mining company's activities in the region.

Through the results obtained in the activities described in the Chapter 2, an updated version of the groundwater flow conceptual model already used by the mining company was produced. The conceptual flow model improvement permitted the elaboration of a more accurate numerical flow model capable of better portraying the real groundwater dynamics in the study area. The advancements were based on inserting the most relevant hydrogeological brittle structures and karst conduits in local scale, introduced colluvial-alluvial and epikarst cover layers in the areas close to the river. We also expanded the domain to move the model boundaries away from the region of greatest pumping influence.

The numerical procedure used in the groundwater flow model was the Finite Element Method (FEM). This method discretizes the domain into polygonal geometric elements, commonly triangular or tetrahedral, in which the hydraulic heads are calculated as a function of nodal values interpolation expressed at each vertex. Due to the possibility of refinement in specific mesh zones and free geometric representation of the aquifer, the FEM is indicated for the modeling of geologically complex regions formed by folds, faults, fractures, and discontinuities. The computational algorithm used to simulate the groundwater flow was the FEFLOW – Finite Element Subsurface Flow and Transport Simulation System (Diersch 2014) – which uses the FEM to solve the partial differential equations that describe the flow. This software allows the insertion of discrete planar (2-D) and linear (1-D) features by selecting arbitrary nodes that compose the model mesh. It makes it possible to insert and manipulate geological structures such as sinkholes, surges, faults, fractures, and karst conduits at any modeling stage without changing the mesh (Ninanya et al. 2018).

3.1. Model Description

3.1.1. Model mesh

The 3-D model comprises 1,753,056 triangular mesh elements and 935,883 nodes, with a depth of 1,437 m. The hydrogeological units were represented through 18 numerical layers that make up the geological model (Figure 18). The minimum thickness of each layer was set at 7 m so that the epikarst and the covers associated with each lithotype were properly represented. The mesh was refined in the regions around rivers and drainages, brittle structures, and the underground mine, with 7 m triangular elements.

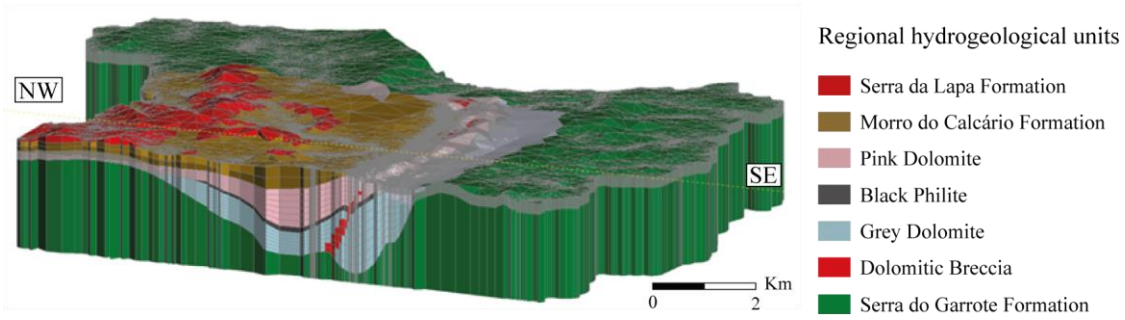

Figure 18 - Geological model in NW-SE section with the spatial distribution of the modeled regional hydrogeological units.

3.1.2. Domain and boundary conditions

The model domain (Figure 19a) was defined through the integrated analysis of the water bodies and the regional geological framework, covering 398.8 km². The delimitations in the plan view corresponded to the drainages that border the Serra da Lapa, and Serra do Garrote formations. The dolomitic basin defines the fractured aquifer outcrop region, composed by the Morro do Calcário and Serra do Poço Verde formations.

The model topographic base (Figure 19b) was created interpolating remote sensing data and *in situ* topographic surveys. The Digital Elevation Model (DEM) was obtained by the Alos Palsar sensor through the Alaska Satellite Facility's virtual platform, with a spatial resolution of 12.5 m. The topographic base accuracy was increased by including the wells' altimetric elevation, and SCR surroundings detailed topographic data provided by the mining company in the map interpolation.

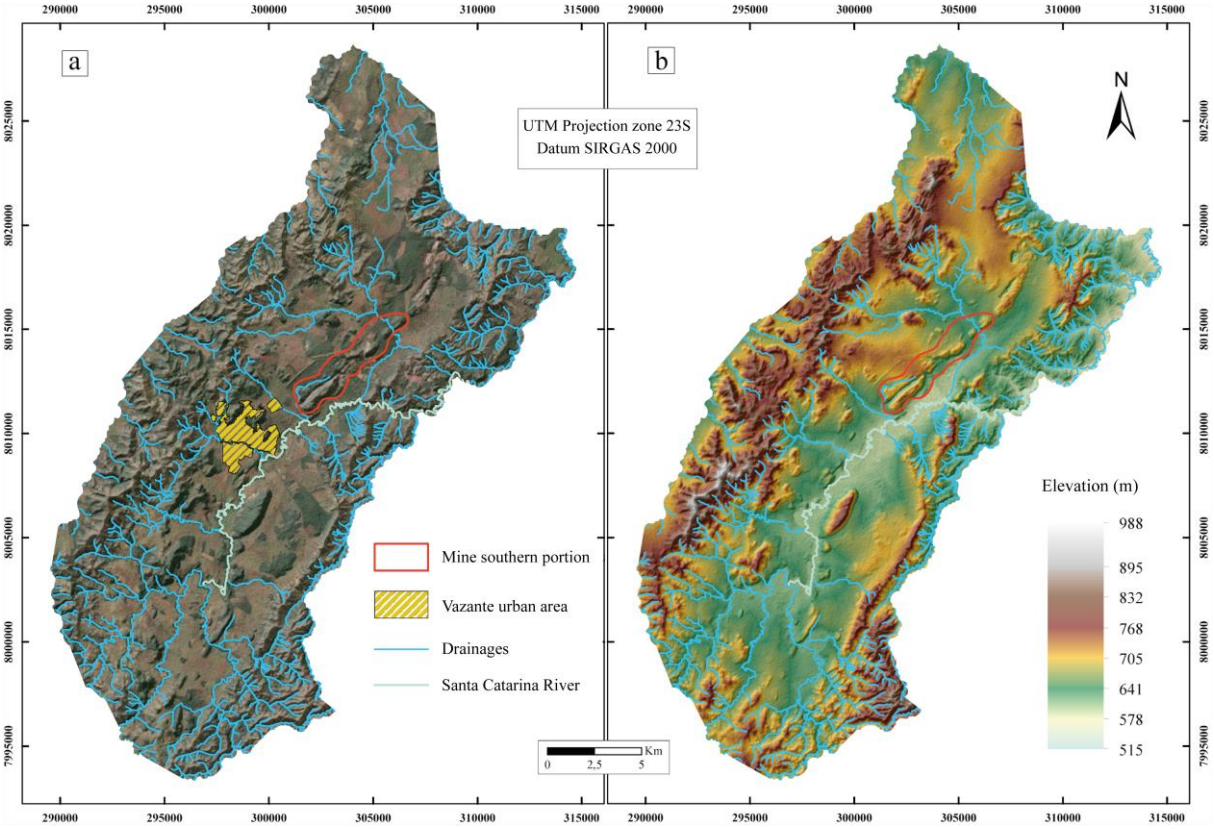

Figure 19 – a) Modeled area hydrographic map; b) Domain altimetric representation by hypsometry.

The modelled area has watershed divides close to its western and eastern limits. The Serra da Lapa Formation is a drainage divide, in the west boundary with altitudes between 832 m and 895 m. The east limit comprises the watershed divide formed by the Serra do Garrote Formation, which has elevations between 641 m (NE portion) and 832 m (SE portion). The surface runoff occurs mostly from these topographic highs towards the dolomitic basin interior with discharge into the SCR.

The groundwater flow is concentrated inside the dolomitic basin with a preferential direction towards the underground mine (Figure 20) through the hydrogeological units of Morro do Calcário Formation, Pink Dolomite, Black Philite, and Grey Dolomite. The Pink Dolomite unit represents the Morro do Calcário Formation in the region close to the mine. This division was created to improve the conceptual model detailing in the area of greatest groundwater level drawdown. The same procedure was applied to represent the Serra do Poço Verde Formation, segmented into Black Philite and Grey Dolomite units. In these units, the flow occurs preferentially by secondary porosity formed by fracture systems and by dissolution features developed and conditioned along the main fracture zones.

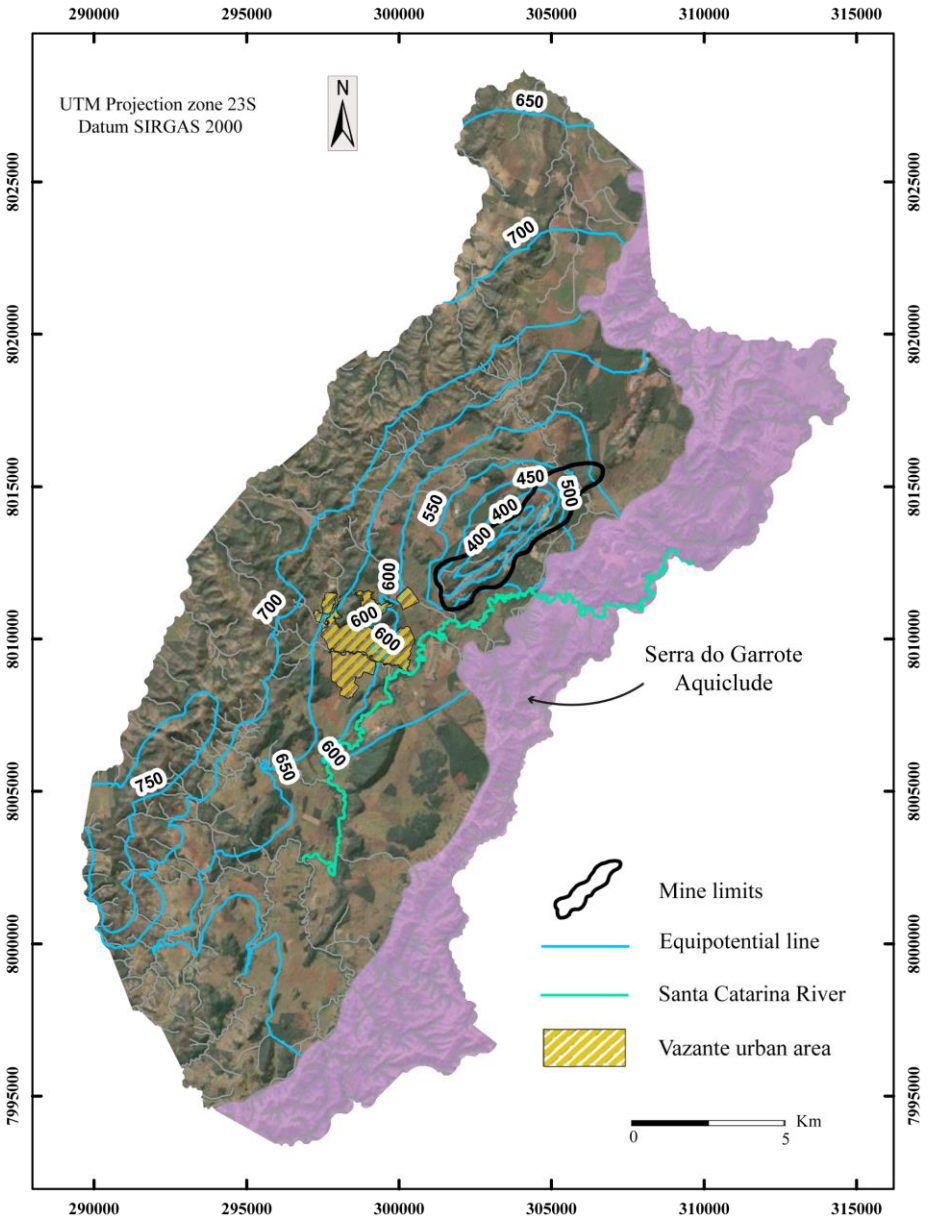

Figure 20 - Shallow potentiometric map for May 2015.

Downward groundwater flow also occurs in the more superficial hydrogeological units (Colluvium-Alluvial Cover and Epikast) and between fractures and karst conduits that develop in the carbonate rock massif (Figure 21). The Colluvium-Alluvial Cover unit forms a shallow aquifer, of primary porosity, with a direct connection to the SCR. The Epikarst unit is located beneath the Colluvium-Alluvial unit, and it presents a complex system of hydraulic connections through fractures and karst conduits that hydraulically connect the surface sediments to the carbonate massif.

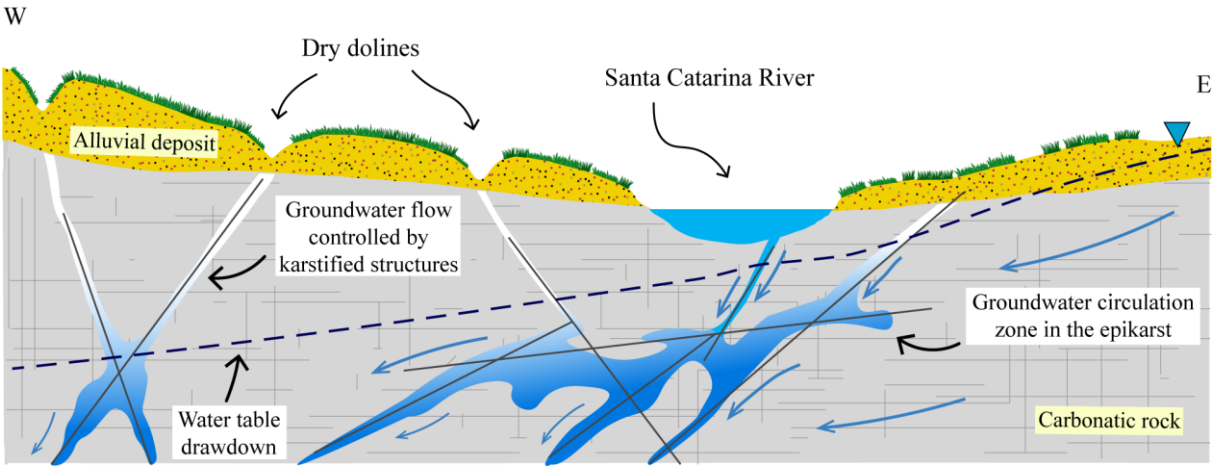

Figure 21 - Schematic diagram summarizing the conceptual groundwater circulation model of the Santa Catarina River losing stretch during the dry season.

The boundary conditions chosen for the model elements are described below:

• Perennial and intermittent drainage (Figure 22a): 3rd type boundary condition (Cauchy) makes the flow dependent on the reference river hydraulic head and the bed conductance rate. In the model solution, the flow in the drains will vary while the hydraulic heads keep changing. Flow restrictions were imposed for the intermittent drainages to only act as an aquifer discharge area when the hydraulic head is above the drainage level. The in-flow and out-flow transfer rates (conductance) for the drainages were set at 10^{-7} $s^{-1}$and 10^{-5} s^{-1}, respectively, based on a 1 m thick clogging layer. The out-transfer rate is generally greater than the in-transfer rate due to the absence of suspended material in the aquifer water. On the other hand, surface water infiltration tends to clog porous spaces due to the presence of suspended material. At the edge of the model, no-flow conditions were defined below the riverbeds.

• Mine (Figure 22b): 1st type boundary condition (Dirichlet) keeps the hydraulic head value fixed as a function of the underground gallery's levels. The advances of the underground galleries were represented monthly for the model calibration, validation, and simulation periods.

• Model bottom: a no-flow condition was defined for the bottom of the model due to the impermeable unit of the Serra do Garrote Formation that delimits the dolomitic basin vertically.

• Recharge: recharge condition restricted to the top of the model. This condition limits the entry of water into the modeled area only through the first layer.

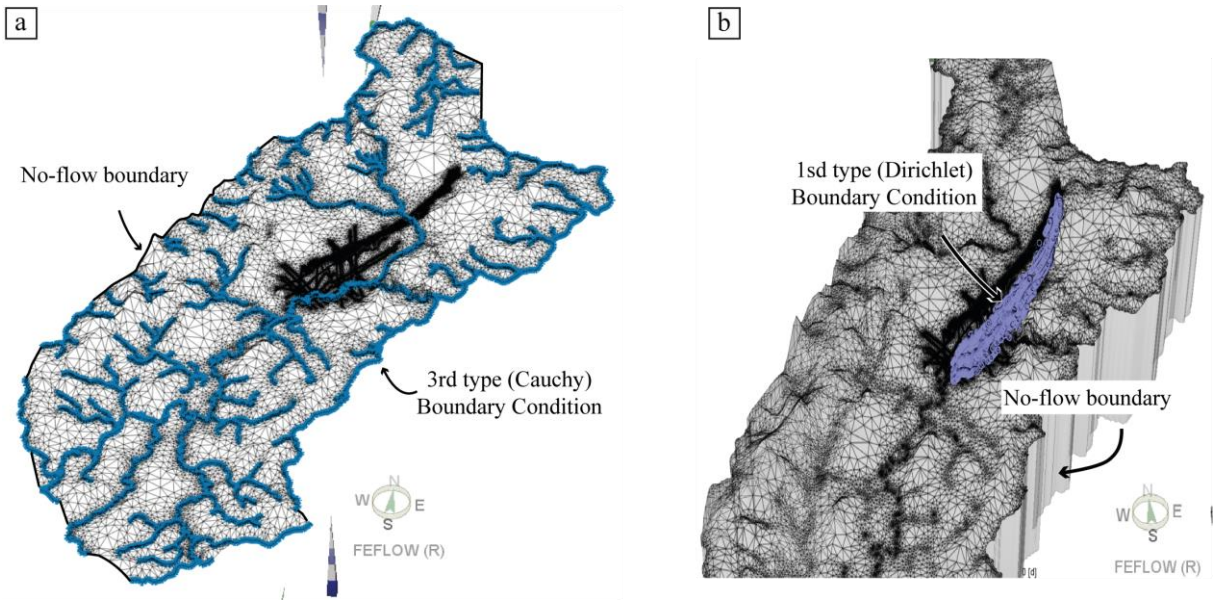

Figure 22 - Boundary conditions associated with a) drainages and b) the underground mine.

The model recharge rates were estimated through the monthly average precipitation provided by the mine's rainfall measurement stations. Based on water balance calculations for each micro basin that compose the dolomitic basin (Hidrovia, 2011), recharge intervals between 20% and 30% of monthly rainfall were estimated for the modeled aquifer units. For the units representing the Serra da Lapa and Serra do Garrote aquitards, the recharges were estimated in an order of magnitude less compared to the aquifer units.

To the west, subsurface dolomites continuity goes beyond the hydrographic limits that bound the basin, characterizing an underground flow regime not controlled by the Serra da Lapa watershed divide. Thus, drainages were used as limits of the model, in which it is possible to insert type 3 boundary conditions.

3.1.3. Initial parameters

A steady-state calibrated model representing the conditions of May 2015 was elaborated to generate the first piezometric surface (initial condition, t=0) for the transient model. This date was used as an initial condition since i) the river was flowing throughout its entire course, and ii) there was no precipitation between May and September 2015. The hydraulic heads in the wells shown in Table 2 were used to calibrate the steady-state model.

The brittle structures included in the model were classified into regional and local. The regional ones (Figure 23) have already been used in the mathematical models developed by the mining company. The local structures were inserted in this numerical model based on the results

described in item 2.4.4, obtained throughout this work. They were discretized in more detail as they exert greater control over the hydrogeological flow of the SCR drying region. The discrete features' hydraulic parameters inserted in the model are presented in Table 3. The values of these parameters were exported from the numerical model that had previously been used by the mining company.

Table 2 - Hydraulic heads in piezometers used to the initial condition referring to May 2015.

Piezometer	Hydraulic head (m)	Piezometer	Hydraulic head (m)
116li	578.7	**236li**	594.1
117al	577.2	**237li**	592.7
117li	577.2	**238ca**	596.5
118al	583.5	**240li**	605.0
118li	577.9	**241ma**	637.9
119al	594.6	**242ca**	616.7
119li	594.8	**243ma**	596.7
120al	592.2	**244ca**	596.4
120li	592.3	**246ca**	595.9
126ls	552.7	**247ca**	596.8
131fi	580.3	**249ca**	595.2
134ca	589.1	**250fi**	561.5
135ca	623.5	**275li**	461.6
140ca	553.4	**277ca**	592.8
141ca	575.3	**279fi**	596.2
142ls	558.3	**280ca**	613.5
143ls	579.4	**282ls**	592.4
143ma	601.8	**283ma**	592.9
145ma	591.3	**287ls**	587.3
146ca	587.4	**288ca**	586.0
147ca	588.7	**290ls**	591.6
152al	586.1	**291ca**	579.0
153li	573.6	**292ca**	552.1
154li	568.5	**68ma**	583.9
155li	557.9	**89li**	542.4
157li	545.4	**90li**	571.5
158li	530.1	**91ls**	544.4
184li	501.5		

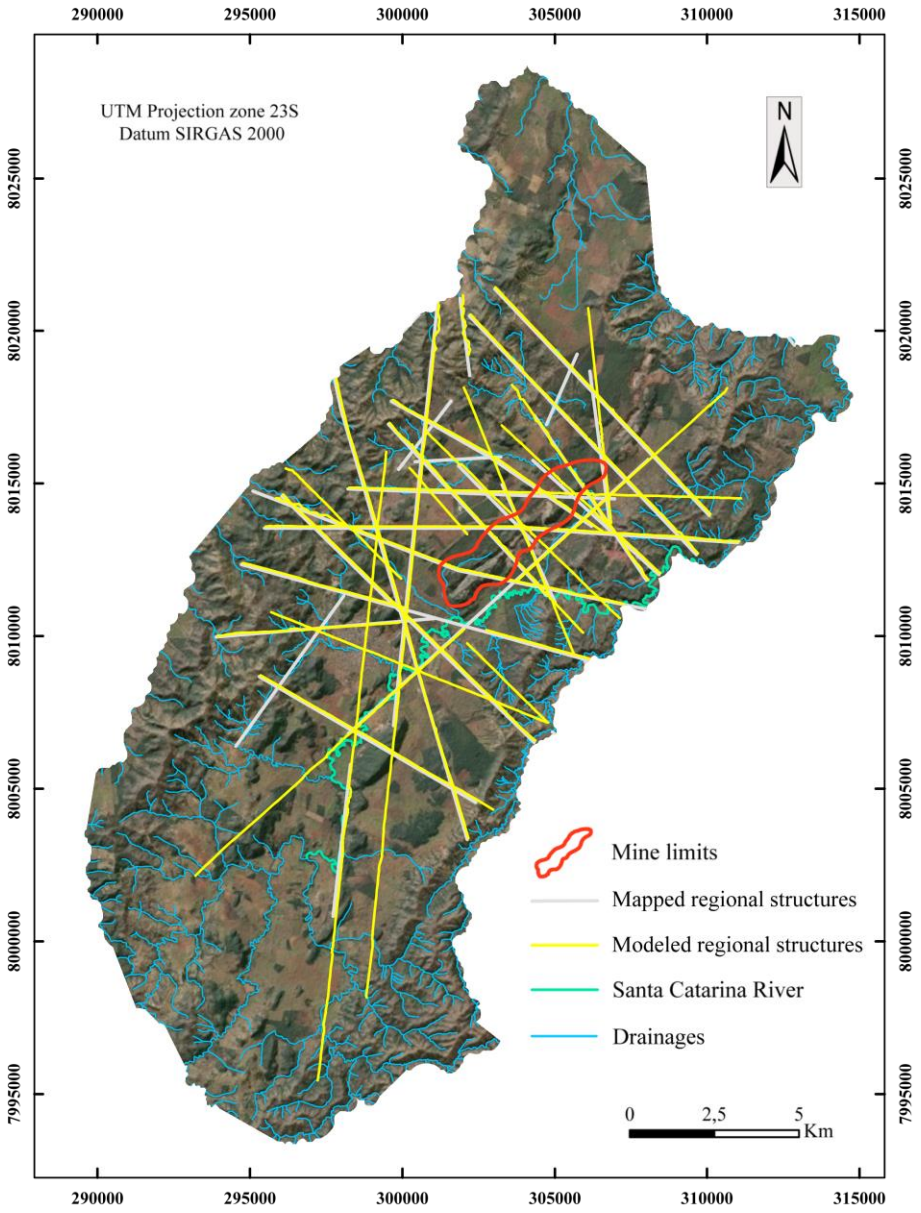

Figure 23 - Regional brittle structures.

The first estimates for the hydraulic conductivity and specific storage values were made through pumping tests carried out by the mining company in 1990. The hydrogeological unit's hydraulic conductivity (K) and specific storage initial values were estimated based on the numerical model that has been previously used by the mining company. For the Colluvial-Alluvial covers and the Epikarst, the horizontal hydraulic conductivity values (Kx and Ky) were taken from slug tests carried out by the IPT in October 2020.

Table 3 - Discrete elements hydraulic parameters inserted in the model.

	Conduits	**Local brittle structures**		**Regional brittle structures**
		High potential	**Medium potential**	
Roughness ($m^{-1/3}/s$)	8	-	-	-
Cross-sectional area (m^2)	0.25	-	-	-
Aperture (m)	-	0.15	0.10	0.10
Hydraulic conductivity (m/day)	-	864	864	864

The hydrogeological units Dolomitic Breccia, Black Phyllite, Pink Dolomite, and Grey Dolomite, as well as the Serra da Lapa, Morro do Calcário, and Serra do Garrote formations were included in the model under isotropic hydraulic conditions, where the horizontal hydraulic conductivities are equivalent to the vertical ones. In general, sedimentary structures developed in unconsolidated sediments or sedimentary rocks generate longitudinal patterns of grain imbrication, which favor the groundwater flow in horizontal directions. Thus, the sedimentary cover's vertical hydraulic conductivities were estimated in an order of magnitude below compared to the horizontal hydraulic conductivities.

3.1.4. Simulated scenarios

Four scenarios of possible mitigation solutions for the SCR drying-up problem were simulated. They were based on the intervention scenarios proposed by the mining company: i) upstream water adduction, ii) riverbed waterproofing, iii) partial, and iv) total obstruction of sinkholes. A fifth scenario was simulated to estimate the possible impacts of an extreme drought event over the SCR flow.

It was simulated in a transient regime for the period between January 2022 and December 2030, guided by the progress foreseen by the mining company for the underground galleries (Figure 24). The baseline scenario for comparison with the simulations described above considered only the progress of the underground galleries between 2022 and 2030.

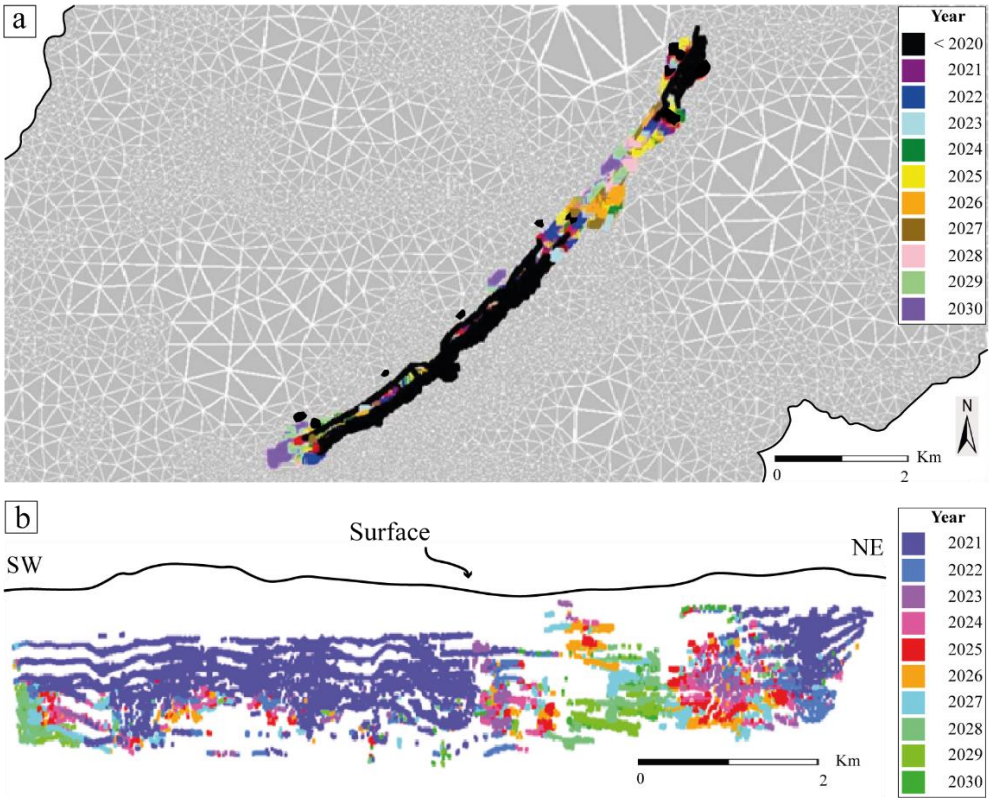

Figure 24 - Mine schematic a) map and b) cross-section of the estimated underground galleries progress between 2020 and 2030.

The recharge values for all simulations, except for the drought simulation, were estimated considering the historical monthly precipitation average between 1970 and 2020. Historical precipitation data were taken from rainfall monitoring stations that have been recording meteorological data in the region for over 50 years. Recharge rates were set at 26% of the historical average monthly rainfall based on the results of the model's calibration step. For the less conductive formations (Serra da Lapa and Serra do Garrote formations), recharge rates were 2.6% of the historical average monthly rainfall.

Recharge rates were entered into the model under an annual cyclical condition. The single recharge values were fixed and repeated for each month between January and December throughout the simulation periods (Figure 25).

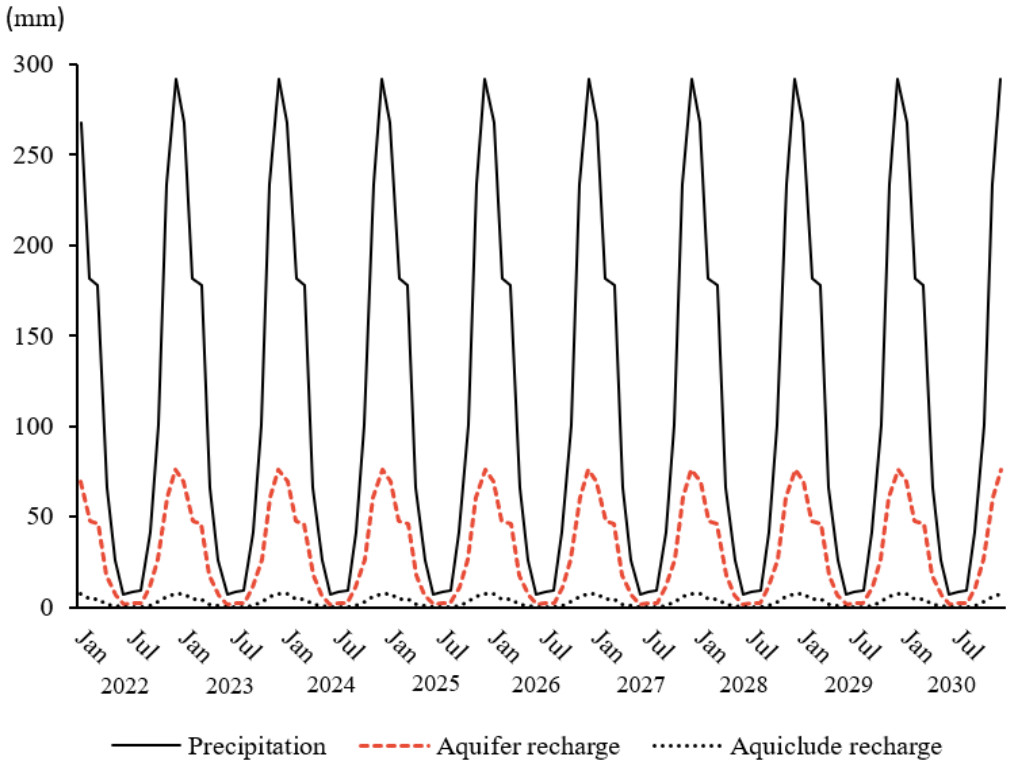

Figure 25 - Cyclical precipitation and recharge values over the simulation period.

The SCR drying stretch was represented in the model under annual cyclical conditions based on the drying pattern observed in the river between 2018 and 2020. Between July and November, progressive river drying extensions were fixed. These constraint-flow rate segments (Figure 26) were inserted under nodal conditions of maximum flow rate equal to zero.

SCR flow loss estimates were evaluated for the river stretch between the Montanhesa and Bambuzal fluviometric stations that delimit the influent river stretch (Figure 27). There will be the possibility of future comparison between the flow loss values calculated by the model for each simulated scenario and the values measured in the field through the fluviometric stations.

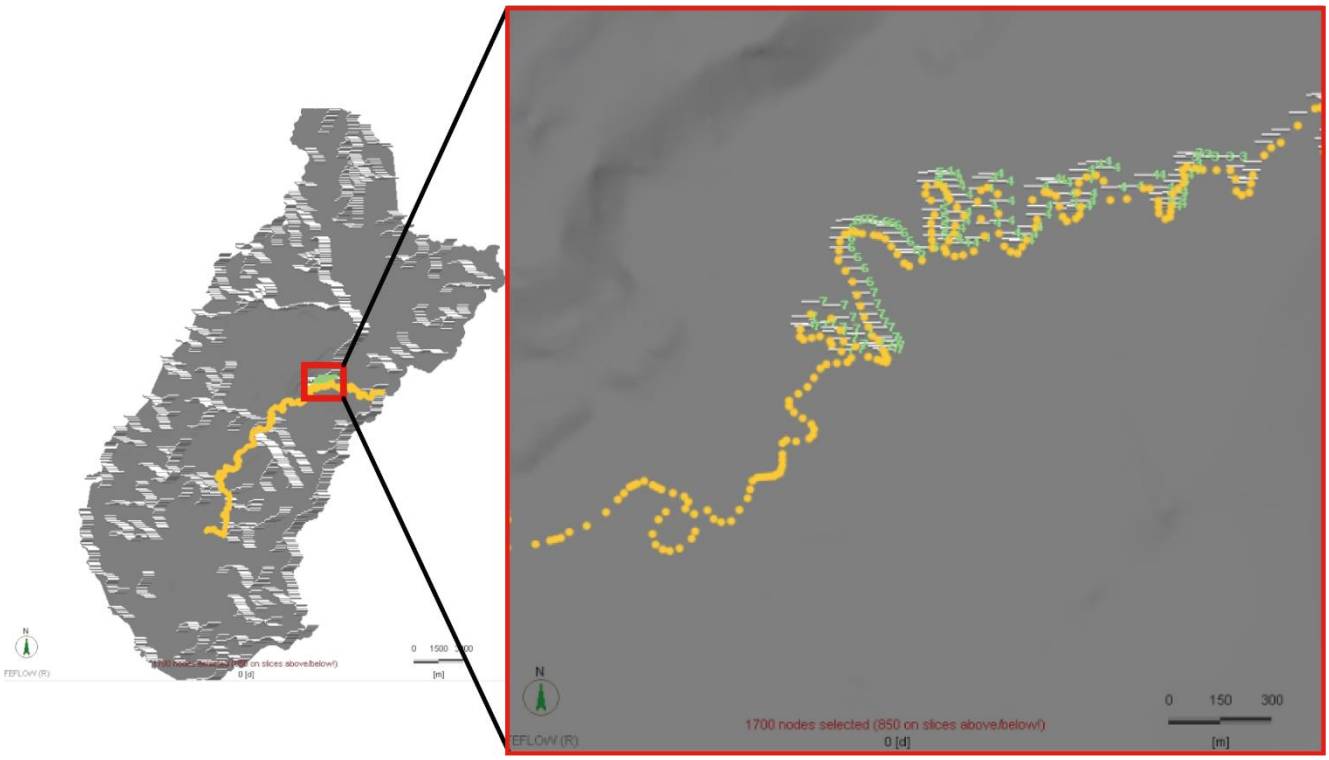

Figure 26 - Santa Catarina River nodal representation (in yellow) with the cyclical drying stretches discretized in green.

3.1.4.1. Upstream Water Supply

The upstream water supply simulation was carried out for the period between January 2022 and December 2030. The period was chosen based on the mining company's guidelines for the construction of supply lines. This solution consists of transporting water through pipes to portions just above the river-influent stretch (Figure 27). This simulation aimed to quantify the expected flow loss from the river to the aquifer if there is a full replacement of water to keep the river flowing.

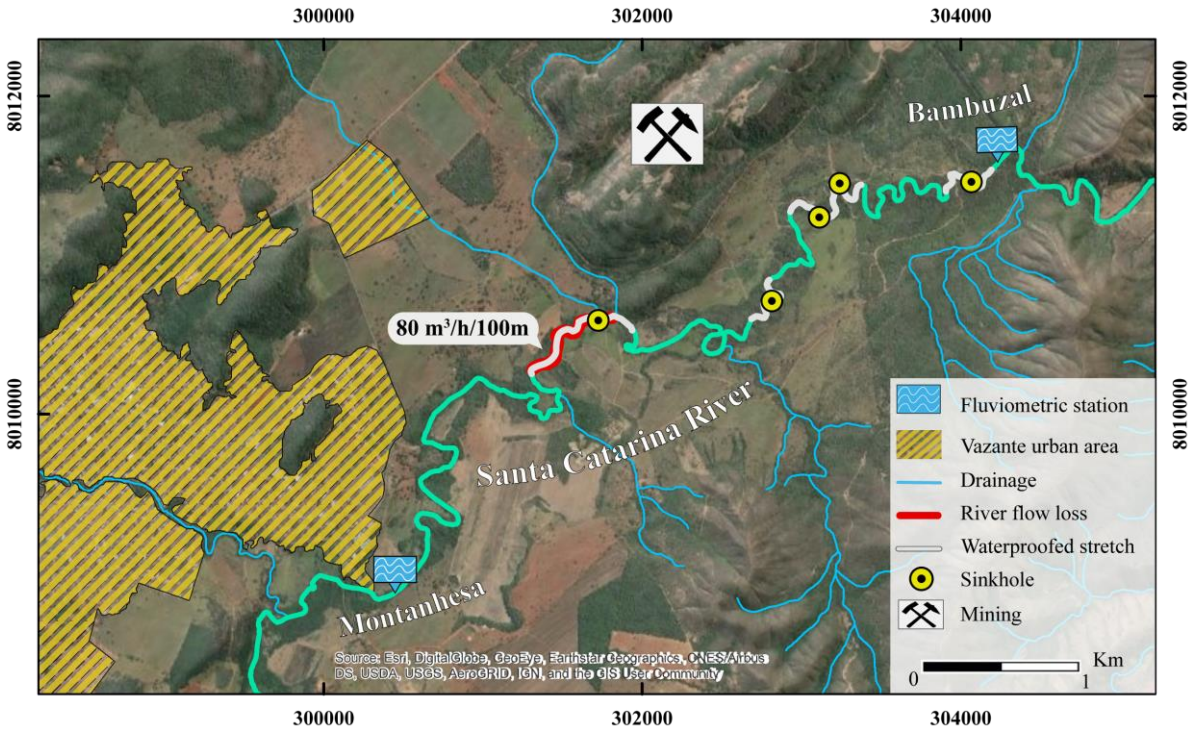

Figure 27 - Map showing the mitigation interventions in the SCR for each simulated scenario.

To simulate the upstream water supply scenario, the cyclical flow loss restrictions in the river drying stretches were removed (Figure 26). The boundary condition represented by the SCR (Cauchy type) acted as an unrestricted source of recharge for the aquifer, generating a river of perennial flow throughout the entire simulation period. In this way, the water demand for the aquifer could be estimated for each simulated scenario. It should be noted that such a boundary condition was also necessary for the simulations of riverbed waterproofing and obstruction of sinkholes because this groundwater flow model does not quantify flow variations in surface water bodies.

3.1.4.2. Riverbed-Waterproofing

This simulation quantified the influence of waterproofing some sections of the river on its flow loss to the aquifer. The simulation was carried out for the period between January 2025 and December 2030 based on the mining company's forecast for the waterproofing works.

The waterproofing sections (Figure 27) were defined by the location of the sinkholes and the zone with the highest measured river flow loss (80 m³/h/100m). Waterproofing sections of 500 m (250 m upstream and 250 m downstream) were inserted in the vicinity of each sinkhole located in the SCR drying stretches.

The sections selected for waterproofing were represented in the numerical model through the insertion of nodal conditions of a maximum flow rate equal to 0 m³/day between the SCR and the aquifer, restricting the hydraulic communication between them.

3.1.4.3. Obstruction of Sinkholes

Obstruction of sinkhole simulations was carried out to evaluate the influence of the total (100 %) and partial (50 %) reduction of its cross-sectional areas on the SCR flow loss.

The simulations were carried out between January 2022 and December 2030 based on the mining company's estimate for the execution of the karst conduits obstruction works with grout and/or polyurethane injections.

3.1.4.4. Extreme Drought Event

It was evaluated the impacts that a year of extreme drought can cause on the SCR flow loss. The choice of this scenario was based on the increasing occurrence of extreme weather events worldwide due to climate changes (Easterling et al., 2000; Sanghi and Mendelsohn, 2008; Field et al., 2012; Diffenbaugh et al., 2017; Cunha et al., 2019).

The simulation period was between January 2022 and December 2030. The year 2024 was selected to impose drought conditions. A satisfactory measurement window could be achieved after the drought event in 2024 so that the aquifer drawdown/recovery phenomena were observed over 6 years.

For the year 2024, the monthly rainfall rates for the dry season were measured between April 2016 and October 2017 (Table 4). This period had the lowest rainfall rates in the last 30 years. For the remaining years of the simulation, the cyclical recharges were estimated through the historical monthly precipitation average (Table 5).

Table 4 - Monthly precipitation rate for the extreme drought period recorded between April 2016 and October 2017.

	Month	Monthly precipitation rate for extreme drought period (mm)
2016	April	6.8
	May	5.0
	June	6.5
	July	0.0
	August	17.5
	September	4.3
	October	76.0
	November	206.1
	December	122.9
2017	January	81.9
	February	201.6
	March	40.4
	April	0.7
	May	37.7
	June	0.0
	July	0.0
	August	0.0
	September	14.9
	October	110.5
	November	195.1
	December	313.1

Table 5 - Historical monthly precipitation average recorded between 1970 and 2020.

Month	Historical monthly average precipitation rate (mm)
January	268.0
February	182.0
March	177.8
April	66.1
May	26.0
June	6.6
July	8.1
August	9.0
September	41.5
October	100.8
November	233.2
December	291.9

3.2. Results and Discussion

3.2.1. Model calibration and validation

The parameter estimation software package PEST was used in the calibration and validation steps. It was performed through the graphical user interface FePEST. The system of equations used in the transient model numerical solution was the SAMG – Algebraic Multigrid.

The hydraulic conductivity of the hydrogeological units was calibrated in the initial condition steady-state model (Table 6). The transient model first calibration step was performed in a dry period (Figure 28), without a recharge, between May and September 2015 to calibrate the specific storage (Table 7) of the hydrogeological units. The second calibration step was performed in the rainy period, between September 2015 and April 2016, when the recharge calibration was carried out. It was defined as 26% and 2.6% of the average monthly rainfall for aquifer and aquiclude formations, respectively.

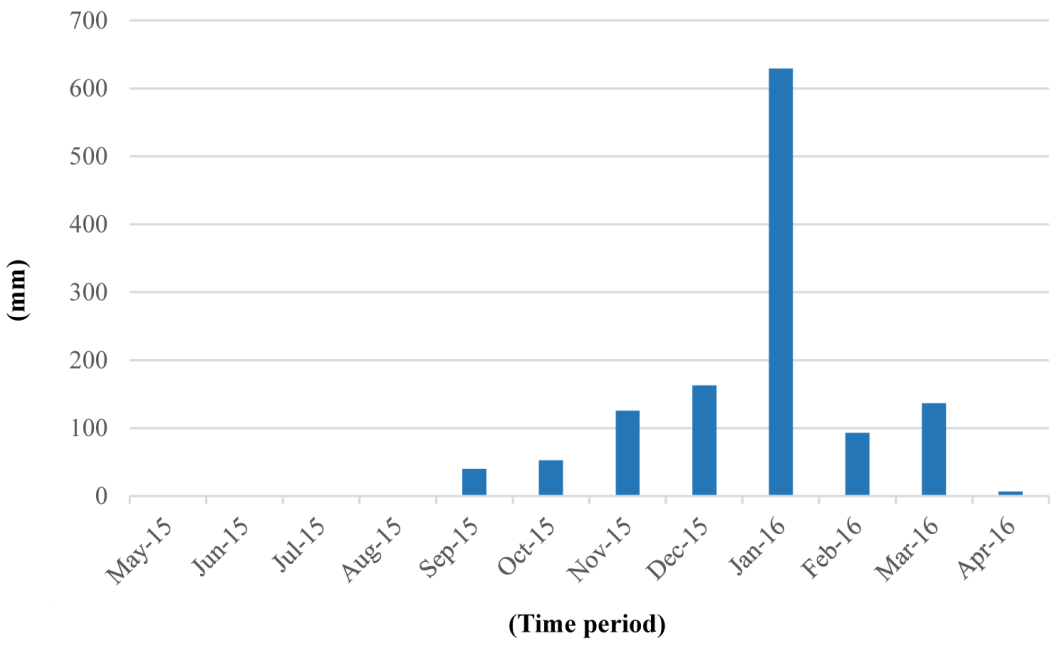

Figure 28 - Monthly precipitation for the model calibration period.

Table 6 - Initial and calibrated hydraulic conductivity values for the modeled hydrogeological units.

Hydrogeological unit	Initial hydraulic conductivity (m/day)		Calibrated hydraulic conductivity (m/day)	
	Kx, Ky	Kz	Kx, Ky	Kz
Dolomitic Breccia	$3.22\ 10^{-2}$	$3.22\ 10^{-2}$	$1.29\ 10^{-2}$	$1.29\ 10^{-2}$
Cover – Grey Dolomite	$2.63\ 10^{1}$	2.63	$2.50\ 10^{1}$	2.50
Cover – Pink Dolomite	$1.76\ 10^{-1}$	$1.76\ 10^{-2}$	$1.08\ 10^{-1}$	$1.08\ 10^{-2}$
Cover – Black Philite	8.03	$8.03\ 10^{-1}$	8.03	$8.03\ 10^{-1}$
Cover - Morro do Calcário Formation	$3.09\ 10^{-1}$	$3.09\ 10^{-2}$	$1.93\ 10^{-1}$	$1.93\ 10^{-2}$
Cover - Serra do Garrote Formation	7.73	$7.73\ 10^{-1}$	7.73	$7.73\ 10^{-1}$
Grey Dolomite	$1.65\ 10^{-2}$	$1.65\ 10^{-2}$	$9.80\ 10^{-3}$	$9.80\ 10^{-3}$
Pink Dolomite	$1.09\ 10^{-2}$	$1.09\ 10^{-2}$	$1.08\ 10^{-2}$	$1.08\ 10^{-2}$
Epikarst	5.91	5.91	6.23	6.23
Black Philite	$2.31\ 10^{-2}$	$2.31\ 10^{-2}$	$2.22\ 10^{-2}$	$2.22\ 10^{-2}$
Serra da Lapa Formation	$1.05\ 10^{-1}$	$1.05\ 10^{-1}$	$1.05\ 10^{-1}$	$1.05\ 10^{-2}$
Morro do Calcário Formation	$8.01\ 10^{-2}$	$8.01\ 10^{-2}$	$1.17\ 10^{-1}$	$1.17\ 10^{-1}$
Serra do Garrote Formation	$4.94\ 10^{-4}$	$4.94\ 10^{-4}$	$4.94\ 10^{-4}$	$4.94\ 10^{-4}$

Table 7 - Initial and calibrated specific storage values for the modeled hydrogeological units.

Hydrogeological unit	Initial specific storage (m^{-1})	Calibrated specific storage (m^{-1})
Dolomitic Breccia	$6.14\ 10^{-5}$	$2.08\ 10^{-5}$
Cover – Grey Dolomite	$5.64\ 10^{-5}$	$1.85\ 10^{-5}$
Cover – Pink Dolomite	$1.00\ 10^{-4}$	$8.23\ 10^{-6}$
Cover – Black Philite	$5.64\ 10^{-5}$	$5.76\ 10^{-5}$
Cover - Morro do Calcário Formation	$1.00\ 10^{-4}$	$7.54\ 10^{-5}$
Grey Dolomite	$2.51\ 10^{-5}$	$1.94\ 10^{-5}$
Pink Dolomite	$2.07\ 10^{-5}$	$9.14\ 10^{-5}$
Epikarst	$6.69\ 10^{-5}$	$4.68\ 10^{-5}$
Black Philite	$2.11\ 10^{-5}$	$6.44\ 10^{-5}$
Serra da Lapa Formation	$3.14\ 10^{-5}$	$2.10\ 10^{-5}$
Morro do Calcário Formation	$2.07\ 10^{-5}$	$2.34\ 10^{-5}$
Serra do Garrote Formation	$1.29\ 10^{-5}$	$1.85\ 10^{-5}$

The calibration was based on hydraulic heads in 55 observation wells (Figure 29). The normalized root mean square error (NRMSE) was calculated as the average of the monthly

NRMSE given by the model for each calibration and validation period (Figure 30, 31). The first calibration step reached a value of 9.89%, and the second one, 7.53%.

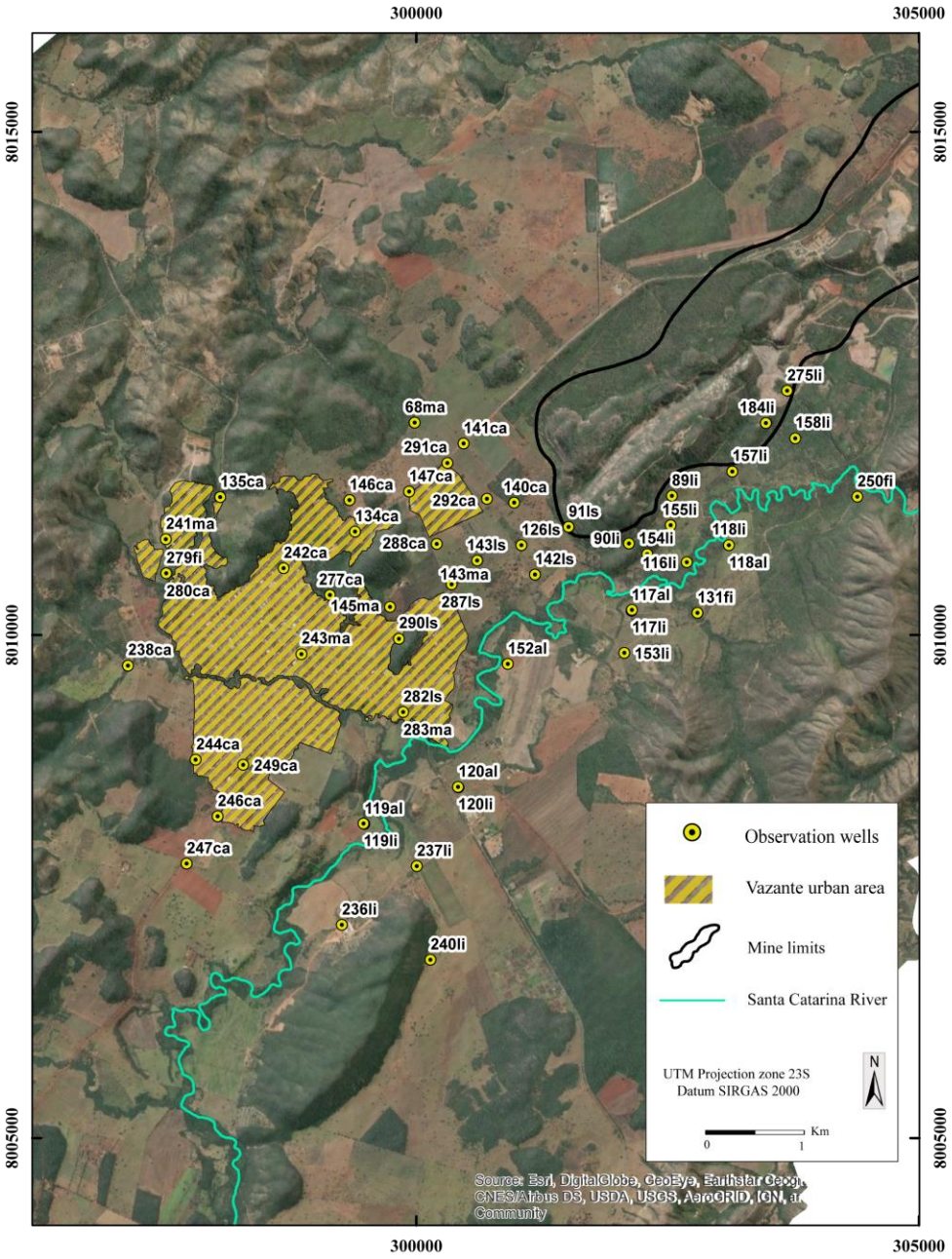

Figure 29 - Map showing the location of observation wells.

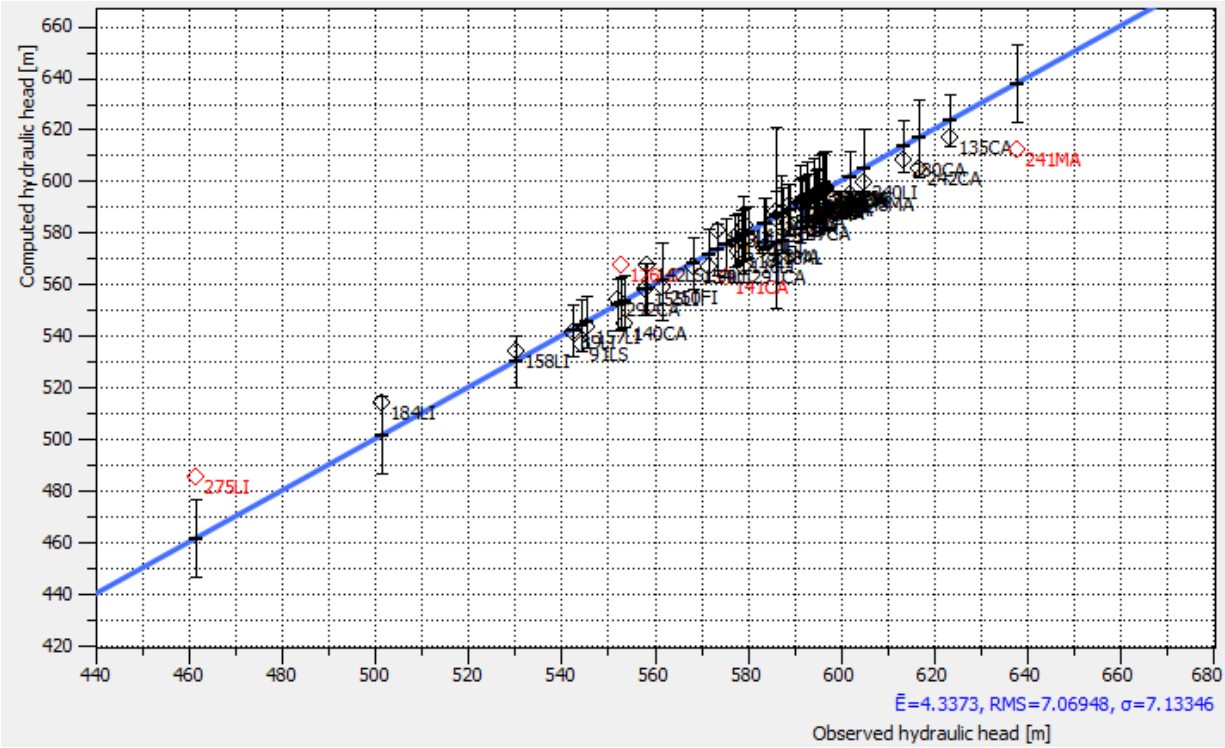

Figure 30 - Example of scatter diagram between calculated and observed hydraulic heads in piezometers for May 2015. The vertical bars represent the acceptable error interval in each well.

The model validation step was carried out after its calibration. During validation, adjustments to some parameters were made to maintain calibration. The chosen validation period was from June 2019 to June 2020. The recharge conditions and cyclical drying of SCR stretches were maintained. Mine evolution data were inserted with the depths of the underground galleries for this period.

Seeking to reduce the NRMSE, a hydraulic parameter was changed. The karst conduits cross-section areas had their values modified from 0.25 m² to 0.39 m² (an increase of 64.1%). In this way, an NRMSE of 9.4% was achieved. In addition to adjusting the hydraulic heads in the observation wells, the validation step was also based on the observed and calculated values of the mine's monthly pumping flow averages for the period (Table 8).

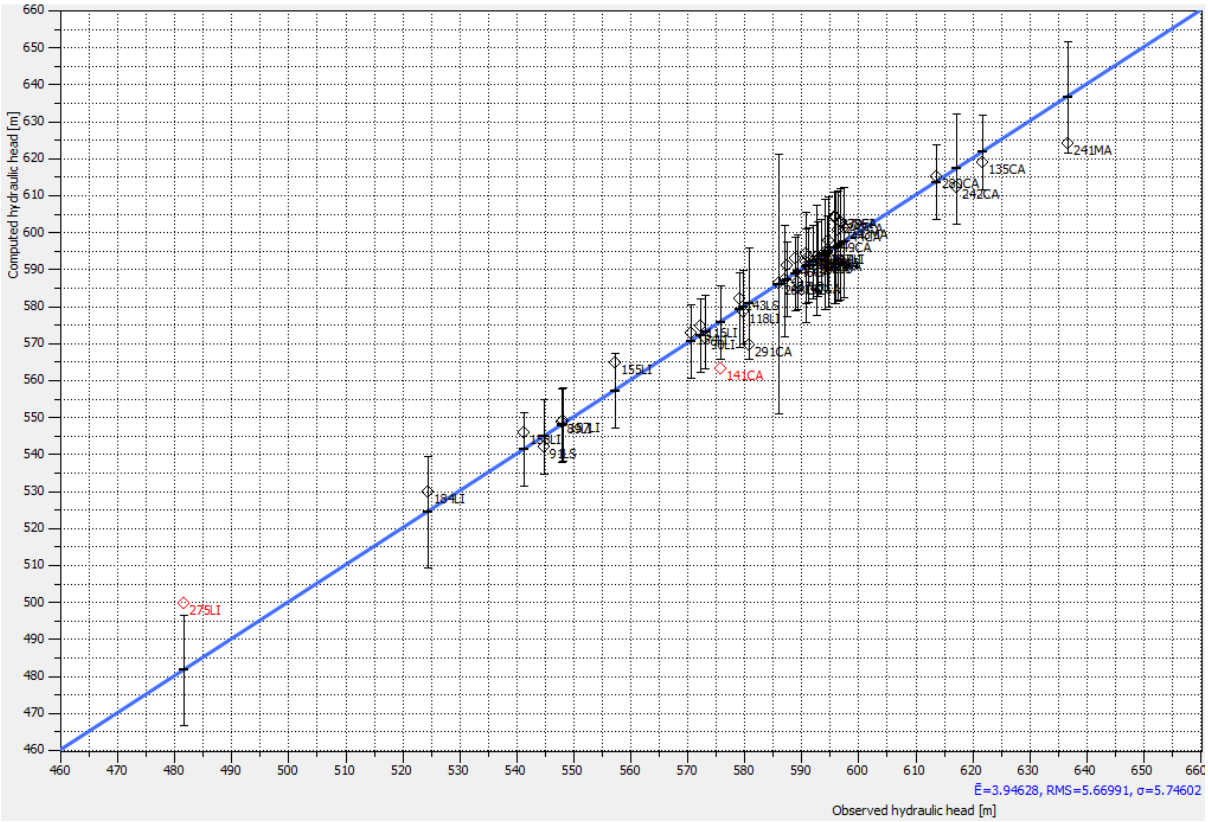

Figure 31 - Example of scatter diagram between calculated and observed hydraulic heads in piezometers for June 2019. The vertical bars represent the acceptable error interval in each well.

Table 8 - Average monthly pumping rate observed in the mine and calculated by the model during the validation step.

Interval	**Observed pumping rate (m^3/h)**	**Calculated pumping rate (m^3/h)**
Jun/2019	10692	10667
Jul/2019	13332	13702
Ago/2019	12949	12857
Sep/2019	11576	12279
Oct/2019	10310	12058
Nov/2019	10712	12216
Dec/2019	12581	13015
Jan/2020	12868	12677
Feb/2020	13617	13030
Mar/2020	15328	12966
Apr/2020	14050	12864
May/2020	13294	12756
Jun/2020	12952	12670

3.2.2. Simulations

All simulations showed a trend of increase in the SCR flow loss related to the advance of the underground mine galleries, followed by stabilization over the simulated periods (Figure 32). This behavior is expected due to the need to increase the mine pumping rates to keep the galleries drained, causing a lateral and vertical expansion of the regional cone of depression. However, the decrease in the underground galleries' advance rates in the final years of the simulations (2029 and 2030) produced a stabilization in the pumping rates (Figure 33). Consequently, the water discharge from the river to the aquifer also stabilized.

There was a significant increase in the river flow loss caused by the upstream water supply (35.1%). The mine pumping rate showed a 7% increase. In this scenario, the river became a perennial source of recharge for the aquifer and no longer presented the cyclical drying stretches during the dry seasons.

The sinkhole obstructions in 50% and 100% represented a notable decrease in the river flow loss at 28.2% and 47.7%, respectively, and 19.7% and 37.9% in the mine pumping rate. The direct hydraulic connections between the SCR and the underground mine, through karst conduits, apparently control a significant part of the river flow loss. The hydrogeological relevance of the karst conduits is also evident in the simulation with riverbed waterproofing, pointing to a reduction of 43.6% in the river flow loss compared to the upstream water supply scenario.

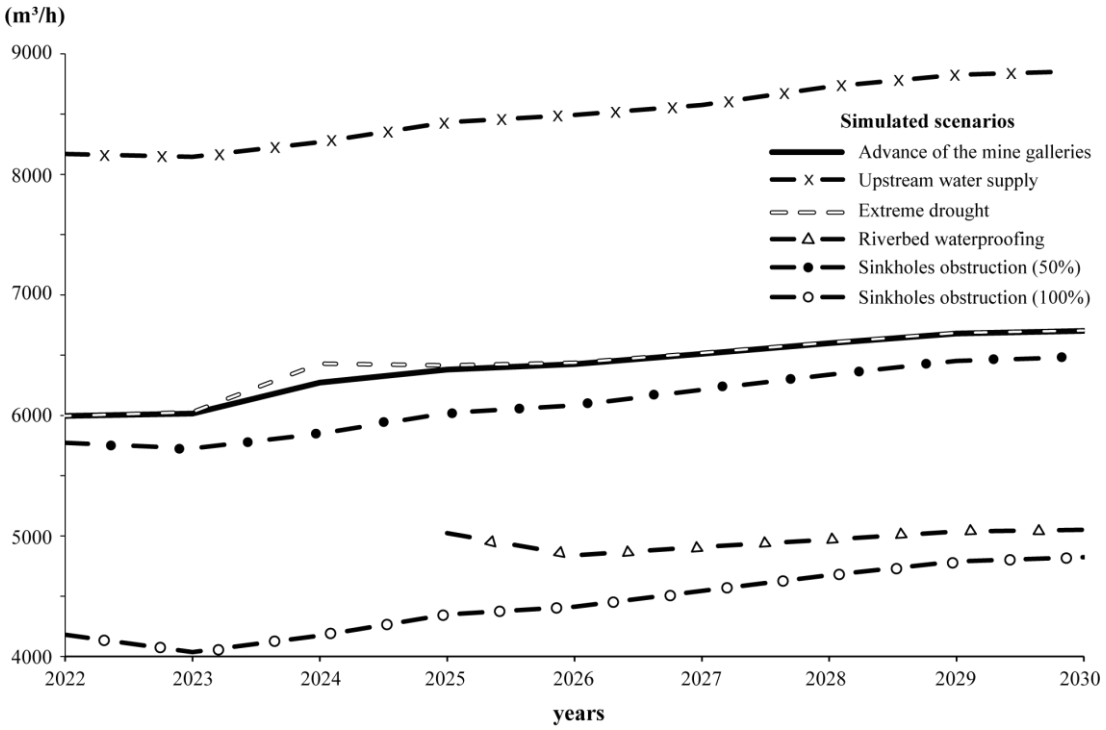

Figure 32 - Estimated Santa Catarina River flow loss between the Montanhesa and Bambuzal fluviometric stations for each scenario during the simulated period.

The extreme drought event simulated for 2024 showed an increase of approximately 2.5% in the SCR flow loss compared to the scenario of the advance of the underground mine galleries. It may be associated with the reduction of surface recharge by rainwater infiltration during the dry period and the maintenance of the mine pumping operation. The aquifer drawdown and consequent lowering of the cone of depression increased the hydraulic gradient between the river and the aquifer, causing the river to release more water into the aquifer. The stabilization observed in the river flow loss from the year following the drought event (2025) represented a rapid hydrogeological rebalancing and recovery of the groundwater circulation dynamics.

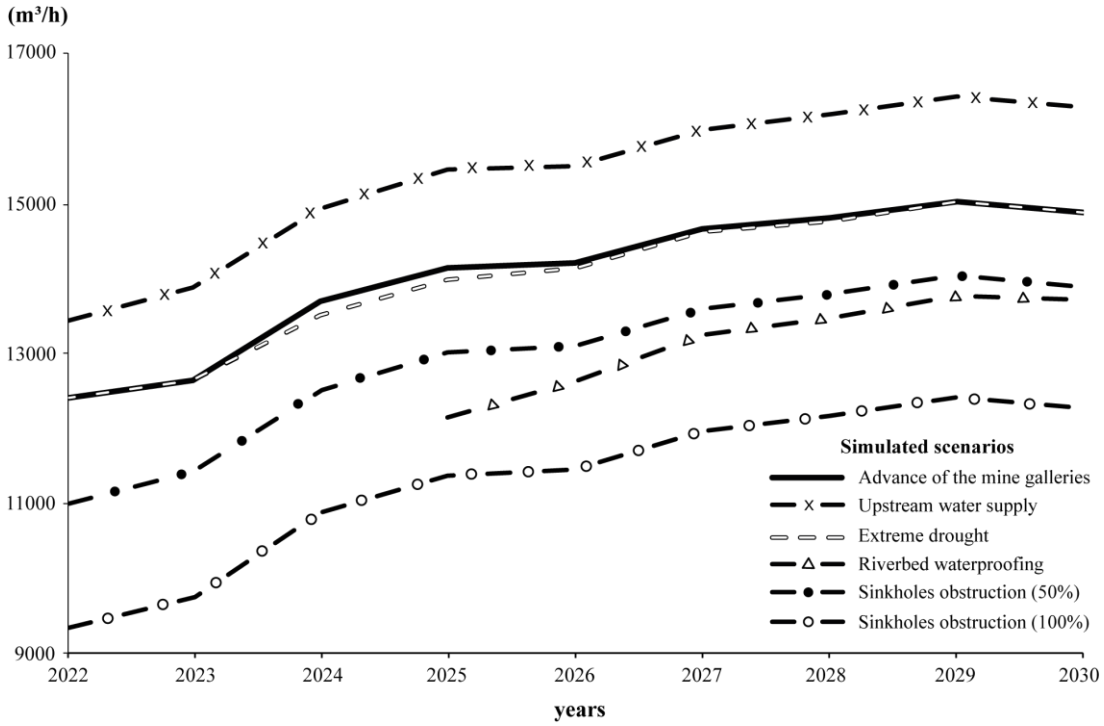

Figure 33 - Estimated mine pumping rate for each scenario during the simulated period.

Table 9 presents the displacements of the cones of depression for each simulated scenario. The 580 m equipotential line marked the outer limit of the cone induced by the mine pumping in the modeled area (Figure 34). It was used to measure the displacements of the cones of depression along an imaginary line that joins the Vazante city hall (the center of the municipality) and the westernmost point of the mine for each simulated scenario. The Appenddix 2 brings the estimated potentiometric maps for December 2030 for all simulated scenarios.

Table 9 - Displacement of the equipotential line 580 m calculated between the final (December 2030) and initial period (January 2022 or 2025) for each simulated scenario.

Simulated scenario	Displacement of equipotential 580 m (m)
Advance of the mine galleries	5
Upstream water supply	83
Riverbed waterproofing	513
Sinkholes obstruction in 50%	89
Sinkholes obstruction in 100%	103

The cone of depression expansion was little expressive (5 m) when considering only the advance of the underground galleries, indicating a balance between the mine pumping rate and

the aquifer recharge rate. However, there was an increase in the river water demand by 604.6 m^3/h to keep the depression cone stabilized.

The riverbed-waterproofing scenario caused the largest advance in the depression cone (513 m). The connection observed between the waterproofing and the cone advance may be associated with an aquifer recharge decrease. The waterproofed sections lose the hydraulic connection with the aquifer and cease to act as a recharge source. The stabilization of the aquifer recharge by infiltration of meteoric water added to the advancement of the underground galleries (and consequent increase in mine pumping) generated an increase in the volume of water withdrawn from the aquifer storage. It can lead to the reduction of hydraulic heads and enlargement of the depression cone influence area.

The models indicated that the obstruction of the sinkholes in the Santa Catarina riverbed significantly reduced the river flow loss without generating major advances in the depression cone (89 m and 103 m, respectively, for obstruction in 50% and 100%), as observed in the waterproofing scenario (513 m). It can be explained by the interruption of the direct hydraulic communication between the river and the deeper zones of the aquifer. The sinkholes obstruction allows the river to transfer more slowly a greater volume of water to the shallow portion of the aquifer through diffuse recharge (in-transfer rate).

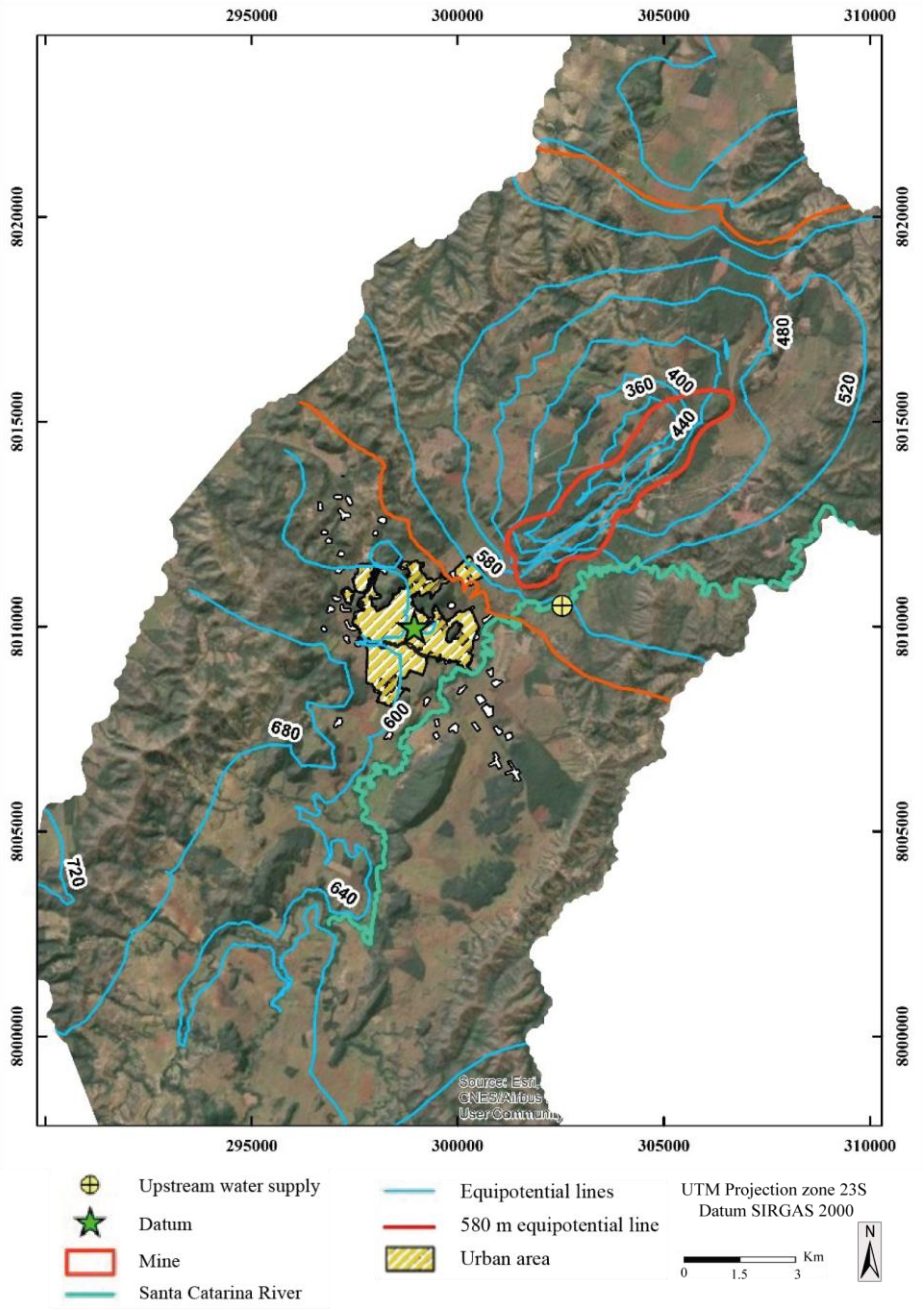

Figure 34 - Potentiometric map for the SCR waterproofing scenario in January 2025 (blue). In orange is the equipotential line of 580 m estimated for the same scenario in December 2030. The datum represents the Vazante city hall.

4. CONCLUSIONS AND RECOMENDATIONS

The refinement of the transient groundwater flow model carried out in FEFLOW proved to be capable of simulating complex hydrogeological scenarios, with abrupt variations in hydraulic conductivity in karst features associated with local and regional systems of faults and fractures.

The hydraulic connections between the Santa Catarina River and the underground mine generated by karst conduits control a significant part of the river flow loss. However, its representation in the numerical model as discrete features (1D) that directly connect the river to the mine, make the model sensitive to the presence of these conduits. It may overestimate the reduction in the river flow loss through mitigation solutions that only predict the sinkholes obstruction. Thus, the mitigation solutions must be tested in the field, seeking to understand their effectiveness in terms of reducing the river flow loss and consequently re-establishing its natural flow in dry periods.

In addition, the consequences related to the depression cone expansion towards the municipality of Vazante must be verified for the riverbed-waterproofing solution, since the reduction of hydraulic connection between the river and the aquifer may cause a deficit in its recharge. The depression cone expansion may unleash a series of undesirable consequences, among them, the hydraulic head reduction in supply wells, the emergence of new dolines and/or the advance of the existing ones, and acceleration of the natural process of karstification in the region.

5. REFERENCES

Almeida F.F.M. (1977). O Cráton do São Francisco. Rev. Bras. Geoc., 7:349-364.

Anderson, M. P., Woessner, W. W., Hunt, R. J. (2015). Applied groundwater modeling: simulation of flow and advective transport. Academic press.

Azmy, K., Kaufman, A.J., Misi, A., Oliveira, T.F. (2006). Isotope stratigraphy of the Lapa Formation, São Francisco Basin, Brazil: implications for Late Neoproterozoic glacial events in South America. Precam. Res. 149, 231–248.

Banks, E. W., Simmons, C. T., Love, A. J., Cranswick, R., Werner, A. D., Bestland, E. A., Wilson, T. (2009). Fractured bedrock and saprolite hydrogeologic controls on groundwater/surface-water interaction: a conceptual model (Australia). Hydrogeology Journal, 17(8), 1969–1989. doi:10.1007/s10040-009-0490-7v.

Bittencourt, C., Auler, A. S., Reis Neto, J. M., Bessa, V., Silva, M. V. A. (2009). The influence of hypogene and epigene speleogenesis in the evolution of the Vazante Karst, Minas Gerais state, Brazil. In Hypogene speleogenesis and karst hydrogeology of Artesian Basins, Simferopol. Conference, Chernivtsi, Ukraine.

Bittencourt, C., Bessa, V., Araújo, E. E. (2008). The Vazante Underground Mine, Brazil — An Example of Controlled Water Table Drawdown in Karstic Areas. Sinkholes and the Engineering and Environmental Impacts of Karst. doi:10.1061/41003(327)71.

Bittencourt, C. e Reis Neto, J. (2012). O sistema cárstico de Vazante - carste em profundidade em metadolomitos do Grupo Vazante - MG. Revista Brasileira de Geociências. 42. 01-10. 10.25249/0375-7536.20124210110.

Bonacci, O. (2015). Surface Waters and Groundwater in Karst. In Karst Aquifers Characterization and Engineering. Professional Practice in Earth Sciences. doi:10.1007/978-3-319-12850-4.

Bonsor, H. C., MacDonald, A. M., Ahmed, K. M., Burgess, W. G., Basharat, M., Calow, R. C., Zahid, A. (2017). Hydrogeological typologies of the Indo-Gangetic basin alluvial aquifer, South Asia. Hydrogeology Journal, 25(5), 1377–1406. doi:10.1007/s10040-017-1550-z.

Campos-Neto, M.C., (1984). Litoestratigrafia, relacões estratigráficas e evolucão paleogeográfica dos grupos Canastra e Paranoá (região Vazante-Lagamar, MG). Revista Brasileira de Geociências 14, 81–91.

Cândido, E., G. (2018). Modelagem hidrogeológica aplicada à análise de transporte de contaminantes: estudo prospectivo da propagação de contaminação em aquífero livre poroso. Dissertação de mestrado, Escola de Engenharia, Universidade Federal de Minas Gerais, Minas Gerais.

Cao, V., Schaffer, M., Taherdangkoo, R., Licha, T. (2020). Solute Reactive Tracers for Hydrogeological Applications: A Short Review and Future Prospects. Water. v.12, n. 3, p. 653.

Carvalho M.O., Valeriano C.M., Aparicio-González P.A., Oliveira G.D., Impiccini A. (2016). The thrust contact between the Canastra and Vazante groups in the Southern Brasília Belt: structural evolution, white mica crystallinity and implications for the Brasiliano orogeny. Brazilian Journal of Geology, 46(4):567-583.

Carvalho, M.O., Valeriano, C.M., Aguiar Neto, C.C., Oliveira, G.D., Heilbron, M. (2019). The Vazante and Canastra groups revisited: Sm-Nd and Sr isotopes - evidence for contribution from Tonian intraplate magmatism during passive margin development along the SW São Francisco margin, Brazil. Brazilian Journal of Geology, 49(1). doi:10.1590/2317-4889201920180081.

Changming, L., Jingjie, Y., Kendy, E. (2001). Groundwater Exploitation and Its Impact on the Environment in the North China Plain. Water International, 26(2), 265–272. doi:10.1080/02508060108686913.

Cook, P. G. (2003). A guide to regional groundwater flow in fractured rock aquifers. Henley Beach, S. Aust: Seaview Press.

Cunha, A. P., Zeri, M., Leal, K., Costa, L., Cuartas, L. A., Marengo, J. A., Ribeiro-Neto, G. (2019). Extreme Drought Events over Brazil from 2011 to 2019. Atmosphere, 10(11), 642. doi:10.3390/atmos10110642.

Custodio, E. (2002). Aquifer overexploitation: what does it mean? Hydrogeology Journal 10, 254–277. doi:10.1007/s10040-002-0188-6.

Custodio, E., Andreu-Rodes, J. M., Aragón, R., Estrela, T., Ferrer, J., García-Aróstegui, J. L., del Villar, A. (2016). Groundwater intensive use and mining in south-eastern peninsular Spain: Hydrogeological, economic and social aspects. Science of The Total Environment, 559, 302–316. doi:10.1016/j.scitotenv.2016.02.107.

Dardenne, M.A. (2000). The Brasília fold belt. In: Cordani, U.G., Milani, E.J., Thomaz-Filho, A., Campos, D.A. (Eds.), Tectonic Evolution of South America. 31st International Geological Congress, Rio de Janeiro, pp. 231– 263.

Divine, C.E. and McDonnell, J.J. 2005. The future of applied tracers in hydrogeology. Hydrogeology Journal, 13, p. 255-258.

Dias, P., Marinho, M., Sotero, M., Vilela, F., Marques, E., Matos, C. (2015). Metalogenia das Províncias Minerais do Brasil: distrito zincífero de vazante, MG. Belo Horizonte: Companhia de Pesquisa de Recursos Minerais - CPRM, 2015. 59p. v.5. (Série Províncias Minerais do Brasil).

Diersch, H. J. G. (2014). FEFLOW: Finite element modeling of flow, mass and heat transport in porous and fractured media. Springer, Heidelberg. Germany. p.996.

Diffenbaugh, N. S., Singh, D., Mankin, J. S., Horton, D. E., Swain, D. L., Touma, D., Rajaratnam, B. (2017). Quantifying the influence of global warming on unprecedented extreme climate events. Proceedings of the National Academy of Sciences, 114(19), 4881–4886. doi:10.1073/pnas.1618082114.

Easterling, D. R., Evans, J. L., Groisman, P. Y., Karl, T. R., Kunkel, K. E., Ambenje, P. (2000). Observed Variability and Trends in Extreme Climate Events: A Brief Review. Bulletin of the American Meteorological Society, 81(3), 417–425. doi:10.1175/1520-0477(2000)081<0417:ovatie>2.3.co;2.

Enemark, T., Peeters, L. J. M., Mallants, D., Batelaan, O. (2019). Hydrogeological conceptual model building and testing: A review. Journal of Hydrology, 569, 310–329. doi:10.1016/j.jhydrol.2018.12.007.

Esteller, M. V. and Diaz-Delgado, C. (2002). Environmental Effects of Aquifer Overexploitation: A Case Study in the Highlands of Mexico. Environmental Management, 29(2), 266–278. doi:10.1007/s00267-001-0024-0.

Field, C. B., Barros, V., Stocker, T. F., Dahe, Q. 2012. Managing the risks of extreme events and disasters to advance climate change adaptation: special report of the intergovernmental panel on climate change. Cambridge University Press.

Ferreira, O. B., Suhogusoff, A. V., Tavares, T. S. (2021). Determinação do fator de retardamento da uranina em sedimentos quaternários do aquífero São Paulo. Águas Subterrâneas, 35(1), 65–77. https://doi.org/10.14295/ras.v35i1.29951.

Fleckenstein J. H., Niswonger R. G., Fogg E. G. (2006). River-Aquifer Interactions, Geologic Heterogeneity, and Low-Flow Management. 44(6), 837–852. doi:10.1111/j.1745-6584.2006.00190.x.

Fuck R. A., Pimentel M. M., Silva L. J. (1994). Compartimentação Tectônica na porção oriental da Província Tocantins. In: Congresso Brasileiro de Geologia, 38, Camboriú (SC), Anais, p.215-216.

GeoHydros and DHI. (2013). Estudo da caracterização da dinâmica de fluxos subterrâneos a partir da injeção de técnicas baseadas na utilização de traçadores corantes. Relatório Técnico. p.389.

Geohydros and Water Services and Technologies. (2020). Estudo de caracterização da dinâmica de fluxos subterrâneos a partir da aplicação de técnicas baseadas na utilização de traçadores corantes. Relatório Técnico. Belo Horizonte, p.133.

Hamad, A., Hadji, R., Bâali, F., Houda, B., Redhaounia, B., Zighmi, K., Hamed, Y. (2018). Conceptual model for karstic aquifers by combined analysis of GIS, chemical, thermal, and isotopic tools in Tuniso-Algerian transboundary basin. Arabian Journal of Geosciences, 11(15). doi:10.1007/s12517-018-3773-2.

Hidrovia. (2012). Caracterização hidrogeológica integrada da área de influência da mina de zinco da Votorantim Metais, unidade Vazante. Relatório técnico. p.101.

Hitzman, M. W.; Reynolds, N. A.; Sangster, D. F.; Allen, C. R.; Carman, C. E. (2003). Classification, Genesis, and Exploration Guides for Nonsulfide Zinc Deposits. Economic Geology, 98(4), 685–714. doi:10.2113/gsecongeo.98.4.685.

IBGE - Instituto Brasileiro de Geografia e Estatística. (2010). Available in: <www.cidades.ibge.gov.br/brasil/mg/vazante/panorama>. Accessed in: March 7th, 2022.

Instituto de Pesquisas Tecnológicas do Estado de São Paulo – IPT. (2004). Levantamento geológico-estrutural nos entornos da mina de zinco da NEXA – Unidade Vazante, no município de Vazante, MG, como subsídio aos estudos hidrogeológicos. Relatório Técnico. São Paulo, 56p.

Instituto de Pesquisas Tecnológicas do Estado de São Paulo – IPT. (2005). Complementação do modelo geológico estrutural no entorno das minas de zinco da Votorantim Metais – Unidade Vazante, no município de Vazante, MG, como subsídio aos estudos hidrogeológicos. Relatório preliminar.

Jamali, M. Y., Mustapha, N., Amir, S. (2020). The Impact of Over-exploitation of Groundwater along the Irrigated Perimeter of Tadla, Oum Errabia Basin, Morocco. Desalination and water treatment, 195, 201-212. doi:10.5004/dwt.2020.25877.

Kalhor, K., Ghasemizadeh, R., Rajic, L., Alshawabkeh, A. (2019). Assessment of groundwater quality and remediation in karst aquifers: A review, Groundwater for Sustainable Development,Volume 8,104-121.https://doi.org/10.1016/j.gsd.2018.10.004.

Karlovic, I., Markovic, T., Vujnovic, T., Larva, O. (2021). Development of a Hydrogeological Conceptual Model of the Varaždin Alluvial Aquifer. Hydrology, 8(1), 19. doi:10.3390/hydrology8010019.

Kresic, N. and Mikszewski, A. (2012). Hydrogeological conceptual site models: data analysis and visualization. CRC press.

Leibundgut, C., Maloszewski, P., Kulls, C. (2009). Tracers in Hydrology. John Wiley e Sons, Ltda.

Lekula, M., Lubczynski, M. W., Shemang, E. M. (2018). Hydrogeological conceptual model of large and complex sedimentary aquifer systems – Central Kalahari Basin (Botswana). Physics and Chemistry of the Earth, Parts A/B/C. doi:10.1016/j.pce.2018.05.006.

Machado, M. e Silva, S. (2010). Geodiversidade do estado de Minas Gerais. CPRM. 131 p.

Masciopinto, C. and Palmiotta, D. (2012). Flow and Transport in Fractured Aquifers: New Conceptual Models Based on Field Measurements. Transport in Porous Media, 96(1), 117–133. doi:10.1007/s11242-012-0077-y.

Mengistu, H., Demlie, M. B., Abiye, T. A., Xu, Y., Kanyerere, T. (2019). Conceptual hydrogeological and numerical groundwater flow modeling around the moab khutsong deep gold mine, South Africa. Groundwater for Sustainable Development, 100266. doi:10.1016/j.gsd.2019.100266.

Mengistu, H., Tessema, A., Abiye, T., Demlie, M., Lin, H. (2014). Numerical modeling and environmental isotope methods in integrated mine-water management: a case study from

the Witwatersrand basin, South Africa. Hydrogeology Journal, 23(3), 533–550. doi:10.1007/s10040-014-1216-z.

Molina, J. L., García Aróstegui, J. L., Benavente, J., Varela, C., de la Hera, A., López Geta, J. A. (2009). Aquifers Overexploitation in SE Spain: A Proposal for the Integrated Analysis of Water Management. Water Resources Management, 23(13), 2737–2760. doi:10.1007/s11269-009-9406-5.

Monteiro, L.V.; Bettencourt, J.S.; Juliani, C.; Oliveira, T.F. (2006). Geology, petrography, and mineral chemistry of the Vazante non-sulfide and Ambrósia and Fagundes sulfide-rich carbonatehosted Zn-(Pb) deposits, Minas Gerais, Brazil. Ore Geology Reviews, S.N.T., n. 28, p. 201 – 234.

Monteiro, L.V.S., Bettencourt, J.S., Juliani, C., de Oliveira, T.F. (2007). Non-sulfide and sulfide-rich zinc mineralizations in the Vazante, Ambrosia and Fagundes deposits, Minas Gerais, Brazil: mass balance and stable isotope characteristics of the hydro- thermal alterations. Gondwana Res. 11, 362–381.

Mukherjee, A., Bhanja, S. N., Wada, Y. (2018). Groundwater depletion causing reduction of baseflow triggering Ganges River summer drying. Scientific Reports, 8(1). doi:10.1038/s41598-018-30246-7.

NASEM - National Academies of Sciences, Engineering, and Medicine. (2020). Characterization, Modeling, Monitoring, and Remediation of Fractured Rock. Washington, DC: The National Academies Press. https://doi.org/10.17226/21742.

Ninanya, H., Guiguer, N., Vargas, E. A., Nascimento, G., Araujo, E., Cazarin, C. L. (2018). Analysis of water control in an underground mine under strong karst media influence (Vazante mine, Brazil). Hydrogeology Journal. doi:10.1007/s10040-018-1785-3.

Petitta, M., Mastrorillo, L., Preziosi, E., Banzato, F., Barberio, M. D., Billi, A., Doglioni, C. (2018). Water-table and discharge changes associated with the 2016–2017 seismic sequence in central Italy: hydrogeological data and a conceptual model for fractured carbonate aquifers. Hydrogeology Journal, 26(4), 1009–1026. doi:10.1007/s10040-017-1717-7.

Pimentel, M.M., Dardenne, M.A., Fuck, R.A., Viana, M.G., Junges, S.L., Fischel, D.P., Seer, H.J., Dantas, E.L. (2001). Nd isotopes and the provenance of detrital sediments of the

Neoproterozoic Brasília Belt, central Brazil. Journal of South American Earth Sciences 14, 571– 585.

Pinho, J.M., Dardenne, M.A., Rigobello, A.E. (1989). Evolução Tectônica da mineralização de zinco de Vazante. In: Simpósio de Geologia do Núcleo Minas Gerais, 5. Anais, 110:275-276.

Pinho, J. M. (1990). Evolução Tectônica da mineralização de zinco de Vazante. 1990. 115p. Dissertação de Mestrado. UnB, Brasília.

PROGEO. (2007). Aquífero da bacia dolomítica – Modelo hidrogeológico regional. Relatório Técnico.

Rapantova, N., Grmela, A., Vojtek, D., Halir, J., Michalek, B. (2007). Ground Water Flow Modeling Applications in Mining Hydrogeology. Mine Water and the Environment, 26(4), 264–270. doi:10.1007/s10230-007-0017-1.

Rigobello, A.E., Branquinho, J.A., Dantas, M.G.S., Oliveira, T.F., Nieves Filho, W. (1988) Mina de zinco de Vazante, Minas Gerais. In: Principais depósitos minerais do Brasil. v.2. 670p.

Rodrigues Filho, S. e Viana, M. B. (2011). Gestão da água: o desafio do zinco em Vazante (MG). Recursos minerais & sustentabilidade territorial, Grandes minas. v.1. p.333-360.

Rostirolla, S. P., Mancini, F., Reis Neto, J. M., Figueira, E. G., Araujo, E. C. (2002). Análise estrutural da mina de Vazante e adjacências: Geometria, cinemética, e implicacões para a hidrogeologia. Revista Brasileira de Geociências, v. 32, p. 59-68.

Rupérez-Moreno, C., Senent-Aparicio, J., Martinez-Vicente, D., García-Aróstegui, J. L., Calvo-Rubio, F. C., Pérez-Sánchez, J. (2017). Sustainability of irrigated agriculture with overexploited aquifers: The case of Segura basin (SE, Spain). Agricultural Water Management, 182, 67–76. doi:10.1016/j.agwat.2016.12.008.

Saadé-Sbeih, M., Asaad, A. H., Shamali, O., Zwahlen, F., Jaubert, R. (2018). Groundwater balance politics: Aquifer overexploitation in the Orontes River basin. Water Alternatives, 11(3), 663-683.

Sanghi, A. and Mendelsohn, R. (2008). The impacts of global warming on farmers in Brazil and India. Global Environmental Change, 18(4), 655–665. doi:10.1016/j.gloenvcha.2008.06.008.

Sasowsky, D. and White, B. (1994). The role of stress release fracturing in the development of cavernous porosity in carbonate aquifers. Water Resources Research, 30(12), 3523–3530. doi:10.1029/94wr01727.

Schlumberger Water Services. (2008). Avaliação hidrogeológica, quantificação de fluxos e medidas mitigadoras. p. 103.

Silva, L.L., Donnici, C.L., Ayala, J.D., Freitas, C.H., Moreira, R.M., Pinto, A.F. (2005). Traçadores: o uso de agentes químicos para estudos hidrológicos, ambientais, petroquímicos e biológicos. Química Nova. v. 32, n.6, p. 1576-1585.

Singhal, B. B. S. and Gupta, R. P. (2010). Applied hydrogeology of fractured rocks. Springer Science & Business Media.

Slezak, P., Olivo, G., Oliveira, G., Dardenne, M. (2014). Geology, mineralogy, and geochemistry of the Vazante Northern Extension zinc silicate deposit, Minas Gerais, Brazil. Ore Geology Reviews. 56. 234-257.

Stavric, V. (2004). Aquifer overexploitation and groundwater mining. In Balwois Conference on Water Observation and Information System for Decision Support, Ohrid, República de Macedonia (pp. 25-29).

Suhogusoff, A. V., Hirata, R., Ferrari, L. M. (2005). Adsorção do traçador fluorescente uranina em sedimentos quaternários da Bacia de São Paulo. Revista Brasileira de Geociências, v. 35, p. 551-558. https://doi.org/10.25249/0375-536.200537551558.

Taheri, K., Taheri, M., Parise, M. (2016). Impact of intensive groundwater exploitation on an unprotected covered karst aquifer: a case study in Kermanshah Province, western Iran. Environmental Earth Sciences, 75(17). doi:10.1007/s12665-016-5995-5.

Trabelsi, F., Tarhouni, J., Mammou, A. B., Ranieri, G. (2011). GIS-based subsurface databases and 3-D geological modeling as a tool for the setup of hydrogeological framework: Nabeul–Hammamet coastal aquifer case study (Northeast Tunisia). Environmental Earth Sciences, 70(5), 2087–2105. doi:10.1007/s12665-011-1416-y.

Valeriano C.M., Dardenne M.A., Fonseca M.A., Simões L.S.A., Seer H.J. (2004). A evolução tectônica da Faixa Brasília. In: Mantesso-Neto V. e Bartoreli A. (eds.). Geologia do continente sul-americano: evolução da obra de Fernando Flávio Marques de Almeida. São Paulo, Beca, p. 575-593.

Valeriano, C., Teixeira, W., Heilbron, M., Simões, L.S. (2000). Southern Brasília belt (SE Brazil): Tectonic discontinuities, K-Ar data and evolution during the Neoproterozoic Brasiliano orogeny. Revista Brasileira de Geociências. p.30.

Vasconcelos, V. V., Martins Junior, P. P., Hadad, R. M. (2012). Caracterização ambiental da bacia do Rio Paracatu. In Martins Junior, P. P. (Coord.). Projeto SACD. Belo Horizonte Cetec.

White, W. B. (1999). Conceptual models for karstic aquifers. Karst modeling, 5, 11-16.

White, W.B. (2012). Conceptual Models for Carbonate Aquifers. Groundwater, 50: 180-186. doi: 10.1111/j.1745-6584.2012.00923.x.

Worthington, S. R. and Smart, C. C. (2003). Empirical Determination of Tracer Mass for Sink to Spring Tests in Karst. Sinkholes and the Engineering and Environmental Impacts of Karst. doi:10.1061/40698(2003)26.

Zheng, C. and Bennett, G. D. (2002). Applied contaminant transport modeling (Vol. 2, p. 353). New York: Wiley-Interscience.

APPENDIX 1 - HYDROGEOLOGICAL CHARACTERIZATION OF BRITTLE STRUCTURES LOCATED BETWEEN THE VAZANTE UNDERGROUND MINE AND THE SANTA CATARINA RIVER, MINAS GERAIS, BRAZIL

Abstract presented at 47th International Association of Hydrogeologists (IAH) Congress, Online, Brazil (August/2021)

Hydrogeological Characterization of Brittle Structures Located Between the VazanteUnderground Mine and the Santa Catarina River, Minas Gerais, Brazil

Otávio Ferreira[1,2]; Tatiana Tavares[2]; Alexandra Suhogusoff[1]; Vitor Losada[2]; Edmar Araújo[3]; Carlos Gamba[2]; Otávio Gandolfo[2]

[1] Instituto de Geociências, Universidade de São Paulo, USP.

[2] Laboratório de Recursos Hídricos e Avaliação Geoambiental, Instituto de Pesquisas Tecnológicas do Estado de SãoPaulo, IPT.

[3] Nexa Resources

Corresponding Author(s): otavio.barbosa.ferreira@usp.br

The Vazante underground mine, located in Minas Gerais state, southeast region of Brazil, is the most important zinc deposit in the country. The mine is inserted in the geological context of the Meso-Neoproterozoic Vazante Group. It represents a carbonate and siliciclastic metasedimentary sequences associated with a system of thrusts and nappes ina complex geotectonic scenario (Pimentel et al, 2001).

The underground galleries are developed in a deformed sequence of metapelitic and dolomitic rocks, which host an intensely fractured unconfined karst aquifer system. The mining operation depends on a continuous groundwater pumping system so that the extraction of the zinc ore is carried out in a drained environment. The impacts created bythe water table drawdown can be seen in the areas around the mine, where the lower course of the Santa Catarina River is located. Over the past few years, the accelerated formation of sinkholes has been observed in this region. Flow loss and drying up stretches of the Santa Catarina River are being mapped during the dry seasons.

This work aims to classify the hydrogeological potential of brittle structures and karst conduits that can generate hydraulic connections between the Santa Catarina River and the underground mine. The continuity in plan and depth of these features were also defined. In an integrated way, the approach was based on studies related to the structural framework of the region, as well as geophysical data of gravimetry, differential interferometry and electrical resistivity tomography. Evaluation of hydrogeological data over time and field observations were also used for the interpretations. In addition, fluorescent tracer tests were carried out to define leakage zones and preferential flowloss paths along the Santa Catarina River channel.

In a future stage, these structures will be incorporated into a numerical groundwater flow model that is being developed in this region.

APPENDIX 2 – POTENTIOMETRIC MAPS OF SIMULATED SCENARIOS FOR DECEMBER 2030

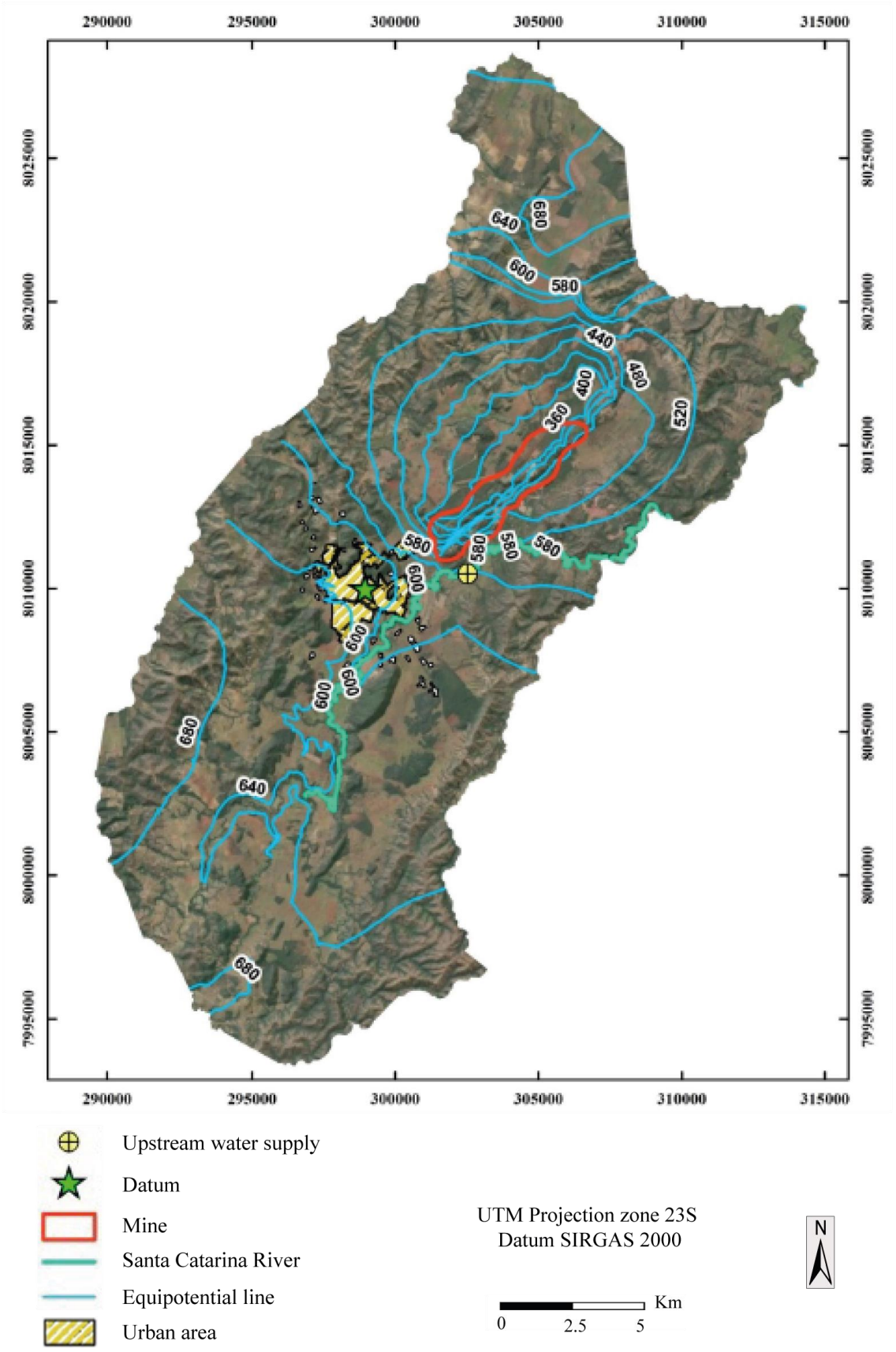

Figure 1 - Potentiometric map for the SCR upstream water supply scenario in December 2030.

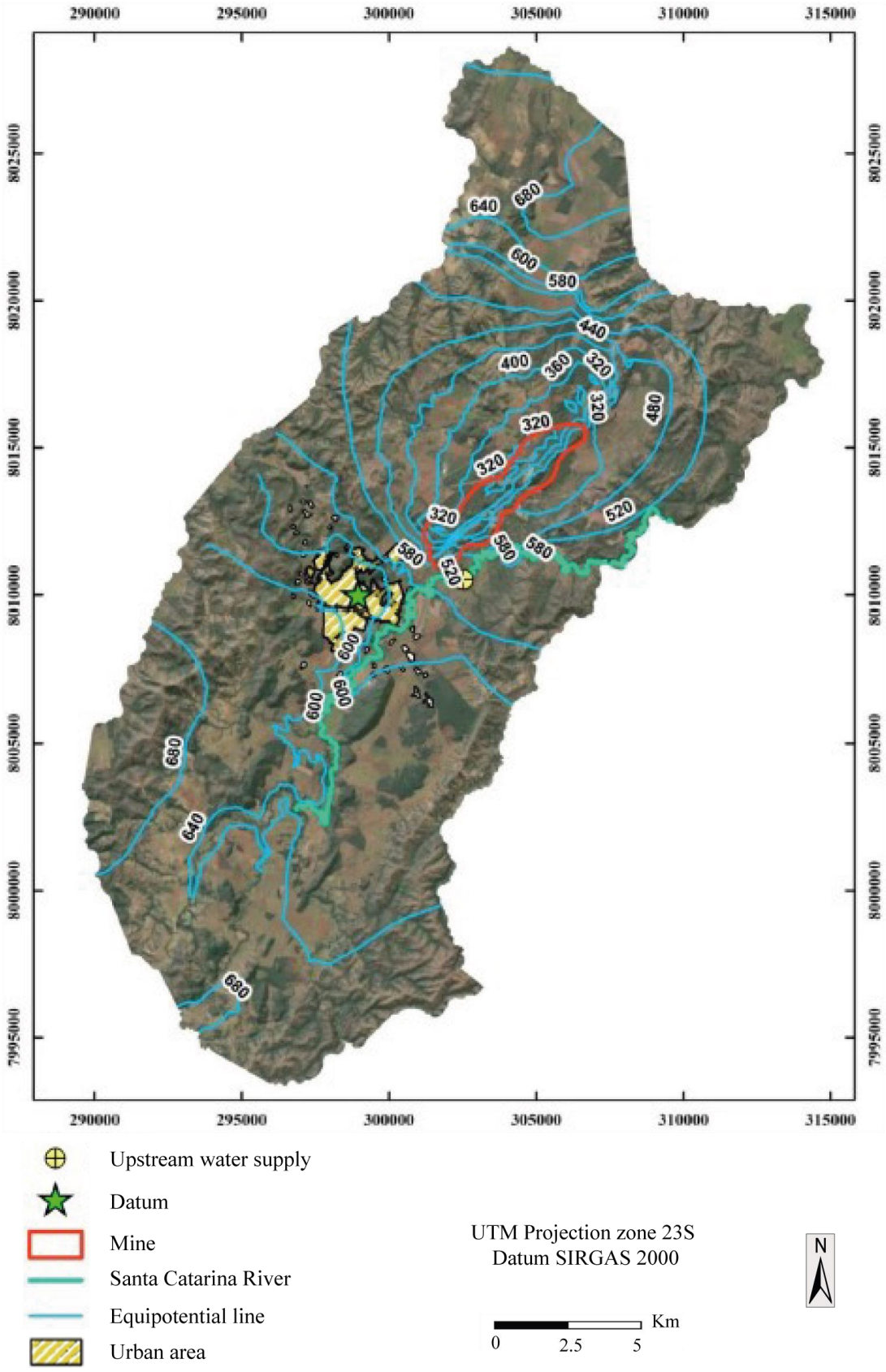

Figure 2 - Potentiometric map for the SCR waterproofing scenario in December 2030.

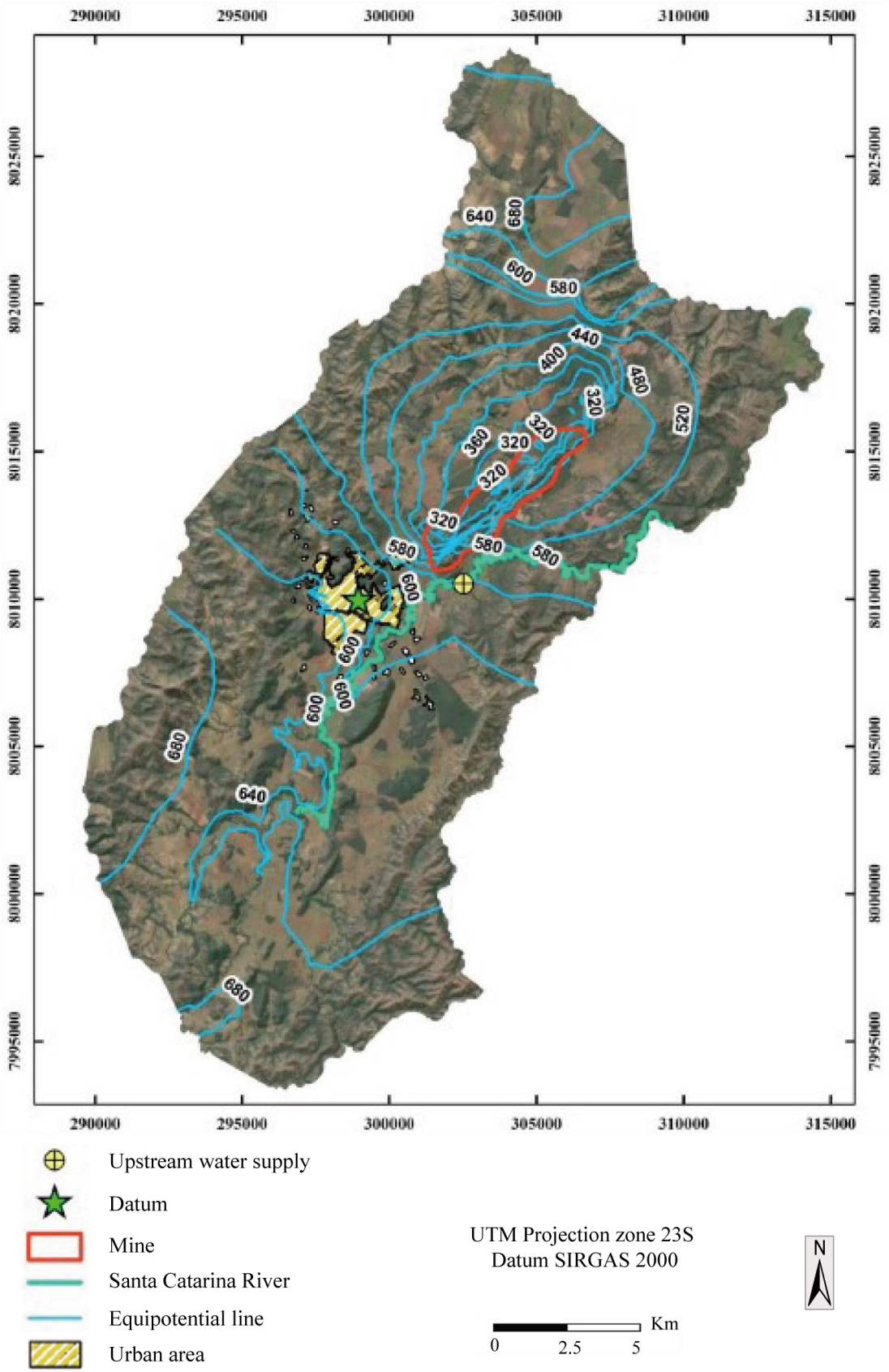

Figure 3 - Potentiometric map for December 2030 representing the scenario of SCR's sinkholes obstruction in 50%.

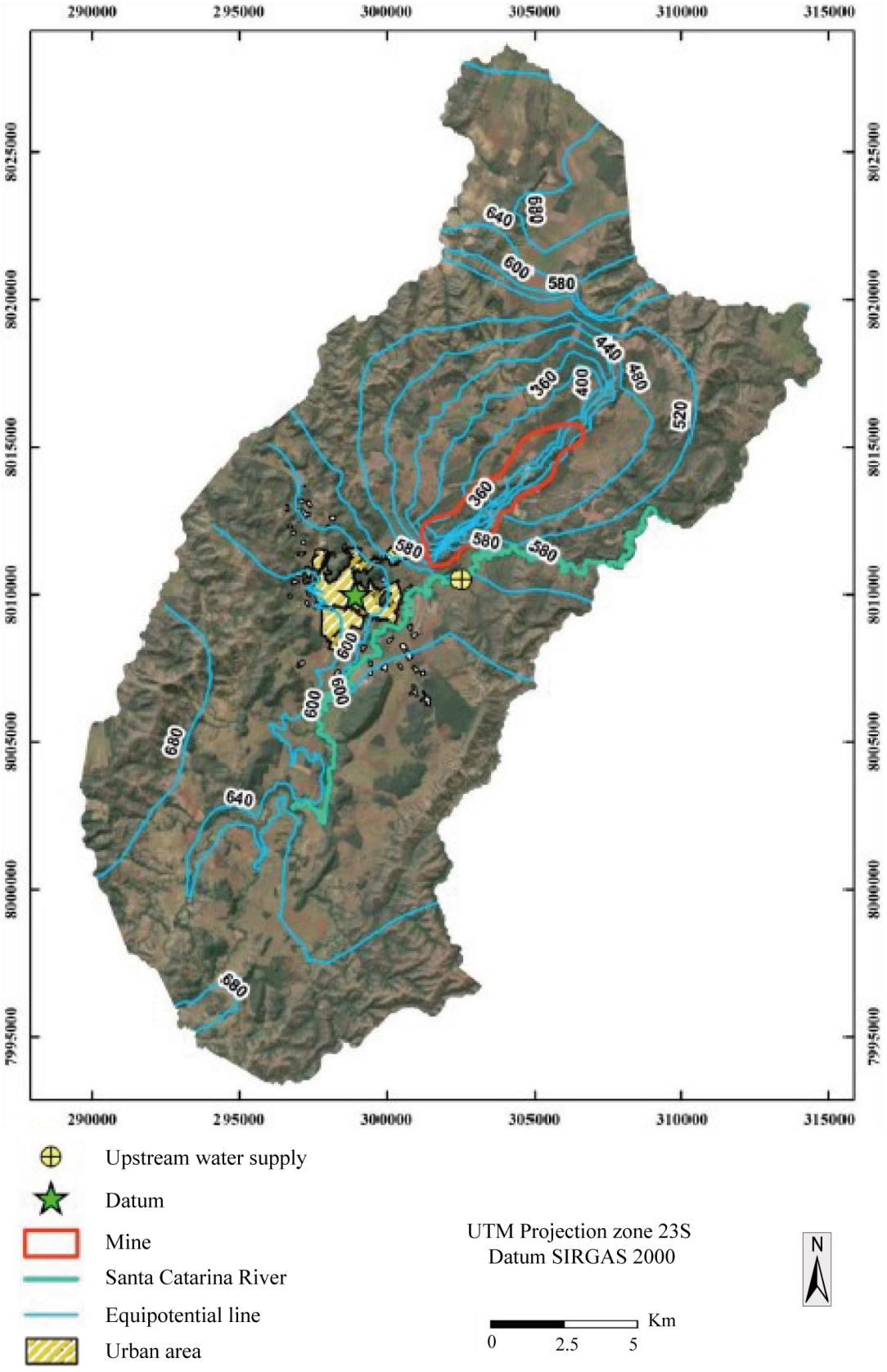

Figure 4 - Potentiometric map for December 2030 representing the scenario of SCR's sinkholes obstruction in 100%.